The role of the BMP antagonist Gremlin2 during cardiac tissue repair

By

Lehanna Nalani Sanders

Dissertation

Submitted to the Faculty of the

Graduate School of Vanderbilt University

in partial fulfillment of the requirements

for the degree of

DOCTOR OF PHILOSOPHY

in

Cell and Development Biology

August, 2016

Nashville, TN

Approved:

Antonis K. Hatzopoulos, PhD
Mark deCaestecker, MB BS, PhD
Stephen R. Hann, PhD
Andrea Page-McCaw, PhD
Joey Barnett, PhD

To my late grandfather, Norman Sanders, who always fostered and supported my desire to become a scientist.

To those in my family who passed away while completing this work: my cousin Maritza Cedeño, my grandmother Sixta Ortíz, and finally my beloved sister, Zulymar Marrero.

To my parents, Phil and Sonia Sanders, in honor of all their sacrifices.

To my partner in life, my husband, Andrew Williams.

ACKNOWLEDGEMENTS

This work was supported by National Institutes of Health grants HL083958 and HL100398 to Antonis Hatzopoulos, GM114640 to Thomas Thompson, our collaborator at the University of Cincinnati and Antonis Hatzopoulos; Institutional Support from Vanderbilt University Medical Center to Antonis Hatzopoulos; and my T32 Program in Cardiovascular Mechanisms: Training in Investigation (HL007411) fellowship.

I want to thank my thesis committee members: Dr. Andrea Page-McCaw, Dr. Joey Barnett, Dr. Steve Hann, and my chair Dr. Mark deCaestecker for providing me with support and advice during as well as outside of each of my committee meetings during my tenure. Their insight was extremely valuable to my education and my work. This work would also not be possible without the tremendous help of those I have collaborated with throughout the years: Dr. Tom Thompson and his lab for synthesizing and providing me with protein whenever it was needed; Dr. Mohamed Saleh and Dr. William McMaster Jr. for helping me conduct experiments that have proven to be extremely valuable to my project; and finally Dr. Ela Knapik and her lab members Dr. Daniel Levic and Gokhan Unlu for always being extremely helpful, enthusiastic and supportive of my efforts.

The Hatzopoulos laboratory has been a great place for conducting my thesis research. From lab meetings that continued until problems were solved

and better understanding was gained, to our annual March Madness brackets, I have thoroughly enjoyed my time in the lab. I have had the pleasure to work with a great group of people past and present that contributed to my work in large ways, including: Dr. Kea Jones, Amrita Mukherjee, Dr. Vineeta Tanwar, Dr. Bryan Fioret, Jeff Bylund, and Dr. David Paik. Everyone made the lab a comfortable and enjoyable place to come into work everyday. At the helm of it all has been my mentor, Dr. Antonis Hatzopoulos.

Antonis has been an extremely supportive mentor, always fostering me intellectually, scientifically, and professionally. I have really enjoyed the time we have spent together and have had the opportunity, thanks to him, to try some of the best chocolates ever from around the world. He has been my advocate and cheerleader through this process and I couldn't have done it without him. I thank him for the long hours he spent one-on-one with me, for believing in me, for helping me through countless trials and tribulations (including being a shoulder to cry on), and for molding me into the scientist that I am today. His office has become a second home throughout the years, and one I will miss going into nearly every day.

While at Vanderbilt University, I have made some of the best friends of my life. Rubin Baskir was one of my first friends and originally a lab mate, and has made my time here memorable and extremely enjoyable. I have since made other lasting relationships, and want to thank the following for always being available for a game night, movie night, or happy hour: Michelle Williams, Patrick

Mulcrone, Dr. Ushashi Dadwal, Dr. Hannah Hankins, and Dr. Kim Riley. However, I need to give special thanks for the love and support of Dr. Meghan Joly. Our countless running dates, costume parties, midnight movies and general conversations were what made my time in Nashville great, and I will forever be grateful for her support and encouragement during what were some of the hardest and darkest times of my life. Outside of the Vanderbilt community, I am also extremely grateful for the great friendships that I have formed with other members of the Joly family: Greg, Valary, and Brent. I also want to thank those friends that I had before coming to Vanderbilt and continued to support me during my PhD career: Jennifer Vernia, Megan Pownall Wyss, Thomas Asare, Scott Goodman, and finally my best friend Jill Shaw. I am so thankful to Jill for always being available via phone, her tremendous support, all her visits here to Nashville, and for sending encouraging letters during my more difficult times.

I have a huge sense of gratitude for the support of my previous mentors, Dr. James Leary and Dr. Paul Todd. I learned so much about science and life in general through their kindness and willingness to spend time with me during my first few years in a research lab. I also want to thank my previous mentor David Kennedy, for his support before joining graduate school as well as his continued support and investment in my career since. I am forever grateful.

There are not enough words to describe the gratitude I have towards my family. I have to thank my grandmother Betty Sanders for all our phone conversations; my Aunt Theresa and Uncle Tom Norton, Titi Millie and Uncle

Carlos Cedeño, and my cousins Maribel and Bret Taylor and Amy and Stephanie Norton for always being extremely encouraging throughout my life and especially during my thesis work. I have also been blessed with an extremely supportive in-law family, especially John and Charlene Williams. The times we have been able to spend together while I have been conducting my thesis research have been extremely valuable and meaningful for the completion of this work.

However, I would not be where I am today without the support of my immediate family. My niece, Bianca, entered the world right before I started graduate school and has been a light in my life during my tenure. At the time of writing this dissertation, she states that she wants to be doctor just like me, so this work is in part for her and her dreams. It is with great sadness that I mention here that her mother, my sister Zulymar, passed away suddenly during my second year. She was almost a second mother to me, always overly protective and amazingly supportive. She would tell everyone she knew that she was so proud of her 'baby sister', and I just wish she could be here to see that I made it, largely in part because I knew that is what she would have wanted. Ever since my sister's passing, my parents, Phil and Sonia, have been taking care of her daughter so that I could stay focused and fully dedicated to completing my thesis. This is only the most recent example of the sacrifices they take for my education and me. My mother dedicated herself to helping me with my schoolwork from a very young age, my father commuted several states away for years so that I could stay in the same school, and they both would do anything to make sure I

had what I needed to foster my desire to be a scientist. They have truly dedicated themselves to making sure I could get to this point, and I will never be able to thank them enough, except simply to say, this is for you.

Lastly, I need to acknowledge the amazing person that is my husband. Ever since we have been together, he has always challenged me to be the best version of myself, while at the same time loving me for who I am. He was there for me everyday during this process, to listen to my triumphs and tribulations, to read over my writing, to be a sounding board of ideas, and even to make me a hot meal. The last year of my thesis work, he also sacrificed himself in a huge way by working an unglamorous job just to help make sure we can pay the bills while I complete my thesis. I will never be able to re-pay this kindness and sacrifice, but I will not only dedicate this work, but also myself to him.

TABLE OF CONTENTS

Page

LIST OF TABLES

Table Page

LIST OF FIGURES

Figure Page

LIST OF ABBREVIATIONS

ACE: Angiotensin converting enzyme
Alk: Activin receptor like kinase
Ang1: Angiopoietin-1
ATP: adenosine triphosphate
BAC: bacterial artificial chromosome
BMP: Bone Morphogenetic Protein
BSA: bovine serum albumin
BZ: border zone
CD: cluster of differentiation
CC, CXC: cysteine-cysteine, cysteine-X-cysteine
CCR: CC chemokine receptor
JNK: c-Jun N-terminal Kinase
DAMPS: danger associated molecular patterns
Dand5: DAN Domain Family Member 5 (also Dante, or Coco)
Dan: Neuroblastoma 1 (Nbl1)
DAPI: 4',6-diamidino-2-phenylindole
DNA: deoxyribonucleic acid
EF: ejection fraction
ES cell: Embryonic stem cell
EM7neo: kanamycin resistance gene under the synthetic bacterial EM7 promoter
EMT: Epithelial to mesenchymal transition
EndMT: Endothelial to mesenchymal transition
Fsp-1: fibroblast specific protein-1
Gapdh: Glyceraldehyde-3-phosphate dehydrogenase
GWAS: Genome wide associated studies
Grem1: Gremlin 1
Grem2: Gremlin 2
H&E: Hematoxylin and eosin
HF: heart failure
HLH: helix-loop-helix
Icam1: Intercellular cell adhesion molecule 1
IF: immunofluorescence
IL: Interleukin
INF: infarct
IP: intraperitoneal
I/R: Ischemia/reperfusion
ICM: Ischemic cardiomyopathy
ID: inhibitor of differentiation

JAK: janus kinase
LAD: Left anterior descending
LV: Left ventricle
LVIDd: Left ventricular internal dimension, diastolic
LVIDs: Left ventricular internal dimension, systolic
MH: mad homology domain
mg: Milligram
mL: Milliliter
µg: Microgram
µl: Microliter
µM: Micromolar
Mo-MLV: Moloney-Murine Leukemia Virus
Mcp-1: Monocyte chemoattractant protein-1
αMHC: Alpha-Myosin Heavy Chain (Myh6)
Mmp: matrix metalloproteinase
MI: Myocardial infarction
Neo: neomycin
NFκB: Nuclear Factor-κB
Nppa/b: natriuretic peptide a/b
OCT: Optimal cutting temperature
PBS: Phosphate buffered saline
PRDC: protein related to Dan and Cerberus
pu(Δ)TK: fusion of puromycin and truncated thymidine kinase genes
RNA: ribonucleic acid
RT-qPCR: real time quantitative polymerase chain reaction
SDF-1: stromal cell derived factor-1
S.E.M.: standard error of mean
αSMA: Alpha Smooth Muscle Actin
SNP: single nucleotide polymorphism
Sost: Sclerostin
STAT: signal transducer and activator of transcription
TG: Transgenic (αMHC-Grem2)
TGFβ: transforming growth factor β
Timp: tissue inhibitor of matrix metalloproteinase
TNFα: Tumor Necrotic Factor alpha
T-reg: T regulatory cells
Twsg1: Twisted Gastrulation BMP Signaling Modulator 1
Vcam1: Vascular cell adhesion molecule 1
Vegfr2: Vascular endothelial growth factor receptor 2 (Flk-1)
WT: Wild type

CHAPTER I

INTRODUCTION

The tissue repair process following a myocardial infarction

Coronary heart disease resulting in myocardial infarction (MI) is the leading cause of death in both men and women, contributing to 1 in 3 deaths (Mozaffarian et al., 2015). Each year about 735,000 people in the U.S. have an MI and most suffer irreversible tissue damage, leading to ventricular remodeling, hypertrophy, deficient contractility, dilatation, and eventually heart failure (HF) (McMurray, 2010; Braunwald, 2015). Despite the fact that overall death rates due to cardiovascular disease have decreased 30% over the last few decades, the number of deaths caused by end-stage heart failure has not changed, demonstrating a need for improving treatments following an acute cardiac injury such as an MI (Braunwald, 2015).

Overview

Following an MI, the adult heart undergoes a sequence of molecular and cellular events that delineate the different stages of tissue repair (Saxena et al., 2015) (**Figure 1**). Cardiomyocytes within infarcted myocardium begin to die via necrosis and apoptosis within minutes after coronary artery occlusion (Itoh et al., 1995; Konstantinidis et al., 2012; Reimer and Jennings, 1979). Toxic products and signals, known as danger associated molecular patterns or DAMPS, released from dying cells induce endothelial cell adhesion proteins, as well as cytokines

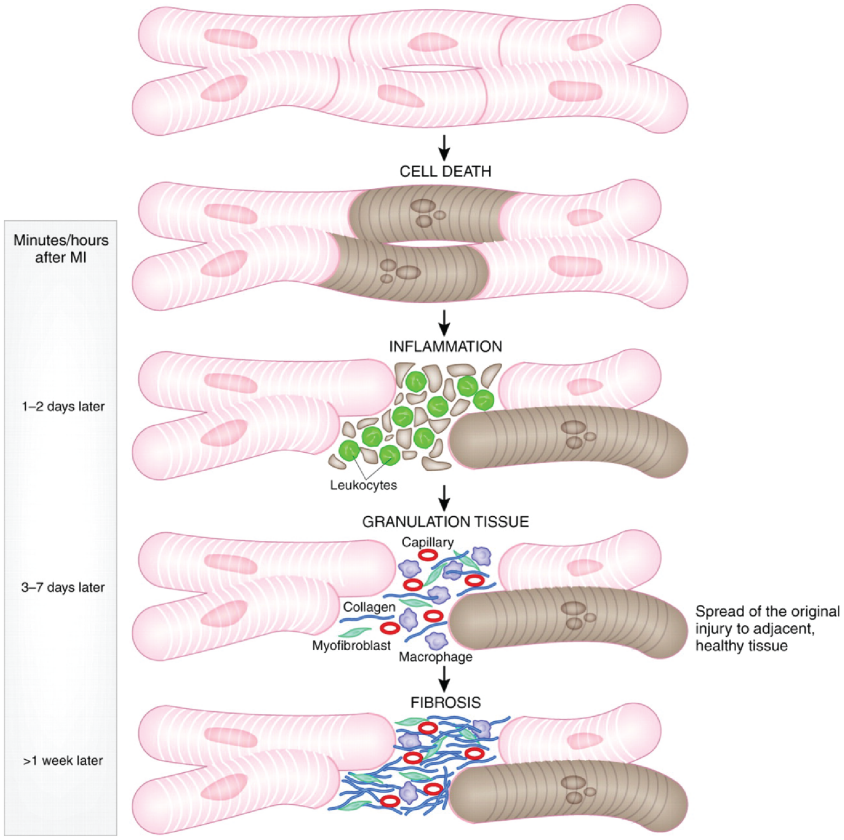

Figure 1. Cardiac tissue repair process following a myocardial infarction. The cardiac tissue repair process begins with massive cell death occurring within the first few hours. A day or so later, an inflammatory response is activated consisting of infiltrating leukocytes to clear the cellular debris. After the debris has been cleared, granulation tissue deposition begins around 3 days post-MI and lasts until day 7. Myofibroblasts and reparative macrophages are the predominant cell types present during this stage. Capillaries begin to form within the injured area in order to restore blood flow, however the formation of a collagen based scar leads to the spread of the original injury into adjacent, previously healthy tissue. By 1 week, the granulation tissue matures into a fibrotic scar. Image source: Boudoulas and Hatzopoulos *Disease Models and Mechanisms* 2009.

and chemokines, to recruit inflammatory cells that remove tissue debris as well as secrete proteases such as matrix metalloproteinase (MMPs) to degrade extracellular matrix (Timmers et al., 2012; Frangogiannis, 2014). After debris is cleared, the gap is filled with granulation tissue that is composed of proliferating cells, mainly endothelial cells that form new capillaries, and myofibroblasts that secrete collagen and other matrix proteins (Boudoulas and Hatzopoulos, 2009; Frangogiannis, 2012). Two to three weeks after the MI, the infarct tissue begins

to mature into a dense, cross-linked, collagen-based scar (Virag and Murry, 2003). These well-documented stages that comprise the tissue repair process are highly regulated in a spatiotemporal manner. However, what regulates these processes both temporally and spatially is not entirely understood. We have recently demonstrated that canonical Wnt signaling activation after MI attenuates fibrosis and promotes arteriole formation and cardiogenesis, suggesting that developmental pathways, critical for embryonic cardiac development, are re-activated after injury in the adult heart to regulate tissue repair (Aisagbonhi et al., 2011; Paik et al., 2015).

Activated inflammatory cells that infiltrate the heart during the initial stages of the tissue repair process can damage surrounding, relatively healthy tissue by inducing secondary apoptosis and necrosis through the secretion of pro-inflammatory cytokines such as TNFα, and by secreting matrix degrading proteins, thereby expanding the size of the initial injury (Entman et al., 1992). Overactive or unresolved inflammation delays and weakens scar formation; preventing proper wound healing (Kattman et al., 2011; Kruithof et al., 2006; Lenhart et al., 2011; Zhang et al., 2014). As a result, deregulated inflammation in MI patients can worsen LV dilative remodeling and systolic function, leading to HF (Frangogiannis, 2014). Therefore a better understanding of how the inflammatory process is regulated is critical for generating therapies that could lead to the improvement of the prognosis of heart failure.

Inflammatory phase of recovery

The inflammatory phase begins with the accumulation of DAMPs, the molecules released by dead or dying cells or generated from the damaged extracellular matrix examples of which include low molecular weight hyaluronic acid and fibronectin fragments. These DAMPs then serve as ligands to activate the complement cascade and Toll-Like receptors. The complement cascade consists of the classical cascade, which activates immunoglobins, and the lectin cascade, which is traditionally associated with a response to microbials, all of which activate C3, leading to the subsequent activation of phagocytosis and neutrophil infiltration.

Free radicals present in the injury area such as reactive oxygen species induce the expression of cytokines and chemokines such as TNFα and IL-1β by endothelial cells, mast cells, and cardiac cells (**Figure 2A**). These cytokines in turn, induce the expression of other chemokines (i.e. MCP-1, IL-6, SDF-1) and cell adhesion molecules present on endothelial cells through NFκB and JAK/STAT pathways activation (Christia and Frangogiannis, 2013; Frangogiannis, 2012; Ma et al., 2013; Zhang et al., 2014). In parallel, DAMPS also activate the NFκB pathway by activating Toll-like receptors or TLRs (Akira and Takeda, 2004; Timmers et al., 2012). NFκB signaling also induces the expression of pro-inflammatory cell adhesion molecules such as E-selectin and VCAM (vascular cell adhesion molecule), which are required for the capture, rolling, adhesion, and extravasation of circulating leukocytes through the endothelial cell layer to the site of injury (**Figure 2B**).

A

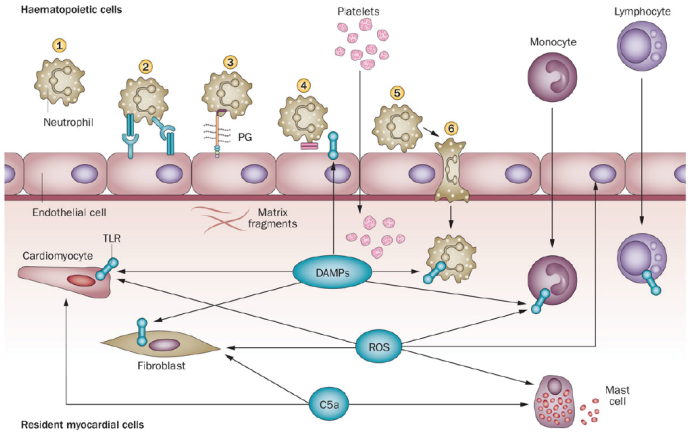

B

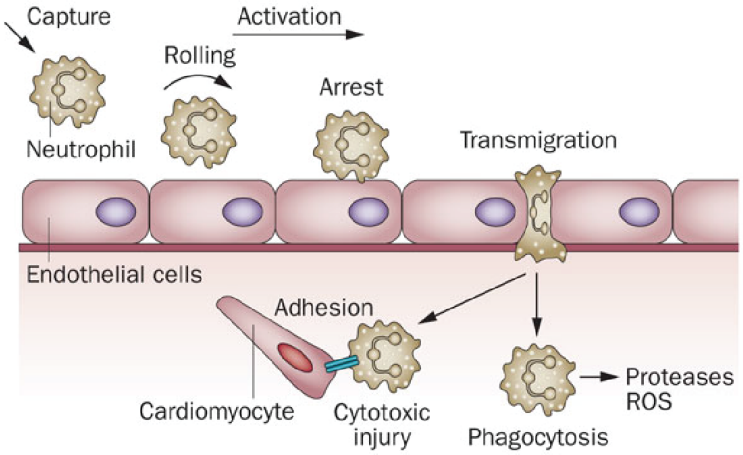

Figure 2. The inflammatory phase of recovery following a myocardial infarction. (A) Danger associated molecular patterns (DAMPS), reactive oxygen species (ROS), and the complement system (C5a) are released immediately following a myocardial infarction. This activates resident cardiomyocytes and fibroblasts to induce the toll-like receptor pathway (TLR). Platelets, neutrophils, monocytes and lymphocytes are then recruited to the site of injury respectively. These inflammatory cell populations traverse through the endothelial cell layer as shown in **(B).** Circulating leukocytes are captured, then begin to roll, attach or arrest, and eventually transmigrate into the injury site in order to clear cellular debris via phagocytosis. These events are regulated by pro-inflammatory cell adhesion molecules. Image source: Frangogiannis *Nature Reviews Cardiology* 2014.

Platelets are the first responding population of cells to enter the site of injury and act to provide a provisional matrix and secrete pro-inflammatory cytokines such as IL-1β, as well as activate the complement cascade. Leukocyte cell populations then enter the scene, beginning with neutrophils, followed by the

pro-inflammatory monocytes/macrophages, and finally adaptive immune cell populations such as regulatory T cells, B cells, and Natural Killer cells (Frangogiannis, 2008; Kain et al., 2014; Yan et al., 2013). These immune cell populations are recruited from a splenic reservoir through Angiotensin II activation, the bone marrow, and heart-draining lymph nodes (Kain et al., 2014; Ma et al., 2013; Swirski and Nahrendorf, 2013; Weirather et al., 2014; Zhang et al., 2014) They act to clear the cellular debris, phagocytose dead cells, secrete MMPs, release pro-inflammatory cytokines.

Resolution of the inflammatory response is a dynamic and active process. The sequence of events that occurs during resolution is initiated by apoptotic neutrophils. These neutrophils express “find me” and “eat me” signals, which include fractalkine, ATPs, and lactoferrin; or annexin and phosphatidylserine respectively. The release of these proteins causes an expansion of the T-reg cell population as well as a phenotypic switch in macrophages, where they transition from a pro-inflammatory phenotype to a reparative phenotype. After this transition, macrophages no longer induce the expression of the pro-inflammatory cytokines, and instead, along with T-reg cells, secrete cytokines responsible for resolving inflammation, TGFβ1 and IL-10. TGFβ1 induces the expression of matrix metalloproteinases (MMPs) that cleave both the CC and CXC families of chemokines and reduces cell-adhesion molecule expression. Il-10 promotes the presence of chemokine receptors such as CCR1, CCR2, and CCR5 thereby trapping circulating cytokines, inhibits production of pro-inflammatory cytokines through mRNA de-stabilization, and contributes to matrix stabilization through the

induction of tissue inhibitor of MMPs (TIMPs) (Christia and Frangogiannis, 2013; Frangogiannis, 2012; Krishnamurthy et al., 2009; Ortega-Gómez et al., 2013; Zhang et al., 2014).

Patients that exhibited increased levels of inflammatory biomarkers also had an increase in the extent of heart failure (Anzai et al., 1997; Frangogiannis, 2014; Ma et al., 2013; Ørn et al., 2009; Zhang et al., 2014). Therefore due to the apparent therapeutic potential, previous clinical trials have attempted to down-regulate the inflammatory response. However, the first trial using the glucocorticoid methylprednisolone actually had detrimental effects to the recovery of the patient group (da Luz et al., 1976). As the understanding of the inflammatory process post-MI has improved, additional clinical trials have been attempted. The ATTACH, RENAISSANCE, and the following larger trial RENEWAL used a recombinant TNFα receptor that prevented TNFα ligand-receptor interactions. These trials also led to increased morbidity and worse outcomes for those patients treated with the TNFα antagonist (Mann et al., 2004). Several trials took more specific approaches and targeted the leukocyte integrin CD11/CD18, following the success seen in animal models. However this treatment did not result in a reduction of infarct size or an improvement in cardiac function in human patients (Baran et al., 2001; Faxon et al., 2002). Using an antibody that binds to a component of the complement cascade also resulted in no change in morbidity (APEX AMI Investigators et al., 2007; Granger et al., 2003). Most recently, intravenous immunoglobulin treatment was used in hopes to balance the cytokine response post-MI but also resulted in no change in infarct

size and cardiac function (Gullestad et al., 2013). On the other hand, inhibitors of activated T-cells such as cyclosporine (Piot et al., 2008) and the P-selectin antagonist inclacumab (Tardif et al., 2013) did show promising results, indicating that modulating inflammation can be beneficial for cardiac repair after MI. Unfortunately, the benefits of cyclosporine use after MI could not be replicated in a larger clinical trial (Cung et al., NEJM 2015). Altogether, the clinical data underscore the need to better understand the mechanisms that regulate the inflammatory response after cardiac tissue injury.

BMP signaling in cardiac development

In order to gain insight into the molecular mechanisms that regulates the cardiac tissue repair process, the Hatzopoulos lab looked to pathways important for cardiac development that are often re-activated during tissue repair and regeneration. One such pathway is the Bone Morphogenetic Protein (BMP) signaling pathway. Originally discovered in the context of bone formation (Umulis et al., 2009), the pathway has since been extensively studied in the context of patterning and development using various models such as chicken embryos, mice, and zebrafish (Dudley et al., 1995; Furtado et al., 2008; Hammerschmidt et al., 1996; Jones et al., 1991; Luo et al., 1995; Schlange et al., 2002; Weaver et al., 1999; Winnier et al., 1995; Wozney et al., 1988). Specifically, BMP signaling has been shown to play an important role during various stages of the complex cardiac development process and is necessary for the initiation of the cardiac gene program.

The process of cardiac differentiation begins with the formation of a linear cardiac tube. The tube then undergoes a series of looping and jogging events in order to generate the 4-chambered heart (**Figure 3**).

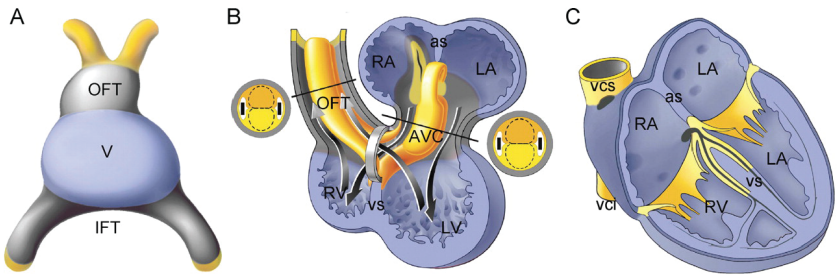

Figure 3. Overview of cardiac development. Cardiac development is a dynamic process dependent upon precise molecular signaling levels in order to maintain proper symmetry and asymmetry. **(A)** The heart begins as a linear tube consisting of the primitive outflow tract, the ventricle, and the inflow tract. This tube then undergoes a series of jogging and looping events, where the left and right ventricles and atria begin to form **(B),** eventually maturing into the four-chambered heart shown in **(C).** Abbreviations: OFT: outflow tract; V: ventricle; IFT: inflow tract; AVC: atrioventricular canal; as: atrium septum; vs: ventricle septum; vcs: vena cava superior; vci: vena cava inferior; RA: right atrium; RV: right ventricle; LA: left atrium; LV: left ventricle. Image source: van Wijk et al *Cardiovascular Research* 2007.

Each of these stages is highly regulated and requires different members and levels of the activated BMP pathway. In fact, *Bmp2*$^{-/-}$ mice are embryonic lethal and die shortly after heart tube formation, demonstrating that *Bmp2* is essential for cardiac development to proceed (Zhang and Bradley, 1996). This is in part likely due to the fact that *Bmp2* is responsible for inducing early cardiogenic differentiation of the mesoderm into myocardial and epicardial cell lineages, expression of cardiogenic transcription factors as well as *Bmp10*, and genes encoding various components of the contractile apparatus (Chen et al., 2004; Jain et al., 2015; Kattman et al., 2011; Kruithof et al., 2006; de Pater et al., 2012; Wang et al., 2007). *Bmp2* and *Bmp4* are also required for atrial-ventricular canal and outflow tract formation (van Wijk et al., 2007).

BMP ligands and cardiac differentiation

BMP signaling is responsible for the left-right asymmetry required for normal cardiac morphogenesis to occur. This has been evidenced by its regulation of target genes such as *Pitx2*, promotion of cardiac chamber identity, and through the loss of jogging and looping events when it is inhibited. BMP ligands such as *Bmp4*, *Bmp6*, and *Bmp7* are then again required for cardiac cushion formation through their regulation of cellular events such as endothelial to mesenchymal transition (EndMT), valve and ventricular septation, and endocardial cushion cell number (Kim et al., 2001; Liu et al., 2004; Ma et al., 2005; McCulley et al., 2008; Solloway and Robertson, 1999).

BMP antagonists and cardiac development

It is also clear that it is not just the presence, but also the level of BMP signaling that is necessary for normal cardiac development. In fact, it has been extensively shown that the level of active canonical BMP signaling directly affects cardiac chamber identity and proportion (Chocron et al., 2007; Furtado et al., 2008; Lenhart et al., 2011; Marques and Yelon, 2009). The regulation of active BMP signaling is done primarily through the activity of BMP antagonists. Evidence suggests that these proteins are also important for cardiac developmental processes. For example, mice that lack the BMP antagonist *Noggin* exhibit a thicker myocardium that is rescued with the addition of *Bmp4* (Choi et al., 2007). Therefore, it appears that cardiac development requires tightly regulated BMP signaling activity through the action of antagonists.

BMP signaling in cardiac repair and inflammation

BMP signaling is also induced after ischemic injury in the adult mouse heart. Previous work has shown that *Bmp4* expression is induced in mice after pressure overload, angiotensin II production, or a permanent coronary artery ligation and was implicated in regulating cardiomyocyte apoptosis during ischemia/reperfusion injury through the non-canonical JNK pathway. Treatment with the endogenous antagonist Noggin, as well as chemical inhibitors dorsomorphin and DMH1 reduced mouse infarct size and cardiac hypertrophy. *BMP4*, and BMP receptors BMPR1a and BMPRII, are also expressed in human cardiac tissue during end-stage heart failure or ischemic heart disease (Derwall et al., 2012; Morrell et al., 2015; Pachori et al., 2010; Sun et al., 2013; Wu et al., 2014). *Bmp2* levels are significantly increased specifically in the myocardium and not in the serum, which was confirmed using histological analyses that showed strong induction of *Bmp2* in the peri-infarct cardiomyocytes (Chang et al., 2008). However the exact role of BMP signaling in cardiac tissue repair and how BMP signaling is regulated after cardiac injury is not well understood.

Previous studies have also linked BMP ligands to the stimulation of the pro-inflammatory phenotypes. The pro-inflammatory cytokine TNFα induces *BMP2* expression via mRNA stabilization and transcriptional up-regulation in an NFκB dependent manner. This occurs via the NFκB binding sites located within the promoter region of BMP2 (Feng et al., 2003; Fukui et al., 2006). Shear stress and pressure overload leads to the BMP driven adhesion of leukocytes to endothelial cells *in vitro* (Csiszar et al., 2005, 2006; Helbing et al., 2011; Sorescu

et al., 2003; Sucosky et al., 2009). Likewise, BMP signaling has been associated with promotion of inflammation in models of atherosclerosis and with anemia caused by chronic inflammatory conditions. For example, *Bmp2* and *Bmp4* produced by vascular smooth muscle cells in atherosclerotic lesions induce monocyte chemotaxis through BmpRII (Chen et al., 2004; Sucosky et al., 2009; Pi et al., 2012; Simões Sato et al., 2014; Steinbicker et al., 2011; Zhao et al., 2013; Mayeur et al., 2014). Conversely, BMP antagonists such as BMPER and Gremlin 1 in the context of atherosclerosis, and Noggin in the aortic valve (AV) leaflet and in diabetic mice, can inhibit inflammation by reducing the expression of pro-inflammatory cell adhesion molecules (Koga et al., 2013; Pi et al., 2012; Sucosky et al., 2009) and administration of chemical inhibitors of BMP signaling such as LDN-193189 and dorsomorphin reduced vascular inflammation and atherosclerosis (Derwall et al., 2012; Helbing et al., 2011; Morrell et al., 2015; Saeed et al., 2012).

BMP signaling

Bone Morphogenetic Proteins (BMPs) belong to a subclass of the Transforming Growth Factor β (TGF-β) superfamily of heterodimeric secreted ligands. They contain a cystine knot structure common to this family of proteins. BMP ligands bind to hydrophobic type I and type II receptors, leading to phosphorylation in the GS box of the N-terminal kinase domain and activation of the type I receptor by its type II partner. When BMP dimers bind to their heterotetrameric receptor complexes, the type I receptor binds to what is called

the wrist epitope of the BMP ligands and the type II receptors binds to the knuckle region. Type I receptors are often referred to as activin receptor-like kinase (ALK). The type I receptors fall into 2 categories based on structural similarity and have distinct binding properties conferring signal specificity. For example BMP2/4 specifically bind to type I receptors ALK3/6 (Bragdon et al., 2011; Lowery and de Caestecker, 2010; Miyazono et al., 2010; Sieber et al., 2009) (**Figure 4**).

Canonical BMP signaling occurs through SMADs

Activated type I receptors phosphorylate SMAD1/5/8 at the SXS motif at the C-terminus, leading to the formation of a complex with SMAD4 and subsequent translocation of the complex to the nucleus (Euler-Taimor and Heger, 2006). SMAD proteins contain two homology domains, mad homology or MH1 and MH2. MH1 contains the nuclear localization signal as well as the DNA binding domain, whereas MH2 interact with the Type I receptor. Smad complexes then bind DNA at AGAC where they regulate expression of target genes such as the ID family of transcriptional repressors (Hinck, 2012; Yadin et al., 2015). ID's are inhibitors of DNA binding and thereby inhibit the differentiation of certain cell lineages. They belong to the helix-loop-helix family of transcription factors, however they lack the DNA-binding domain. Instead, they associate with other members of the family and prevent their binding to DNA or

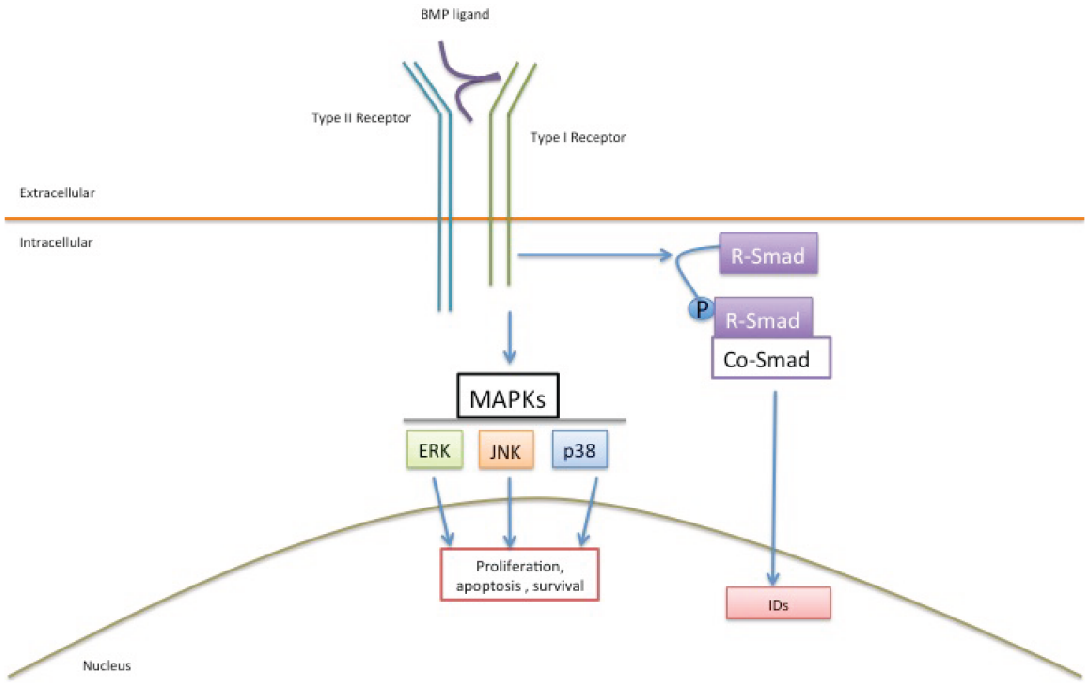

Figure 4. BMP signaling pathway. The BMP pathway is activated upon ligand binding to the heterotetrameric receptor complex. Type II receptors activate type I through phosphorylation of their GS domain, a region containing Glycine and Serine repeats. This in turn activates the receptor to then phosphorylate receptor-Smads (R-Smads). This phosphphorylation event allows the R-Smad to then form a complex with Co-Smads. This complex then translocates to the nucleus to activate target gene transcription. This arm of the pathway is known as the canonical pathway, and targets inhibitor of DNA binding proteins or IDs. During non-canonical BMP signaling, type I receptors are capable of phosphorylating mitogen activated protein kinases (MAPKs) such as extracellular signal-regulated kinase (ERK), c-Jun N-terminal kinase (JNK), and p38.

from forming active heterodimers. They most commonly interact with enhancer or E-box proteins that bind to the enhancer region located upstream transcription start sites (ID family of HLH proteins) (Miyazono et al., 2005). In addition to canonical signaling, there is also a branch of non-canonical signaling, where MAPKs such as JNK and ERK are activated in lieu of SMADs (Sieber et al., 2009).

BMP antagonists

BMP signaling is modulated in the extracellular space by a large number of secreted, structurally diverse antagonists, such as Chordin, Noggin and members of the DAN family (Yanagita, 2005). These antagonists also contain the cystine knot structure common in the ligands themselves and predominantly act by binding to the BMP ligands and thereby prevent ligand binding to their receptors. Namely, the large protein members such as Noggin and BMPER bind to both the type I and type II receptors binding domains present on the BMP ligands. However, a unique form of antagonism exists in the Chordin, Tolloid, and Twisted gastrulation (Tsg) system. Intact Chordin forms a complex with Tsg and BMP to inhibit BMP. Tolloid cleaves Chordin and twisted gastrulation's presence ensures this cleavage, freeing BMPs to interact with their receptors (Groppe et al., 2002; Umulis et al., 2009; Walsh et al., 2010; Zhang et al., 2008).

Besides extracellular antagonist interactions, other modes or models of antagonism are thought to occur. The exchange model occurs when low concentrations of the antagonist actually provides BMP ligands to the receptors and prevent any non-specific binding, whereas high concentrations sequester ligands. The sink-source model, where BMP activity is decreased in a spatial as well as concentration dependent manner, is thought to contribute to the generation of signaling gradients (Ramel and Hill, 2012). Extracellular regulation also occurs through heparin sulfate proteoglycans interactions that are capable of binding to BMPs and thereby limit their interaction with their receptors (Walsh et al., 2010). These mechanisms are in place in order to generate the level or

gradient of BMP morphogen signaling that is required for its pleiotropic effects on several developmental and physiological processes.

Gremlin 2

Gremlin 2 (Grem2), also called Protein Related to Dan and Cerberus (PRDC), belongs to the DAN family of BMP antagonists together with its close paralog Gremlin 1 (54% identity), Dan, Dante (or Coco), Cerberus-like 1, Uterine sensitization-associated gene-1 (USAG-1), and Sclerostin. The Dan family consists of single domain proteins that have a conserved 8-membered cystine ring contained within the highly conserved “Dan” domain (Avsian-Kretchmer and Hsueh, 2004; Nolan and Thompson, 2014; Pearce et al., 1999). It is this Dan domain, a hydrophobic region at the dimer interface that binds to BMP ligands. In the case of Grem2, this cystine ring consists of an odd number of cysteines, leaving one un-paired. Grem2 uniquely consists of 2 independent head to tail protein dimers, which differs from Noggin head to head dimerization (**Figure 5**). These dimers are in fact highly stable and resistant to di-sulfide bond reduction due to the fact that hydrogen bonding and van der Waal forces are what are responsible for keeping the tertiary structure of the protein together due to the un-paired cysteine. The N-terminus of Grem2 includes two N-linked glycosylation consensus sequences, as well as a flexible latch that allows for the required large hydrophobic interactions between antagonist-ligand. It also works to hide the BMP binding epitope to prevent any non-specific binding. Purified Grem2, prepared in the collaborating laboratory of Dr. Tom Thompson, was used to

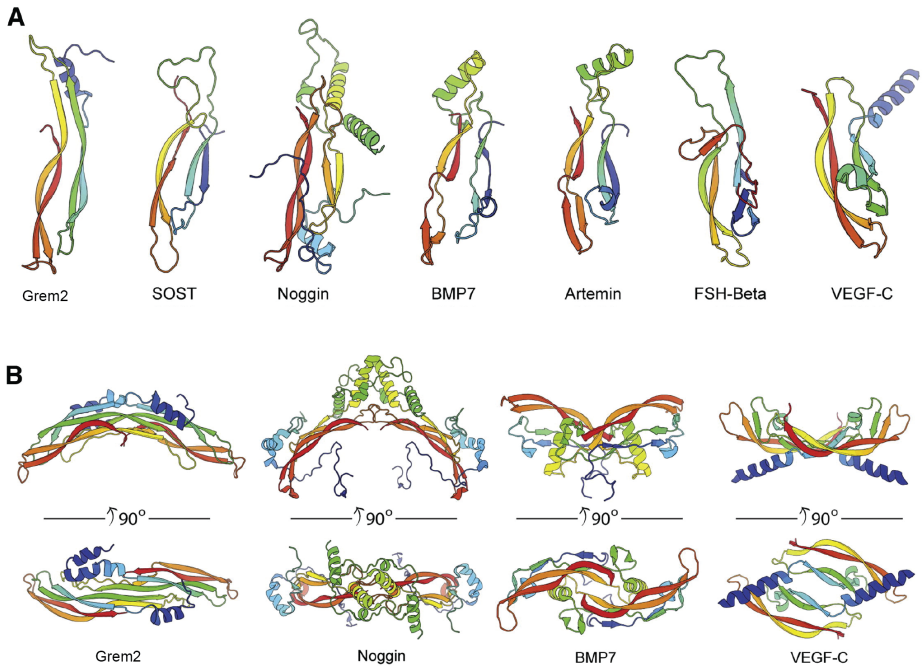

Figure 5. The tertiary structure of Grem2 is unique among other members of the protein family. **(A)** Ribbon diagrams of the central cystine-knot domain present in this family of proteins, demonstrating the differences in the number and orientation of beta-strands and alpha-helices. **(B)** Representations of the indicated proteins as dimers, showing the unique head-to-tail conformation of Grem2, differing from the head-to-head confirmation of other BMP antagonists such as Noggin. Image source: Nolan et al *Structure* 2014.

asses its binding affinity to BMP ligands and was calculated to have an IC50 of less than 1nM, (**Figure 6**) (Kattamuri et al., 2012a, 2012b; Nolan et al., 2013).

Grem2 was first discovered 15 years ago (Pearce et al., 1999), but its biological function and mechanism of BMP inhibition have remained largely obscure. Grem2 expression has been detected in the developing spinal cord and lung mesenchyme (Lu et al., 2001; Minabe-Saegusa et al., 1998), and Grem2 has been implicated in follicle, neuronal, bone and craniofacial development (Ideno et al., 2009; Kriebitz et al., 2009; Sudo et al., 2004; Zuniga et al., 2011). Grem2 *in vivo* has been shown to inhibit canonical BMP signaling and *in vitro*

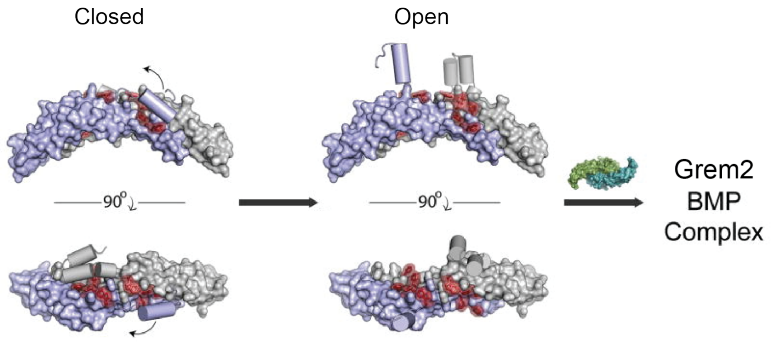

Figure 6. Structural representation of BMP binding site on Grem2. The tertiary structure of Grem2 demonstrates that the BMP binding site located within the DAN domain of the protein, contains a flexible finger-like N-terminal region that opens. This generates a large hydrophobic interface to become available in the presence of BMP ligands, thereby conferring binding specificity. BMP binding regions are shown in red. Image source: Nolan et al *Structure* 2014.

inhibits Bmp2 and Bmp4, but not Tgfβ or Activin (Sudo et al., 2004). Several DAN-family members such as Dante and Grem1 have been linked to a number of pathophysiological states. Dante has been shown to promote cancer metastasis, and Gremlin 1 has been shown to be induced in endothelial cells during pulmonary arterial hypertension, in fibroblasts during idiopathic pulmonary fibrosis, and actually promotes Tgfβ directed epithelial to mesenchymal transition. Grem1 is induced during chronic kidney disease such as diabetic nephropathy and is known to promote the cancer stem phenotype (Cahill et al., 2012; Gao et al., 2012; Koli et al., 2006; Lappin et al., 2002; Owens et al., 2015). Although other members of the DAN family have been implicated in various pathological conditions, little is known about the role of Grem2 in disease.

Grem2 in cardiac development and differentiation

The Hatzopoulos laboratory recently established that during embryonic development in zebrafish, grem2 first appears in the ventral portion and

pharyngeal arch mesoderm next to the forming heart tube (**Figure 7**) (Müller et al., 2006; Muller et al., 2013). Loss- and gain-of-function approaches demonstrated that Grem2 is necessary for proper cardiac tube jogging and looping, cardiac laterality, to promote normal cardiac rhythm and cardiomyocyte differentiation by suppression of Smad1/5/8 phosphorylation (**Figure 8**) (Muller et al., 2013).

Moreover, *Grem2* is expressed in the cardiac field in E8 mouse embryos and promotes differentiation of pluripotent mouse embryonic stem (ES) cells to atrial-like cardiomyoctyes through activating atrial transcription factors and suppressing ventricular (**Figure 9**). Grem2 expression begins during the differentiation stages of mesodermal and endodermal progenitor cells and that Grem2 treatment on CGR8 ES cells lead to an increase in p-JNK that was not seen with the treatment of other antagonists such as Noggin. The increase in cardiomyoctyes via Grem2 was diminished when cells were treated with the JNK pathway inhibitor SP60 but not the BMP pathway inhibitor dorsomorphin.
Therefore, Grem2-induced cardiomyocyte differentiation occurs via activation of the non-canonical BMP pathway JNK (Tanwar et al., 2014).

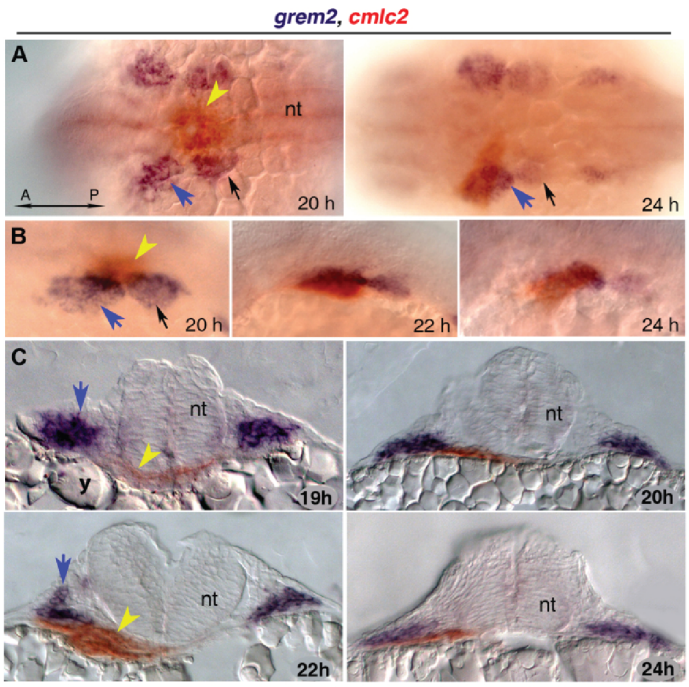

Figure 7. *Grem2* is expressed adjacent to the cardiac forming regions in zebrafish. **(A, B)** Whole mount in situ hybridization demonstrates that *grem2* (purple) is expressed symmetrically around the cardiac tube shown here via staining of the *cardiac myosin light chain 2* (*cmlc2*, red). **(C)** Cross-sectional views of zebrafish embryos also demonstrate the nascent localization of *grem2* to developing heart regions. Abbreviations: h: hours post fertilization; A: anterior; P: posterior; nt: neural tube; y: yolk. Image source: Muller et al *Disease Models and Mechanisms* 2013.

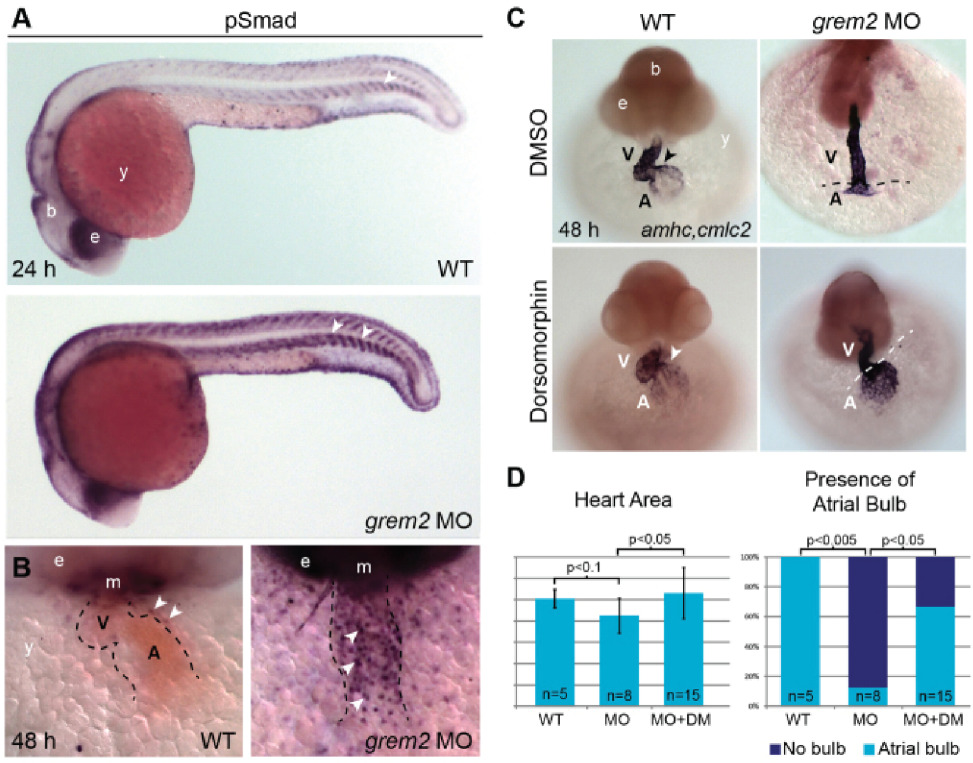

Figure 8. *Grem2* regulates canonical BMP signaling *in vivo* and is necessary for normal cardiac morphogenesis in zebrafish. (A, B) Whole mount antibody staining reveals that knock-down of *grem2* expression via morpholino injection results in an increase of pSmad staining in both the somites and in the developing cardiac tube. **(C)** In situ hybridization using probes for *atrial myosin heavy chain (amhc)* and *cardiac myosin light chain (cmlc2)* demonstrates that *grem2* morphant embryos (MO) also exhibited defects in cardiac jogging and looping processes. This was rescued by the injection of the chemical BMP antagonist dorsomorphin. This is quantified in **(D)** as a measure of total heart area. Of note, the affects of *grem2* knock-down (MO) was more pronounced in the atria as demonstrated by the presence of an atrial bulb, which was also rescued by dorsomorphin injection (MO+DM). Abbreviations: b: brain; e: eye; m: mouth; y: yolk; v: ventricle a: atria; h: hours post-fertilization. Image source: Muller et al *Disease Models and Mechanisms* 2013.

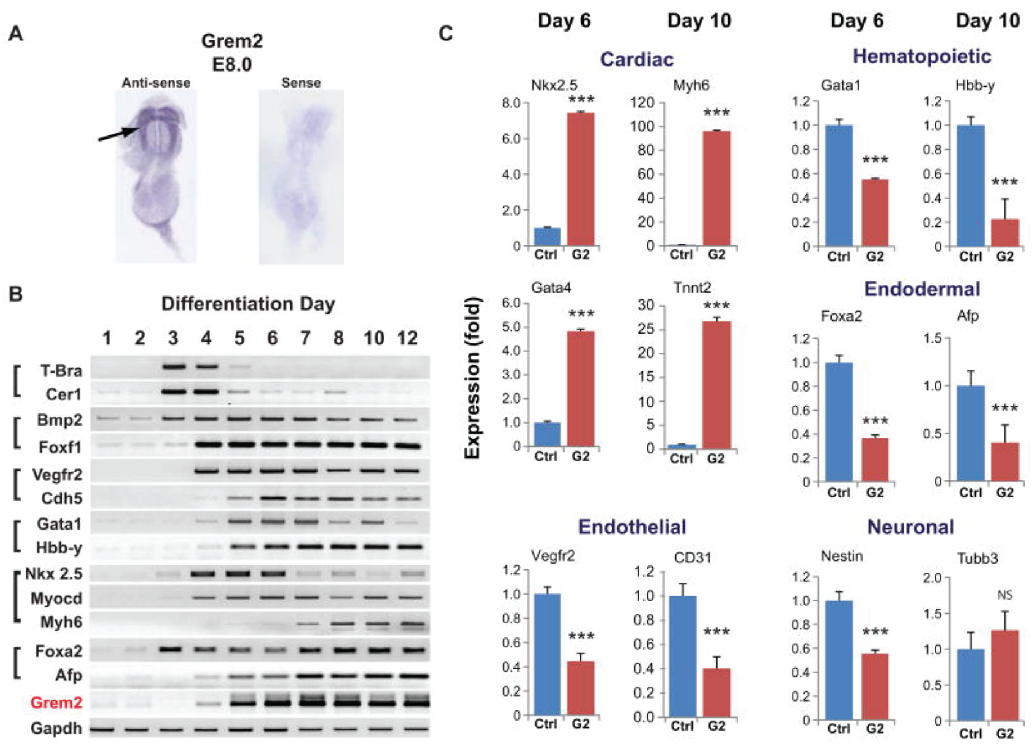

Figure 9. Grem2 is expressed during mouse cardiac development and promotes cardiac differentiation from embryonic stem (ES) cells. (A) In situ hybridization demonstrates that *Grem2* is expressed within the cardiac field during mouse embryonic day 8 (E8). **(B)** RT-qPCR analysis at the indicated differentiation days of CGR8 ES cells places *Grem2* gene induction after the induction of mesodermal genes (*Bmp2, Foxf1*) and the beginning of the cardiac gene program (*Nkx2.5, Myocd, Myh6*). Abbreviations: *Afp: α Fetoprotein; Bmp2: Bone morphogenetic protein 2; Cer1, Cerberus-like 1; Cdh5: Vascular endothelial cadherin; Chrd: Chordin; Foxa2: Forkhead box A2; Foxf1: Forkhead box F1; Gapdh: Glyceraldehyde-3-phosphate dehydrogenase; Gata1: GATA binding protein 1; Grem1: Gremlin 1; Grem2: Gremlin 2; Hbb-Y; Hemoglobin Y, beta-like embryonic chain; Myocd: Myocardin; Myh6: Myosin Heavy chain 6, or α Myosin heavy chain; Nkx2.5: NK2 Homeobox 5; Nog: Noggin; Nbl1: Neuroblastoma suppressor of tumorigenicity 1 precursor (Dan); T-bra: T-brachyury; Vegfr2: Vascular endothelial growth factor receptor 2 (Flk-1).* **(C)** RT-qPCR analysis from CGR8 ES cells at differentiation days 6 and 10 demonstrates that Grem2 treatment (G2) results in a significant increase in cardiac genes (*Nkx2.5, Myh6, Gata 4, Tnnt2*) and a significant down-regulation in genes of other lineages, such as hematopoietic, endodermal, endothelial, and neuronal compared to control (Ctrl). Abbreviations: *CD31: Cluster of differentiation 31, or Platelet Endothelial Cell Adhesion Molecule-1; Gata4: GATA binding protein 4; Tnnt2: Troponin T type 2; Tubb3: tubulin, beta 3 class III*. Image source: Tanwar et al *Stem Cells* 2014.

Summary and hypothesis

The cardiac tissue repair process following an acute injury such as a myocardial infarction is highly regulated in both a temporal and spatial dependent manner. The inflammatory phase of tissue repair is a highly dynamic process and has been directly implicated with patient outcome and survival. Previous clinical studies targeting direct players of the inflammatory process has produced mixed results. Taking clues from cardiac developmental processes that often get

re-activated during an injury response, focus has been brought to the BMP signaling pathway. BMP signaling is necessary for normal cardiac morphogenesis to occur and is re-activated post-MI. The level of BMP signaling is important for its downstream effects, and BMP antagonists are responsible for regulating the canonical BMP pathway. We recently determined that a relatively unstudied antagonist, Grem2, is important for cardiac development, and therefore sought to determine if it also plays a role during the cardiac tissue repair process.

According to current work conducted by the Hatzopoulos laboratory, Grem2 is not essential for mouse embryonic development. However, in the adult heart, Grem2 is highly induced in peri-infarct cardiomyocytes at the end of the inflammatory phase after MI. Based on the role of BMP signaling during inflammation, we hypothesized that Grem2 regulates the inflammatory response and keep inflammation in check through suppression of canonical BMP signaling. We therefore investigated the role of Grem2 in the cardiac tissue repair process and in functional recovery.

CHAPTER II

BMP SIGNALING AND GREM2 ARE INDUCED IN THE HEART AFTER A MYOCARDIAL INFARCTION

Introduction

The cardiac repair process following an acute injury such as a myocardial infarction consists of well-documented stages that are highly spatiotemporally regulated. However, the molecular pathways that regulate these processes are not entirely understood. The Hatzopoulos laboratory has recently demonstrated that developmental pathways necessary for cardiac morphogenesis are re-activated after injury and in fact play important roles in the recovery process (Aisagbonhi et al., 2011; Paik et al., 2015), and that a BMP antagonist, Grem2 is important for cardiac development and differentiation (Muller et al., 2013; Tanwar et al., 2014). BMP signaling is a pathway that has been extensively studied in the context of cardiac development and has been shown to be induced after ischemic injury in the adult mouse heart (Pachori et al., 2010; Wu et al., 2014). Histological analyses placed BMP signaling induction in peri-infarct cardiomyocytes (Chang et al., 2008). However the exact role of BMP signaling and whether it is regulated after cardiac injury has not been extensively studied.

To place BMP signaling components within the context of the MI repair process, we analyzed whole mouse heart RNA samples prepared at distinct time points after left anterior descending (LAD) artery ligation, namely at day 0 (baseline, prior to injury), 1, 2, 3, 5, 7 and 21 after MI. We also conducted

histological analysis in order to determine the localization of canonical BMP signaling components, namely the cell types producing both pathway components as well as important pathway regulators.

Materials and methods

Experimental MI

Mice underwent open chest surgery, a 10-0 nylon suture was placed through the myocardium into the anterolateral left ventricular wall around the left anterior descending (LAD) artery and the vessel was permanently ligated (Aisagbonhi et al., 2011). Male mice at 12-16 weeks of age fed with a normal chow diet were euthanized at defined time points following surgery to obtain cardiac tissue for molecular and histological analyses.

RNA analysis by Reverse Transcription and quantitative Polymerase Chain Reaction (RT-qPCR)

Whole hearts were dissected at the indicated time points after MI, perfused to remove blood cells and RNA was obtained using TriZol Reagent according to the manufacturer's instruction (Life Technologies). Reverse transcription was conducted by incubating 100 ng of oligo$(dt)_{15}$ (Promega) with 3 µg RNA for 5 min at 70°C. 20 mM of dNTPs (GE Healthcare), 200 U/µl of Mo-MLV reverse transcriptase with 5x associated buffer (Promega), 40 U/µl RNasin (Promega) and water were added to the RNA solution and incubated at 40°C for 1 hour, followed by a 5 minute incubation at 95°C in order to inactivate enzyme

activity. 1:100 of the final cDNA solution or ~20 ng served as template for quantitative Real Time PCR with GoTaq qPCR Master Mix (Promega) using a C1000 Thermal Cycler (BioRad) as previously described (Aisagbonhi et al., 2011). 0.5 µM of *Gapdh* primers were included as an internal control and relative gene induction levels were determined using the $2^{(-DDCt)}$ formula (Beck et al., 2008; Livak and Schmittgen, 2001). Experiments were done in triplicates. The sequences of gene-specific primers have been included in **Table 1**.

Immunofluorescence and immunohistochemistry analyses

For IF on cardiac tissue sections, freshly isolated hearts were perfused with 1X Phosphate Buffered Saline (PBS), bisected transversely, embedded in Optimal Cutting Temperature (OCT) compound, frozen on dry ice, cut into 10 µm thick sections and stored at -70^{o}C until use. Before antibody staining, slides were thawed at room temperature, immersed in cold 1:1 acetone: methanol and fixed for 5 minutes on ice. Slides with cardiac tissue sections were washed three times in 1X PBS for 5 minutes each wash, and incubated with blocking buffer containing 1% bovine serum albumin (BSA) and 0.05% saponin in 1X PBS for 1 hour at room temperature. Next, sections were stained with primary antibodies overnight at 4°C in blocking buffer. Afterwards, slides were washed five times in 1X PBS for 5 minutes each, incubated with secondary antibodies and DAPI for 1 hour at room temperature in blocking buffer, washed in 1X PBS three times for 5 minutes each, and mounted with VECTASHIELD fluorescent mounting medium

(Vector Laboratories). The Vanderbilt Histology Core provided histological services, including tissue sectioning.

Primary antibodies used for IF analysis were as follows: rat monoclonal anti-mouse CD31/PECAM1 (BD Pharmingen; 1:100, Cat. No. 553370), rabbit monoclonal anti-mouse p-Smad1/5/8 (Cell Signaling; 1:50, Cat. No. 9511), mouse monoclonal anti-mouse MF20 (Developmental Studies Hybridoma Bank; 1:5, Cat. No. MF 20, RRID:AB_2147781), rabbit polyclonal anti-human Grem2 (GeneTex; 1:100, Cat. No. GTX108414), rabbit monoclonal Id2 (Biocheck Can. No. BCH-3/#9-2-8), and mouse monoclonal α-Actinin (Sigma; 1:800, Cat. No. A7811). Secondary antibodies used for IF were: goat anti-mouse Cy3-conjugated (Cat. No. 115-165-146), goat anti-rat Cy3 (Jackson ImmunoResearch, Cat. No. 712-165-150), and goat anti-rabbit Alexa-Fluor-488-conjugated (Life Technologies, Cat. No. A21206). Cy3 antibodies were used at a 1:200 dilution and Alexa-Fluor-488 was used at a 1:400 dilution. Cardiac tissue sections were stained with the fluorescent dye 4',6-diamidino-2-phenylindole (DAPI, 1:5000 dilution; Invitrogen) to mark cellular nuclei. Images were taken on the Olympus FV-1000 inverted confocal microscope and processed using the FV10-ASW 1.6 Viewer software (Olympus).

p-Smad1/5/8^{+} cardiomyocytes were quantified using ImageJ 1.46r (NIH) color thresholding, as a percentage of cells double positive for MF20 and p-Smad1/5/8 amongst all DAPI positive cells in the viewing field; at least 4 viewing fields were used for calculations.

The human heart tissue samples were obtained from Vanderbilt Cardiology Main Heart Registry/Biorepository. The study was approved by Vanderbilt Institutional Review Board and written informed consent was obtained from all heart tissue donors or organ donor families. Explanted heart from patients with ischemic cardiomyopathy or organ donors whose heart were unmatched for transplantation was collected into the Biorepository. At the time of explantation, a section of left ventricular (LV) free wall tissue was immediately frozen in liquid nitrogen, and a small piece of LV tissue from the same section was embedded in OCT media and stored at -80oC until used for immunofluorescence analysis.

Statistical Analysis

Statistical analysis was performed using GraphPad Prism software. Data are represented as the mean ± SEM. Student's two-tailed unpaired *t*-test was used for comparison between two groups, *one-way ANOVA* was used to compare multiple groups, and *two-way ANOVA* was used to compare gene induction in each mouse model over time. Dunnett's and Bonferroni's multiple comparisons test was used post-hoc. **P<0.05*, ***P<0.01*, ****P< 0.001, ****P<0.0001* were considered significant.

Results

Dynamic induction patterns exist for members of the inflammatory and fibrotic pathways

Using qPCR, with typical inflammatory gene markers, such as *Il-1β* and *E-selectin*, and markers of granulation tissue formation and fibrosis, such as *Tgfβ1* and *alpha Smooth Muscle Actin* (*αSma*), we determined that pro-inflammatory genes are induced early and peak at days 1-2 after MI, whereas fibrosis genes are induced at day 5, as expected (Frangogiannis, 2014; Paik et al., 2015; Virag and Murry, 2003). Gene induction of inflammatory genes returned to baseline levels between days 3 to 5, whereas *Tgfβ1* expression returned to baseline at day 21. *αSma* levels declined, but were still detectable at day 21, reflecting the presence of myofibroblasts during the scar maturation phase (**Figure 10A**).

Dynamic changes in the expression of BMP pathway components and their antagonists occur after a myocardial infarction

Investigation of BMP ligands after MI showed that *Bmp2* is the earliest induced ligand of the BMP family at day 1 with its expression peaking at day 3, a pattern that corresponds to the inflammatory stage of cardiac repair. Previous work documented Bmp2 protein induction occurs primarily in peri-infarct area cardiomyocytes and not in recruited immune cells (Chang et al., 2008). *Bmp2* is subsequently downregulated to pre-injury levels by day 7 after MI. *Bmp2* suppression coincides with up-regulation of *Bmp4*, *Bmp6*, and *Bmp10*, the expression of which starts around day 5 and persists during fibrosis and scar

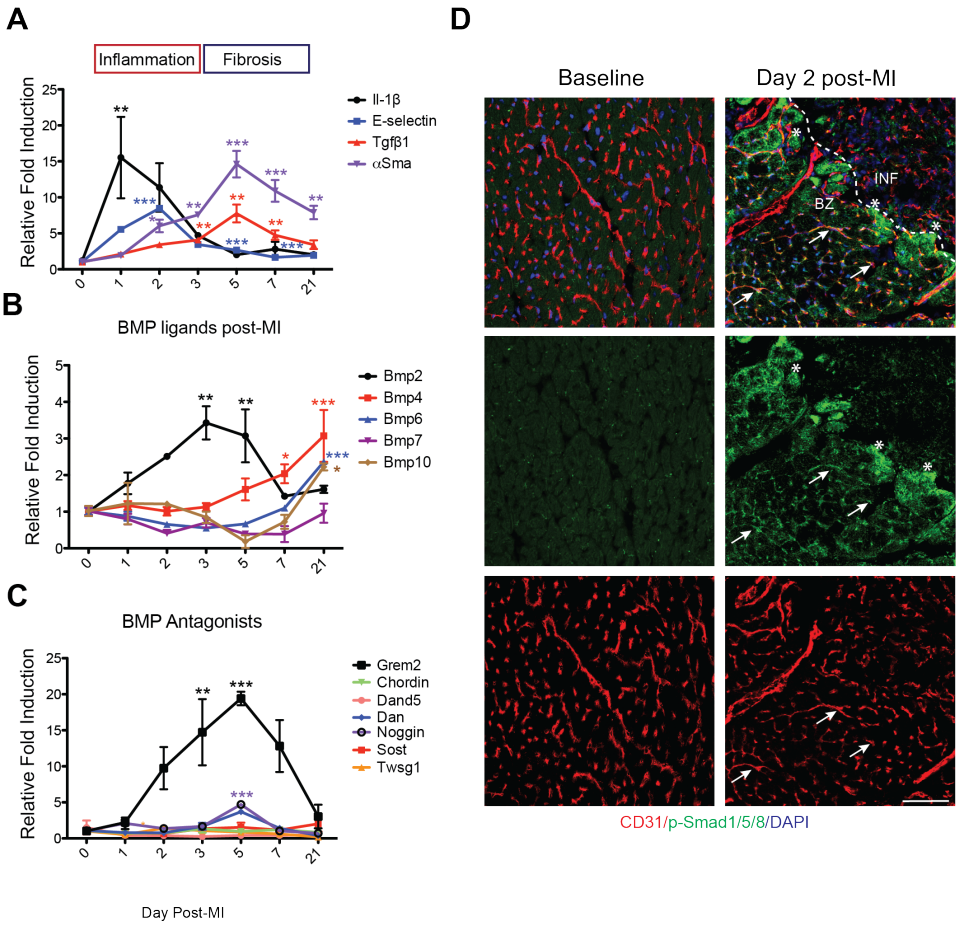

Figure 10. Dynamic changes in the expression of BMP signaling components and BMP antagonists after myocardial infarction. (A-C) Whole mouse heart RNA samples were isolated at day 0 (baseline, prior to injury), 1, 2, 3, 5, 7 and 21 post-MIand analyzed by qPCR. Values at baseline were set as 1. **(A)** Sequential induction of inflammation (*Il-1β* and *E- selectin*) and fibrosis (*Tgfβ1* and *αSma*) associated genes after MI. **(B)** Expression analysis of BMP ligands shows that *Bmp2* is transiently induced during the inflammatory phase of the post-MI repair process, followed by induction of *Bmp4*, *Bmp6*, and *Bmp10*. **(C)** Expression analysis of BMP antagonists shows *Grem2* is the main antagonist induced after MI, starting at the late inflammatory stage and peaking at day 5. ** P < 0.05*; *** P < 0.01*; **** P< 0.001* compared to day 0. One-way ANOVA with Dunnett's multiple comparisons test. N=3 for all time points. All data are means ± SEM. **(D)** Immunofluorescence (IF) analysis with antibodies recognizing p-Smad1/5/8 (green) and CD31 (red) shows that Smad1/5/8 is not present in normal cardiac tissue at baseline prior to MI, but is activated in peri-infarct area endothelial cells at day 2 post-MI (representative examples marked with arrows) and in cardiomyocytes (asterisks). DAPI (blue) marks cellular nuclei. Scale bar, 50 μm. Abbreviations: BZ=border zone; INF=infarct; *Il-1β: Interleukin 1β; Tgfβ1: Transforming growth factor β1; αSma: alpha Smooth muscle actin; Grem2: Gremlin 2; Dand5: DAN domain family member 5 (also Dante, or Coco); Dan: Neuroblastoma 1 (Nbl1); Sost: Sclerostin; Twsg1: Twisted gastrulation BMP signaling modulator 1*.

formation (**Figure 10B**). Consistent with the induction of distinct BMP ligands during different stages after MI, there was an overlapping expression of the only BMP signaling target gene that showed a significant induction post-MI throughout

the repair process, *Id2* (**Figure 11A**). BMP receptor induction illustrated that BmpR2 was the only receptor with a significant induction (**Figure 11C).** In contrast, analysis of BMP signaling antagonists showed minimal changes in their expression levels after MI with the notable exception of *Grem2* that is induced at day 2, peaks at day 5 after MI and returns to pre-injury levels at day 21 (**Figure 10C,** with absolute expression values after GAPDH normalization in **Figure11B**). The *Grem2* induction pattern follows the pattern of *Bmp2* with one-day delay. We did not detect a signal for its close paralog *Grem1* at baseline, or at the tested time points after MI (**Figure 11B**). Although Grem2 is the most prominently induced BMP antagonist after MI, absolute expression values indicate that during homeostasis the heart maintains expression of *Dan*, *Sost*, *Twsg1* and *Chordin* which, however are at least 40 (Chordin) to 400 (Dan, Twsg1) times less potent BMP inhibitors than Grem2, or do not bind directly to BMP ligands (Sost) (**Figure 11B**; Nolan et al., 2015; Zhang et al., 2008).

Consistent with the *Bmp2* induction pattern after MI, immunofluorescence (IF) analysis at day 2 post-MI, using antibodies recognizing the phosphorylated, i.e., activated form of Smad1/5/8, demonstrated activation of canonical BMP signaling in endothelial cells in the peri-infarct area and cardiomyocytes at the border zone of the infarcted tissue. In contrast, we did not detect active Smad1/5/8 within ventricular tissue prior to injury (**Figure 10D**).

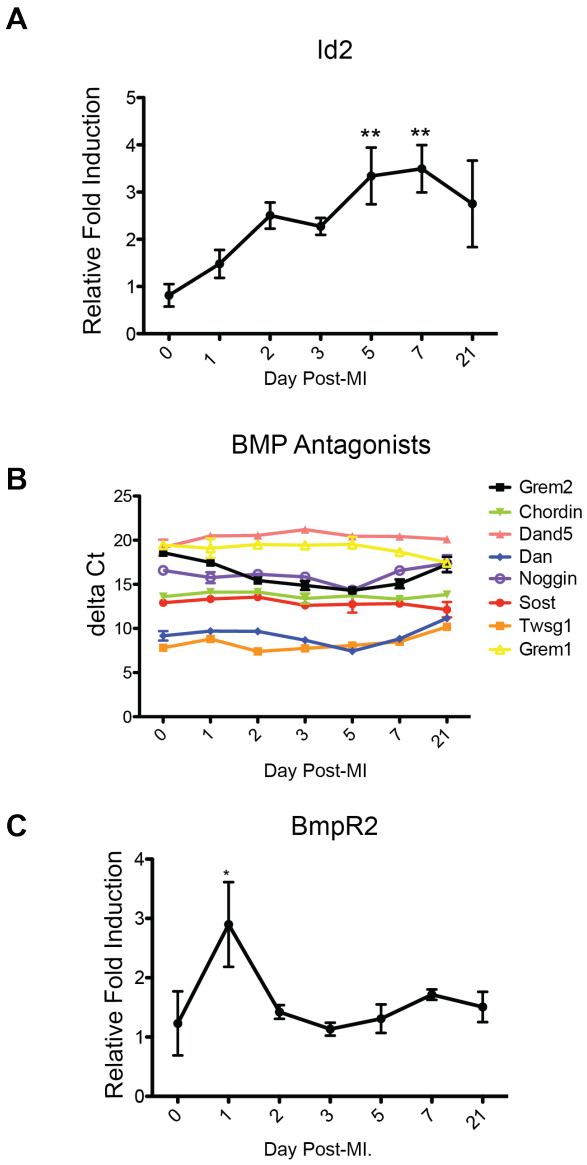

Figure 11. Induction of canonical BMP signaling target gene *Id2* and *BmpR2,* as well as relative expression of BMP antagonists after MI. (A) qPCR analysis of whole heart RNA samples isolated from *WT* mice at days 0, 1, 2, 3, 5, 7 and 21 post-MI shows *Id2* gene induction throughout the cardiac tissue repair process. *** P < 0.01* compared to day 0. One-way ANOVA with Dunnett's multiple comparisons test. N=3 for all time points. All data are means ± SEM. *Id2: Inhibitor of DNA binding 2.* **(B)** Absolute expression of BMP antagonist genes following normalization to *Gapdh*. delta Ct= Ct_{gene}- Ct_{Gapdh}. All data points (N=3) are means ± SEM. **(C)** qPCR analysis demonstrates that the BMP receptor BmpR2 is induced early, at day 1 post-MI. * *P < 0.05* compared to day 0. One-way ANOVA with Dunnett's multiple comparisons test. N=3 for all time points. All data are means ± SEM.

BMP pathway components are expressed in the border zone and infarct areas post-MI

Immunofluorescence analysis indicated that BMP pathway components are expressed at higher levels in the border zone and infarct area compared to distal or uninjured tissue areas. IF staining with antibodies recognizing the phosphorylated, i.e., active form of Smad1/5/8, showed that canonical BMP signaling is active in peri-infarct cardiomyocytes of *WT* mice in agreement with previous reports showing that BMP ligands are expressed in this region and not present in cardiomyoctyes distal to the infarct (Chang et al., 2008). (**Figure 12A** and **B**). *Id2* expression is mainly localized within the infarct, likely in inflammatory cells (**Figure 12C**).

Antibody staining revealed that the robust induction of Grem2 protein expression after MI takes place primarily in peri-infarct cardiomyocytes with no Grem2 detected in distal areas away from the infarct (**Figure 12D**). In the case of human patients, very little Grem2 is expressed within the heart tissue of healthy patients, however Grem2 is expressed within the cardiomyocytes of ischemic cardiomyopathy patients (**Figure 12E**).

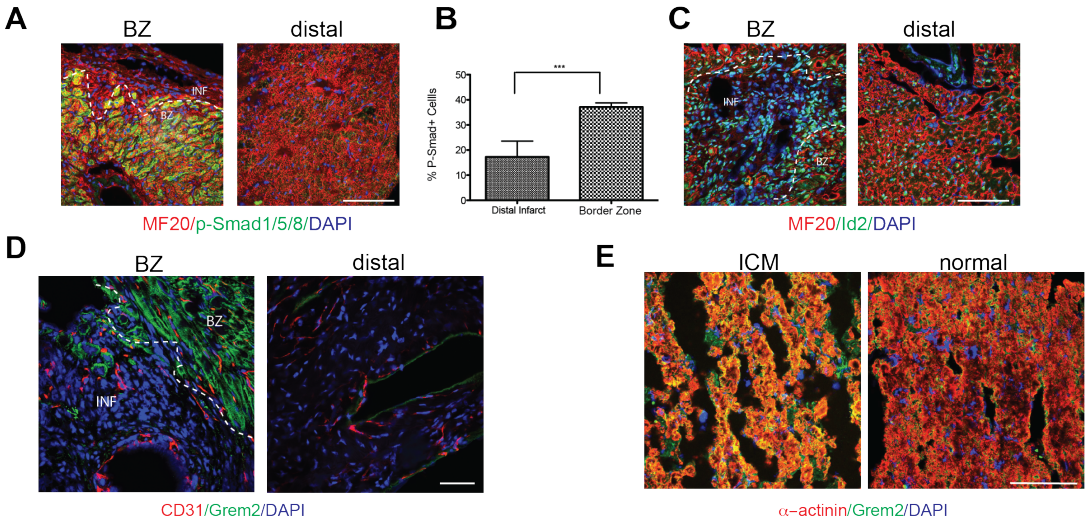

Figure 12. BMP signaling components are expressed in the peri-infarct and infarct areas. (A, C) IF analysis of cardiac tissue sections 7 days post-MI using antibodies recognizing p-Smad1/5/8 or Id2 (green) and Myosin Heavy Chain (MF20, red) shows activation of canonical BMP signaling in the peri-infarct border zone and within the infarct respectively and not in areas distal to the infarct. DAPI marks cellular nuclei. Scale bars, 100 μm. BZ=infarct border zone; INF=infarct. **(B)** Quantification of p-Smad1/5/8$^+$ cells as a percentage of total MF20$^+$ cells per viewing area. *** $P < 0.001$. Student's two-tailed unpaired *t*-test. N=3. All data are means ± SEM. **(D)** IF analysis with antibodies recognizing Grem2 (green) and CD31 (red) shows that Grem2 protein is induced in the peri-infarct area and not in regions distal to the infarct. Grem2 expression appears primarily in cardiomyocytes, but not CD31$^+$ endothelial cells. DAPI marks cellular nuclei. Scale bars, 100 μm. BZ=border zone, INF=infarct. **(E)** IF analysis of cardiac tissue sections taken from human patients illustrates that Grem2 (green) is expressed in the cardiomyocytes (α–actinin, red) of ischemic cardiomyopathy patients (ICM) and not in the cardiomyocytes from a normal patient (normal). DAPI marks cellular nuclei. Scale bars, 100 μm.

Discussion

In conclusion, our data indicate a bi-phasic pattern of BMP ligand induction after MI, i.e., early upregulation of *Bmp2* expression during the inflammatory stage, followed by a second phase during granulation tissue and scar formation that is dominated by several ligands, including *Bmp4*, *Bmp6*, and *Bmp10*. Conversely, *Grem2* is the prominent BMP antagonist induced after MI with its expression starting at day 2, peaking during the transition from inflammation to granulation tissue formation, and returning to baseline levels during scar formation. BMP pathway components are being induced in the infarct or border zone areas, with Grem2 being produced by cardiomyocytes in

both the mouse model of acute MI as well as human ischemic cardiomyopathy patients.

The cellular response following a myocardial infarction has been well described, but the molecular pathways responsible for regulating each phase of the response is not entirely understood (Boudoulas and Hatzopoulos, 2009). Our data indicate that BMP signaling is involved in the cardiac repair process after MI, as has been previously reported (Chang et al., 2008; Pachori et al., 2010; Wu et al., 2014). However, to our knowledge, ours is the first study to show that canonical BMP signaling activation after MI coincides with the induction of inflammatory process genes. We are also the first group to investigate the roles of endogenous antagonists in the cardiac repair process. Specifically, we show that the BMP antagonist Grem2 is robustly and transiently induced after myocardial infarction during the late inflammatory phase and early proliferative phase of granulation tissue formation. Grem2 protein is synthesized primarily in peri-infarct cardiomyocytes, a domain that overlaps both with the expression of Bmp2 after MI and the area of p-Smad1/5/8, i.e., canonical BMP signaling activation. Some p-Smad1/5/8 persists in cardiomyocytes, even with Grem2 induction, which may be due to the presence of ligands such as GDFs or Activins that can induce Smad1/5/8 phosphorylation, but are not inhibited by Grem2 (Sudo et al., 2004). Persistent activity suggests that additional canonical BMP signaling inhibition may be required after MI to supplement Grem2. Previous reports have linked activation of BMP signaling to cardiomyocyte apoptosis (Pachori et al., 2010) during the early stages of ischemia/reperfusion injury, as

well as fibrosis and hypertrophy (Sun et al., 2013), so Grem2 may also have direct cardioprotective properties.

However, the question remains if the timing of BMP pathway induction directly correlates with the regulation of the inflammatory process following a myocardial infarction. In order to test if this is a case, mouse models that are engineered to have changes in the expression of BMP pathway components could be challenged with an MI. Since Bmp2 is the ligand induced during the inflammatory phase, a conditional cardiac cell specific knockout mouse could be used to test if its presence is necessary for the inflammatory phase to occur, or if lack of Bmp2 alters the inflammatory response in any way. This would lead to determining whether BMP signaling regulates the inflammatory response, but would not lead to directly determining a therapeutic target. Since our data also demonstrate that the relatively unstudied protein, Grem2 is the only endogenous antagonist induced at the end of the inflammatory response, it would therefore be valuable to investigate if Grem2 is necessary to regulate the inflammatory response post-MI. These investigations are the topics of the following chapters.

Acknowledgements

I thank members of the Cardiovascular Pathophysiology and Complications Core of the Mouse Metabolic Phenotyping Center, the Cell Imaging Shared Resource, the Translational Pathology Shared Resource, the Transgenic Mouse/ES Cell Resource, and the Molecular Cell Biology Resource at Vanderbilt University Medical Center for technical assistance. This work also

utilized the core(s) of the Vanderbilt Diabetes Research and Training Center funded by grant 020593 from the National Institute of Diabetes and Digestive and Kidney Disease. I thank Lianli Ma and Lin Zhong for performing mice surgeries; Mark Magnuson and Jennifer Skelton for generation of the Grem2 mouse lines; Daniel Levic and Ela W. Knapik for help with histological analyses; and David T. Paik for assistance in providing mouse heart samples for histological analysis.

CHAPTER III

LOSS OF GREM2 LEADS TO AN INCREASE IN THE MAGNITUDE OF INFLAMAMTION, THEREBY WORSENING CARDIAC FUNCTION POST-MI

Introduction

The inflammatory phase following a myocardial infarction is a highly dynamic process that exerts pleiotropic effects on the subsequent stages of the cardiac repair process. The purpose of inflammation in this context is to clear the cellular debris present after the loss of blood flow that leads to massive cell death. However the inflammatory response that gets activated after acute injury may be more severe (i.e. prolonged) than is necessary. As a result, excessive inflammation leads to an increase in cell death and in the fibrotic response; all together leading to the injury into what was previously healthy tissue (Frangogiannis, 2014).

Excessive inflammation has been linked to worse outcomes after a myocardial infarction in both animal models and in human patients. Therefore several clinical trials have been attempted in order to limit this inflammatory response. However so far these trials have been largely unsuccessful since they have directly targeted components of the inflammatory response, a process that is necessary for cardiac repair to occur (Christia and Frangogiannis, 2013).

BMP signaling has been implicated in promoting inflammation as well as induced by pro-inflammatory mediators in other disease states such as

atherosclerosis and anemia (referenced in CHAPTER I). Our data also indicate that BMP signaling is activated during the inflammatory phase of cardiac recovery post-MI and is followed by the induction of the pathway antagonist Grem2. Therefore we hypothesized that pro-inflammatory mediators increase the inflammatory response in both magnitude and duration by activating the BMP pathway post-MI, and that Grem2 is necessary to limit and terminate this inflammatory response.

Materials and methods

Generation of genetically engineered Grem2 mice

In order to inactivate the *Grem2* gene and generate *Grem2*$^{-/-}$ mice, Dr. John Schoenhard and Amrita Mukerjee in our laboratory first constructed an insertion vector (kindly provided by Dr. Mark Magnuson) containing two fragments from the *Grem2* gene locus (fragments B and C, each 0.5 kb in length) flanking a *kanamycin selection* gene cassette under the synthetic *EM7* prokaryotic promoter (*EM7neo*) and a fusion puromycin/truncated herpes simplex virus *thymidine kinase* gene [pu(Δ)TK; **Figure 13A**)]. Fragment B is located within the *Grem2* single intron just upstream of exon 2, which contains the entire *Grem2* coding sequence. Fragment C resides within the 3' UTR. The truncated thymidine kinase was incorporated to facilitate clone selection in future recombination strategies. Homologous recombination between a BAC containing the *WT Grem2* locus and the insertion vector replaced the entire coding sequence and part of the 3' UTR of the *Grem2* gene with the pu(Δ)TK/EM7neo

cassette. A vector containing two additional small fragments of the *Grem2* gene locus (Fragments A and D), also 0.5 kb in length, were used to retrieve the resultant targeting vector from the modified BAC (**Figure 13A**).

200 g of the targeting vector were linearized and double-electroporated into 3.5 x 10^7 129/Sv mouse embryonic stem cells at the Vanderbilt Transgenic Mouse/Embryonic Stem Cell Shared Resource (TMESCSR). After puromycin selection at 1.5 g/ml, 483 colonies were picked and 25 colonies were identified as having properly recombined by Southern blotting using 5' and 3' probes outside the targeting vector (the location of the probes are marked in **Figure 13A**). The targeting efficiency was 5.2%. Six positive clones were subsequently expanded and confirmed by secondary screening. Two selected clones were then injected into C57BL/6 blastocysts and blastocysts were transplanted into pseudopregnant females. Both clones gave germline transmission generating two independent *Grem2*$^{-/-}$ mouse lines that displayed identical physiological phenotypes and response to myocardial ischemic injury. The *Grem2*$^{-/-}$ mice and littermate *WT* controls (*WT*^{mix}) were kept on a mixed C57BL/6 and 129/Sv background.

Histological, molecular and flow cytometric analyses were conducted using male mice at 12-16 weeks of age fed with a normal chow diet.

Experimental MI

See CHAPTER II.

Echocardiography

Mice underwent echocardiography measurements in order to assess cardiac function post-surgery. Mice were rested and calmed before echocardiography was performed. All mice were conscious and unsedated during imaging using the VEVO 2100 machine and transducer MS-400 (VisualSonics) to measure and calculate cardiac parameters. The left ventricle was located in B-Mode and was traced over five consecutive beats in M-Mode. Left ventricular internal dimension and volume in diastole and systole (LVIDd, LVIDs, LVvold, LVvols) were measured from M-Mode using the short axis and used to calculate fractional shortening and ejection fraction (Paik et al., 2015).

RNA analysis by Reverse Transcription and quantitative Polymerase Chain Reaction (RT-qPCR)

See CHAPTER II. The sequences of gene-specific primers used in this chapter have been also included in **Table 1**.

Immunofluorescence and immunohistochemistry analyses

See CHAPTER II.

Primary antibodies used for IF analysis were as follows: rabbit polyclonal anti-human Tie1 (Santa Cruz Biotechnology, 1:100, Cat. No. sc-342 (C-18), rat monoclonal anti-mouse CD31/PECAM1 (BD Pharmingen; 1:100, Cat. No. 553370), Cat. No. MF 20, RRID:AB_2147781), rabbit polyclonal anti-human Grem2 (GeneTex; 1:100, Cat. No. GTX108414), rat monoclonal anti-mouse

CD62E/E-selectin (BD Pharmingen; 1:100, Cat. No. 550290), rat monoclonal anti-mouse CD45 (BD Pharmingen; 1:100, Cat. No. 550539), and mouse monoclonal -Actinin (Sigma; 1:800, Cat. No. A7811).

Flow Cytometry

Together with Dr. Mohamed Saleh in Dr. David Harrison's laboratory, we prepared single cell suspensions of cardiac cells depleted of cardiomyocytes from freshly isolated whole hearts perfused with 1X PBS to remove blood cells. Briefly, hearts were digested with Collagenase D (2 mg/ml; Roche) and DNase I (100 µg/ml) in a solution of RPMI 1640 (Gibco) containing 10% FBS using an AUTOMacs Dissociator (Miltenyi Biotech), and then incubated at 37°C for 30 minutes in an orbital shaker to prepare single cell suspensions. The digested tissue was then passed through a 70-micron cell strainer and centrifuged at 500 g for 10 minutes. The cell pellet was suspended in 2 ml 1X PBS and centrifuged at 300 g for 5 minutes. Two more centrifugation/wash steps followed, and the pellet was suspended in 100 µl of FACS buffer (1% BSA, 0.5% NaN_3 in 1X PBS). We then added 2 µl of Fc blocker (eBioscience) and cells were incubated for 10 minutes at 4°C to prevent non-specific antibody binding, then washed with 1 ml of FACS buffer and centrifuged at 300 g for 5 minutes. The cells were resuspended in 100 µl of FACS buffer and antibodies were added at 1 µl or 0.25 µg per 1 million cells and incubated for 30 minutes at 4°C. The antibodies used were Brilliant Violet 510–conjugated (BV510) anti-CD45 antibody (Biolegend, Cat. No. 103107), Alexa Fluor 488–conjugated anti-F4/80 antibody (Biolegend,

Cat. No. 123119), PE-Cy7-conjugated anti-Ly6C (eBioscience, Cat. No. 25-5932-80), Brilliant Violet 421-conjugated anti-CCR2 (Biolegend, Cat. No. 150605), PE-conjugated anti-Ly6G (Biolegend, Cat. No. 127607), and APC-Cy7-conjugated anti-CD3 (BD Pharmingen, Cat. No. 557596).

After incubation, cells were centrifuged at 300 g for 5 minutes and washed twice with 1ml FACS buffer. 5 µl of 7-AAD (eBioscience) was added to 100 µl of the solution and incubated for 10 minutes at room temperature for live/dead staining. After 300 µl of FACS staining buffer was added, cells samples were analyzed by flow cytometry using the BD FACSCanto II cytometer. Total cell number was determined by adding 50 µl of counting beads (~49500-52000 beads per µl; Life Technologies). Flow-minus-one was used for gating. Low voltage gating was conducted in order to capture the counting bead population. All leukocyte populations were quantified within the $CD45^+$ gate. Data acquisition was completed using FloView.

Regarding total blood flow sorting, 100 µl of fresh heparinized blood was directly stained with 1.5 µl of each of the previously mentioned antibodies for 30 minutes at 4°C. The samples were then washed with FACS buffer. 2ml of red blood cell lysis buffer was applied per 100µl of blood for 4 minutes at room temperature. Two additional rounds of washing and centrifugation at 1500g for 3 minutes followed. 7-AAD staining was conducted as described for the heart samples.

TTC Staining

Whole mouse hearts were isolated 24 hours post-MI, flash frozen, and then cut into 1mm sections as instructed by Dr. Rich Gumina. The sections were incubated in 1.5% TTC at 37°C for 30 minutes and then fixed in 10% formalin overnight, and finally imaged. ImageJ 1.46r (NIH) was used to outline infarct (white) tissue. Infarct size is reported as a percentage of the total left ventricular (LV) area.

Statistical Analysis

Statistical analysis was performed using GraphPad Prism software. Data are represented as the mean ± SEM. Student's two-tailed unpaired *t*-test was used for comparison between two groups, *one-way ANOVA* was used to compare multiple groups, and *two-way ANOVA* was used to compare gene induction in each mouse model over time. Dunnett's and Bonferroni's multiple comparisons test was used post-hoc. **P<0.05*, ***P<0.01*, ****P< 0.001, ****P<0.0001* were considered significant.

Results

Loss of Grem2 leads to an increase of endothelial pro-inflammatory markers after MI

To determine whether Grem2 has a role in cardiac repair, we generated a loss of function (*Grem2*$^{-/-}$) mouse model by deleting most of exon 2 via

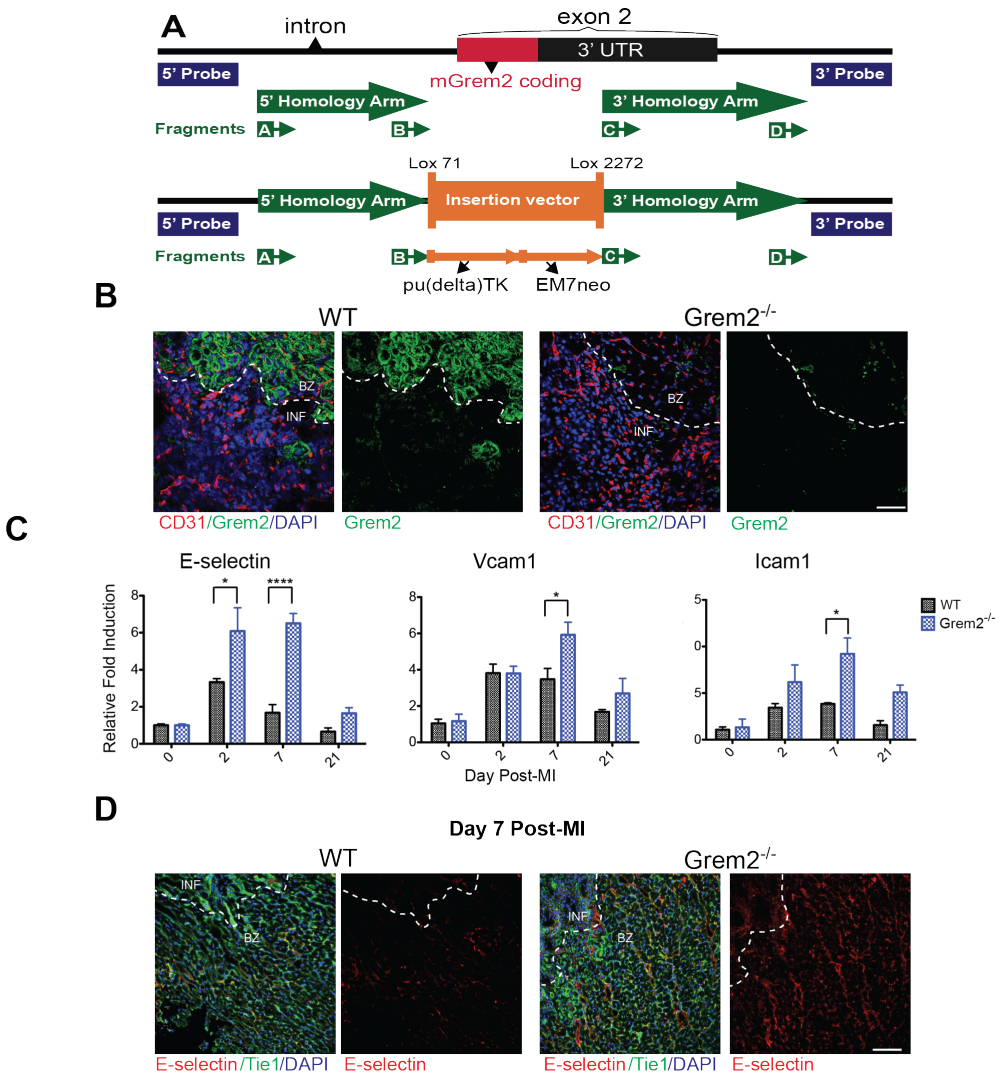

Figure 13. Loss of Grem2 increases expression of genes encoding endothelial cell membrane proteins mediating inflammatory cell recruitment after MI. (A) Schematic diagram of the *Grem2* gene knockout strategy before (upper panel) and after homologous recombination (lower panel). The entire coding region of *Grem2* in exon2 was replaced by the pu(delta)TK/EM7neo selection cassette as described in the Methods. The location of fragments A-D used to modify the corresponding BAC clone, the extent of homology arms, and the position of DNA probes used for screening putative *Grem2*$^{-/-}$ ES clones are indicated. **(B)** IF analysis with antibodies recognizing Grem2 (green) and CD31 (red) shows that Grem2 protein is induced in the peri-infarct area. Grem2 expression appears primarily in cardiomyocytes, but not CD31^{+} endothelial cells. Grem2 protein expression is missing in *Grem2*$^{-/-}$ mice. DAPI marks cellular nuclei. Scale bars, 100 µm. BZ=border zone, INF=infarct. **(C)** qPCR analysis of whole heart RNA samples isolated from *WT* and *Grem2*$^{-/-}$ mice at days 0, 2, 7 and 21 post-MI. Induction levels of gene encoding endothelial cell-specific adhesion membrane proteins *E-selectin*, *Vcam1* and *Icam1* are significantly higher in *Grem2*$^{-/-}$ hearts compared to *WT* counterparts. * $P < 0.05$; **** $P < 0.0001$. Two-way ANOVA with Bonferroni multiple comparisons test. N=3 for all time points. All data are means ± SEM. **(D)** IF analysis of cardiac tissue sections at day 7 post-MI shows E- selectin protein expression (red) persists in endothelial cells (Tie1, green) in the infarct (INF) and peri-infarct border zone (BZ) areas in *Grem2*$^{-/-}$ hearts compared to *WTs*. DAPI marks cellular nuclei. Scale bars, 100 µm. Abbreviations: *pu(Δ)TK*: fusion of *puromycin* and truncated *thymidine kinase* genes; *EM7neo*: *kanamycin resistance* gene under the synthetic bacterial *EM7* promoter; *Vcam1: Vascular cell adhesion molecule 1; Icam1: Intercellular cell adhesion molecule 1.*

homologous recombination (**Figure 13A**; **Figure 14A-C**; see also Methods).

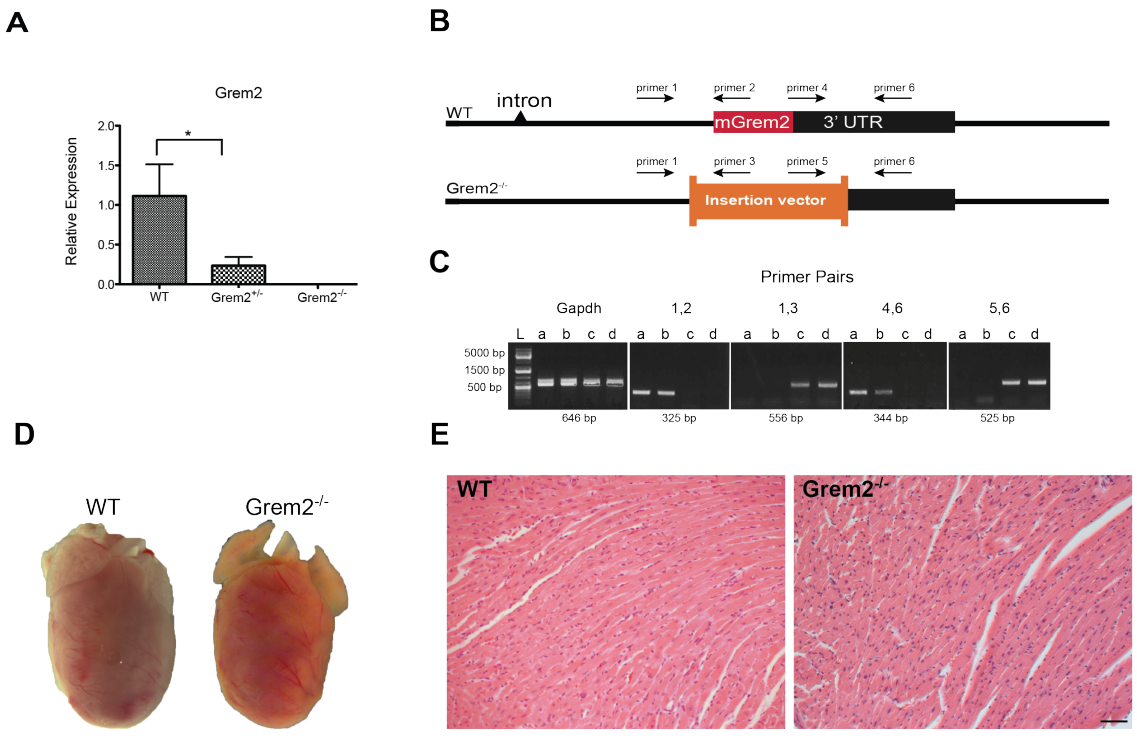

Figure 14. *Grem2* gene inactivation by homologous recombination. (A) qPCR analysis of whole heart RNA samples isolated from *WT*, *Grem2*$^{+/-}$ and *Grem2*$^{-/-}$ mice shows that *Grem2* baseline gene expression levels are approximately halved in *Grem2*$^{+/-}$ mice and completely absent in *Grem2*$^{-/-}$ mice. * $P < 0.05$. Student's two-tailed unpaired *t*-test. N=3 for all groups. All data are means ± SEM. **(B)** Schematic drawing to mark the location of the primer pairs used to genotype *WT*, *Grem2*$^{+/-}$ and *Grem2*$^{-/-}$ mice. Primer pairs 1,2 and 4,6 are specific to the endogenous *WT* locus, whereas 1,3 and 5,6 amplify DNA fragments generated after homologous recombination. **(C)** Example of conventional PCR results using genomic DNA isolated by mouse tail tip clipping. Mice a,b are *WT*, c,d are *Grem2*$^{-/-}$. The expected size of the amplicons is indicated below. *Gapdh* primers served as controls. L: DNA ladder marker. **(D)** Whole mount images of 12-week old *WT* and *Grem2*$^{-/-}$ hearts show no differences in morphology and size between the two genotypes. **(E)** Hematoxylin & Eosin stained cardiac sections fromthe left ventricle of *WT* and *Grem2*$^{-/-}$ show no apparent cellular and tissue abnormalities in *Grem2*$^{-/-}$ hearts.Scale bar, 10 µm.

This approach deleted the entire coding sequence and most of the 3' untranslated region of the *Grem2* gene, leading to complete loss of Grem2 protein. *Grem2*$^{-/-}$ mice are viable without major structural or physiological defects or apparent differences in heart size, cardiac tissue morphology and cardiac function as compared to *WT* siblings, with the exception of a small increase in heart rate (**Table 2**; **Figure 14D,E**). Thus, although the *Grem2* expression pattern has been conserved in zebrafish and mouse embryos, where *Grem2* is

first expressed in the area of the secondary heart field (Muller et al., 2013; Tanwar et al., 2014), Grem2 appears to be dispensable for mouse development. Antibody staining revealed that the robust induction of Grem2 protein expression after MI takes place primarily in peri-infarct cardiomyocytes (**Figure 13B**). There was no Grem2 detected in distal areas away from the infarct (data not shown). There was also a complete absence of Grem2 protein in *Grem2*$^{-/-}$ mice, further corroborating their null phenotype (**Figure 13B**).

In order to test whether the sequential induction of *Bmp2* and *Grem2* during the inflammatory phase plays a role in inflammation after acute injury, we challenged *Grem2*$^{-/-}$ and *WT* sibling mice with experimental MI by permanent ligation of the LAD coronary artery. We then isolated whole heart RNA at day 0, 2, 7 and 21 after MI and analyzed the expression of pro-inflammatory genes. Our data show that induction of genes encoding endothelial cell membrane proteins implicated in the rolling and adhesion of circulating immune cells to the vascular wall are higher in *Grem2*$^{-/-}$ hearts compared to *WT*s. Specifically, RNA analysis showed that expression of *E-selectin*, *Vcam1*, and *Icam1* are further upregulated compared to *WT* controls at day 2 and 7 after MI; however, their expression decreases at day 21 to levels comparable to *WT* hearts (**Figure 13C**). Consistent with the gene induction results, IF analysis of cardiac tissue sections at day 7 after MI revealed that endothelial cells (Tie1) within the infarct and peri-infarct areas stain positively for E-selectin protein in *Grem2*$^{-/-}$ mice, whereas, at this stage, E-selectin is almost undetectable in *WT* controls (**Figure 13D**). Comparison of chemokine expression such as *Ccl2*, *Il-8*, and *Il-1β* showed, that

although chemokines are induced after MI as expected, relative expression levels were comparable between *Grem2*$^{-/-}$ and *WT* mice, except a further 1.7-fold increase of *Ccl2* expression in *Grem2*$^{-/-}$ mice compared to *WT* (**Figure 15**). Thus, our data show that lack of Grem2 enhances the pro-inflammatory phenotype of endothelial cells in and around the injury site after MI.

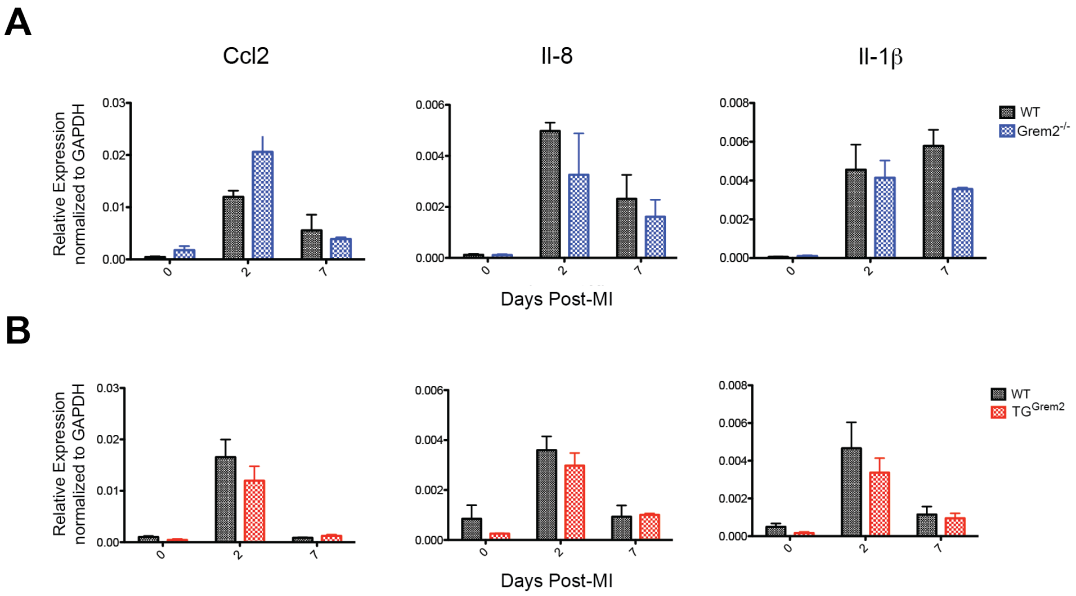

Figure 15. Chemokine expression levels after MI are comparable among *WT* and *Grem2* mouse lines. qPCR analysis of whole heart RNA samples isolated from *WT*, *Grem2*$^{-/-}$, and *TG*^{Grem2} mice at days 0, 2, and 7 post-MI. Relative expression levels of chemokines in *Grem2*$^{-/-}$ **(A)** and *TG*^{Grem2} **(B)** mice before and after MI are comparable to *WT* with the exception of a moderate increase in *Ccl2* in *Grem2*$^{-/-}$ mice. Student's two-tailed unpaired *t*-test between genotypes at various time points. N=3 per group for all time points. All data are means ± SEM.

Loss of Grem2 leads to an increase in the magnitude of inflammation and spread of inflammation

To test whether increased expression of pro-inflammatory makers after MI augments infiltration of immune cells, we isolated hearts at day 5 after MI and analyzed histological sections with an antibody recognizing the leukocyte marker, CD45. The results showed that infiltration of CD45^{+} cells after MI appeared more abundant in *Grem2*$^{-/-}$ hearts compared to *WT* (**Figure 16A**). To quantify the

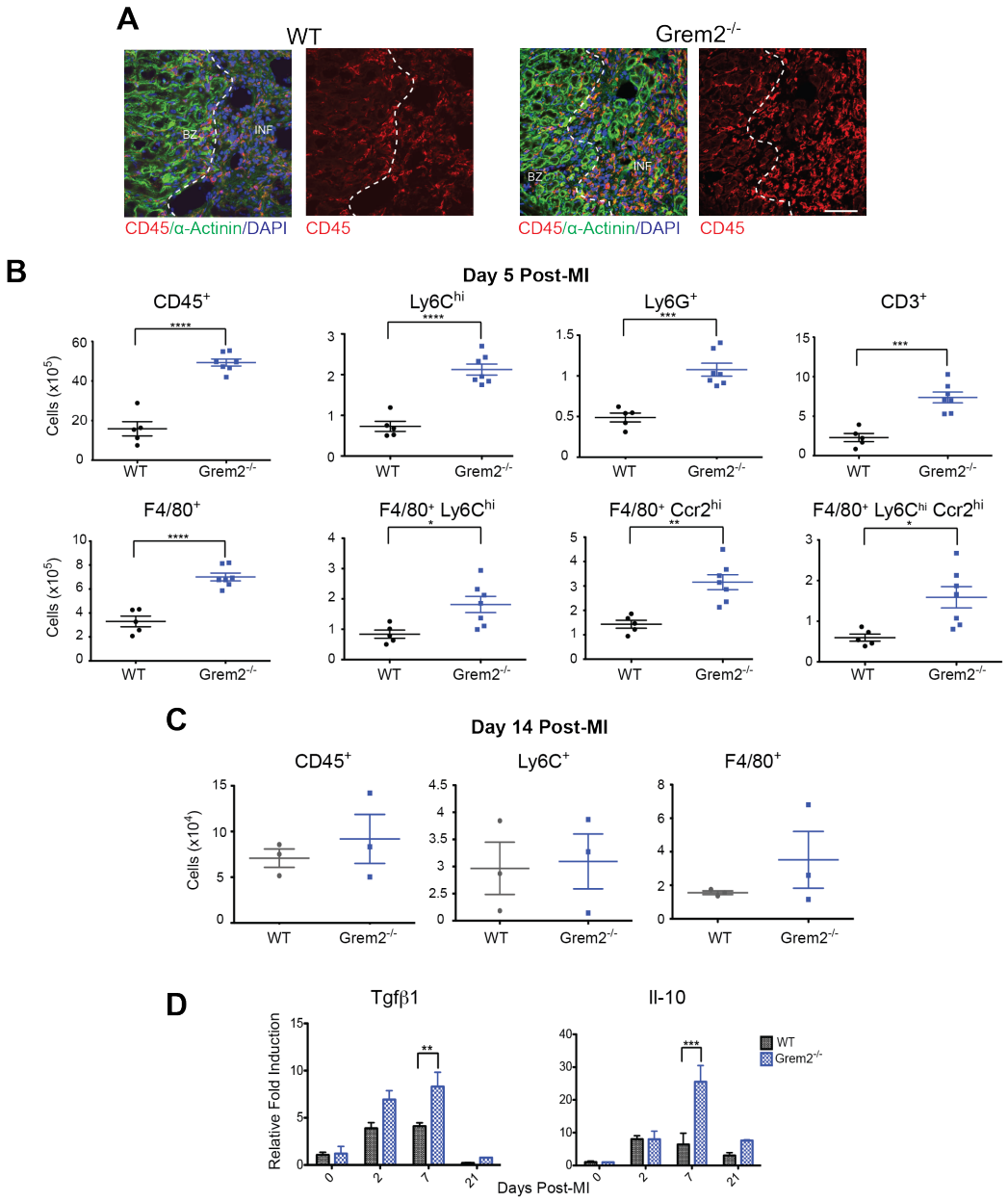

Figure 16. Loss of Grem2 increases the magnitude but not the duration of the inflammatory response after MI. **(A)** IF analysis at day 5 post-MI illustrates that *Grem2*$^{-/-}$ mice have increased levels of infiltrating leukocytes marked by CD45 (red) compared to *WTs*. A-Actinin (green) staining marks cardiomyocytes. DAPI marks cellular nuclei. Scale bars, 50 µm. BZ=border zone, INF=infarct. **(B)** Flow cytometry analysis of single cell suspensions of non-cardiomyocyte cells isolated from whole hearts and analyzed using antibodies recognizing CD45, Ly6C, Ly6G, CD3, F4/80, and Ccr2 shows increased infiltration of inflammatory cells at day 5 post-MI in *Grem2*$^{-/-}$ mice compared to *WTs*. *$P<0.05$; **$P<0.01$; *** $P < 0.001$; ****$P<0.0001$. Student's two-tailed unpaired *t*-test. *WT* N=5, *Grem2*$^{-/-}$ N=7. Bars represent means ± SEM. **(C)** In contrast there are no significant differences in CD45^{+}, Ly6C^{+} and F4/80^{+} cells between the two groups at day 14 post-MI. N=3. **(D)** qPCR analysis of whole heart RNA samples isolated from *WT* and *Grem2*$^{-/-}$ mice at days 0, 2, 7 and 21 post-MI shows higher induction levels of *Tgfβ1* and *Il-10* in *Grem2*$^{-/-}$ hearts compared to *WTs*. ** $P < 0.01$; *** $P < 0.001$. Two-way ANOVA with Bonferroni multiple comparisons test. N=3 per group for all time points. All data are means ± SEM. Abbreviations: *Il-10: Interleukin 10.*

increase in inflammatory infiltrate and better characterize the corresponding cells,

we prepared single cell suspensions of non-cardiomyocyte cells and conducted flow cytometry using antibodies recognizing various immune cell markers such as CD45, Ly6C, Ly6G, CD3, F4/80, and Ccr2 (Nahrendorf et al., 2007; Yan et al., 2013; Hulsman et al 2016). As shown in **Figure 16B**, there was a 3-fold increase in the inflammatory cells, identified as $CD45^+$ cells, in *Grem2*$^{-/-}$ hearts after MI as compared to *WTs*. Within the $CD45^+$ population, there was a 2-3-fold increase in $Ly6C^{hi}$ cells that represent mostly monocytes (but may also include neutrophils and T-cells that express intermediate levels of Ly6C), neutrophils ($Ly6G^+$), T-cell lymphocytes ($CD3^+$), and macrophages ($F4/80^+$). There was a similar increase in *Grem2*$^{-/-}$ hearts compared to *WTs* of pro-inflammatory $F4/80^+$ macrophages expressing high levels Ly6C ($F4/80^+/Ly6C^{hi}$), the Monocyte chemoattractant protein-1 (MCP-1, or Ccl2) receptor Ccr2 ($F4/80^+/Ccr2^{hi}$), or both ($F4/80^+/Ly6C^{hi}/Ccr2^{hi}$). The gating strategy and representative flow cytometry plots are shown in **Figures 17 and 18**.

Analysis of the initial necrosis area using Triphenyl tetrazolium chloride (TTC) staining 1 day after MI showed that infarct sizes were comparable between WT and *Grem2*$^{-/-}$ mice, suggesting that the observed differences in the inflammatory response are not due to more severe infarcts in *Grem2*$^{-/-}$ mice (**Figure 19**). Furthermore, flow cytometry analysis on blood $CD45^+$ cells isolated from *Grem2*$^{-/-}$ and *WT* mice at baseline and 5 days after MI revealed that leukocyte numbers in the blood were not significantly different at baseline. After MI, circulating leukocyte numbers were increased as expected (Swirski et al., 2009), albeit numbers were ~2 times higher in *Grem2*$^{-/-}$ mice, likely because

circulating leukocyte numbers correlate with the magnitude of the inflammatory response (**Figure 20**; Chia et al., 2009).

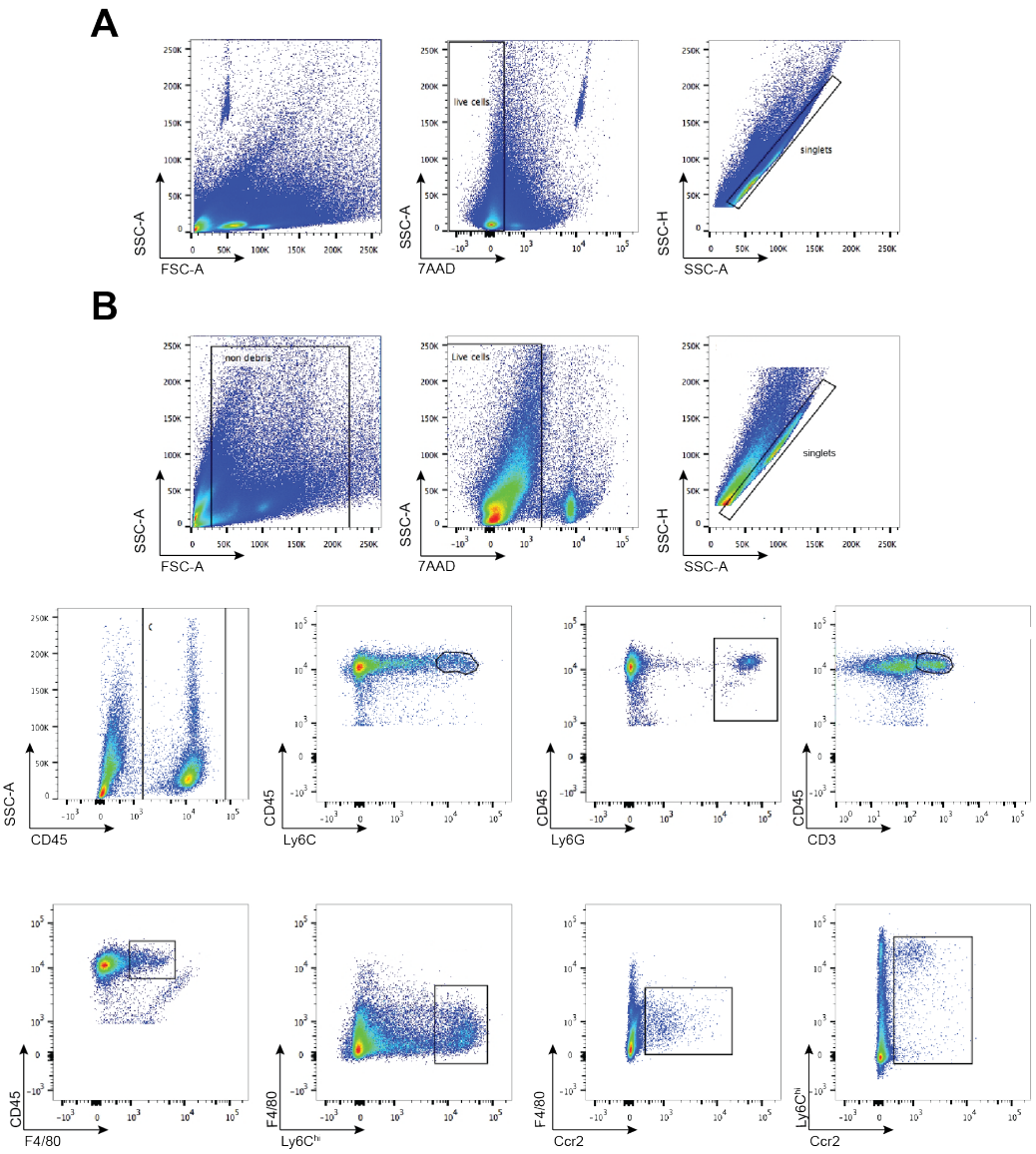

Figure 17. Flow cytometry gating strategy. (A) Representative graphs of the flow cytometry analysis of non-cardiomyocyte cells isolated from whole hearts showing the gating strategy, where we gated out debris first, followed by gating for live cells and then singlets. SSC=side scatter, FSC= forward side scatter, 7AAD= 7-Aminoactinomycin D**. (B)** Representative graphs of the flow cytometry analysis of non-cardiomyocyte single cells from a *WT* mouse. $CD45^{+}$ cells, which represent all leukocytes, were then gated for antibodies used to identity various inflammatory cell subpopulations: $Ly6C^{hi}$ that marks primarily monocytes, Ly6G for neutrophils, CD3 for T-cell lymphocytes, and F4/80 for macrophages. Inflammatory macrophages within the F4/80 population were further characterized as $Ly6C^{hi}$ and/or $Ccr2^{+}$.

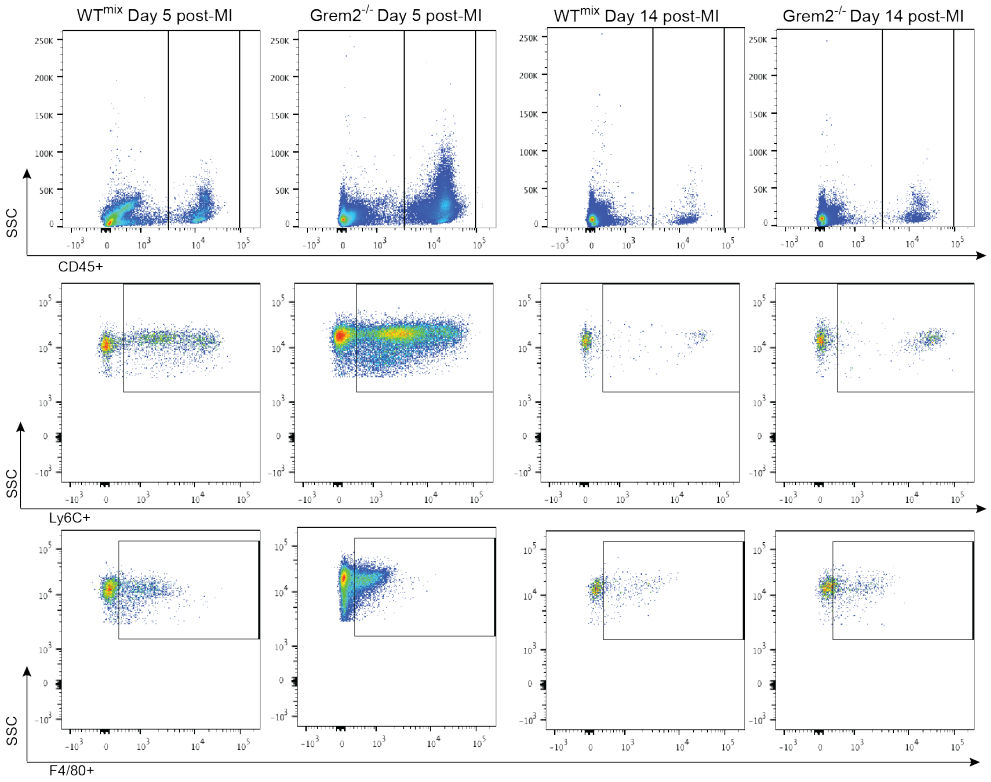

Figure 18. Flow cytometry of inflammatory cells in *WT* and *Grem2*$^{-/-}$ mouse hearts. Representative flow cytometry graphs of single cell suspensions from non-cardiomyocyte cells isolated from whole hearts at 5 and 14 days after MI. CD45^{+} cells represent leukocyte populations. Ly6C^{+} and F4/80^{+} cells are a subset of CD45^{+} cells. SSC=side scatter, FSC=forward side scatter, 7AAD =7-Aminoactinomycin D.

Finally, we investigated whether loss of Grem2, besides increased inflammatory cell infiltration, also leads to prolonged inflammation. To this end, we quantified inflammatory cells by flow cytometry at day 14 after MI, a time point when inflammatory cell numbers return close to baseline levels in *WT* mice. Our results showed a dramatic drop in inflammatory cells in *Grem2*$^{-/-}$ mice to levels comparable to *WT* controls (**Figure 16C**), consistent with the eventual downregulation of cell adhesion molecules in *Grem2*$^{-/-}$ hearts after MI (**Figure 16D**). Specifically, CD45^{+} cell numbers in *Grem2*$^{-/-}$ decreased 40-fold from day 5

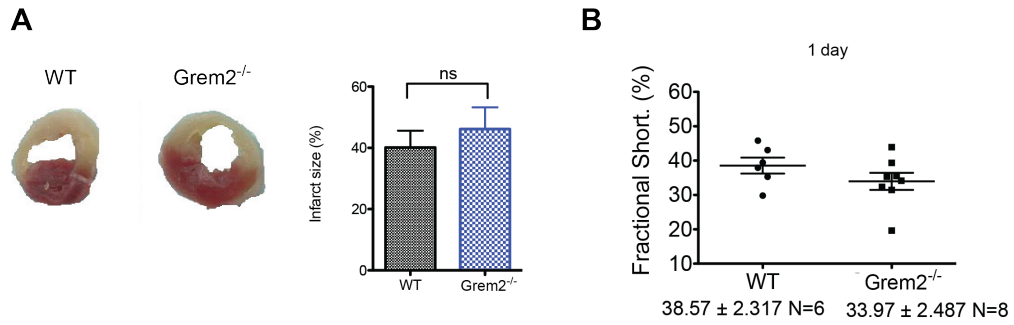

Figure 19. Grem2 does not regulate initial infarct size post-MI. (A) TTC staining on *WT* and *Grem2*$^{-/-}$ mice at day 1 post-MI illustrate no significant differences in initial infarct size. N=6-7 per group. All data are means ± SEM. **(B)** Echocardiography measurements conducted on mice that were utilized for flow cytometry experiments demonstrate comparable %FS at 1 day post-MI, demonstrating that the initial injury in these mice are comparable. N=6-8 per group. All data are means ± SEM.

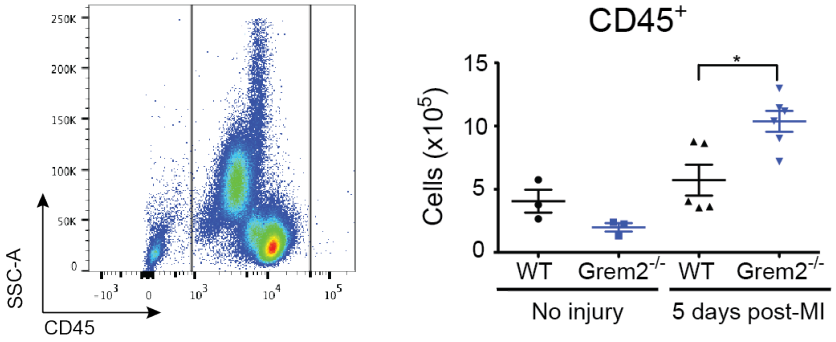

Figure 20. Blood leukocyte levels before and after MI. CD45^{+} cells in blood samples from *WT* and *Grem2*$^{-/-}$ mice demonstrate that there are no differences in circulating leukocytes before injury, however there is a modest increase in the level of leukocytes in *Grem2*$^{-/-}$ mice compared to *WT* counterparts at day 5 post-MI. ** P < 0.05.* Student's two-tailed unpaired *t*-test. N≥3 for all groups. All data are means ± SEM.

to 14, Ly6C^{+} cells 80-fold, and F4/80^{+} cells 10-fold (**Figure 16A,C**). Furthermore, molecular analysis indicated an increase in the induction of genes encoding proteins involved in the resolution of inflammation such as *Tgfβ1* and *Il-10* in *Grem2*$^{-/-}$ mice compared to *WT* animals, which may account for the clearing of excessive inflammatory cells in *Grem2*$^{-/-}$ cardiac tissue (**Figure 16D**). Taken together, our results indicate Grem2 is necessary to regulate the magnitude, but not the duration of the inflammatory cell infiltration after MI.

Loss of Grem2 leads to worse cardiac function post-MI

Excessive inflammation has been linked to poor prognosis after MI both in animal models and human patients (Lefer et al., 1993; Simpson et al., 1988; Anzai et al., 1997; Gonzalez-Quesada and Frangogiannis, 2009; de Lemos et al., 2007; Christia and Frangogiannis, 2013). To determine the effects of Grem2 loss-of-function on cardiac recovery, we compared cardiac functional parameters among *WT* controls and *Grem2*$^{-/-}$ mice by M-mode echocardiography at various time points after MI (**Figure 21**). *Grem2*$^{-/-}$ mice have worse cardiac function compared to their corresponding *WT* siblings of mixed C57BL/6 and 129/Sv background (*WT*^{mix}) as evidenced by higher fractional shortening (FS) and ejection fraction (EF) values 21 days after MI (**Figure 21A**). Specifically, systolic diameters were higher in *Grem2*$^{-/-}$ mice compared to *WT*^{mix} controls, demonstrating that the changes to cardiac function are likely due to the changes in the magnitude of inflammation, since systolic dysfunction is often linked to these phenotypes (**Figure 21B**; (Frangogiannis, 2014; Saxena et al., 2015). *Grem2*$^{-/-}$ mice have comparable ventricular dimensions and functional values to corresponding *WT* control mice at baseline (**Figure 21B**). These data indicate that Grem2 levels directly correlate with functional recovery after acute MI. Original M-mode echocardiography images are shown in **Figure 21C.**

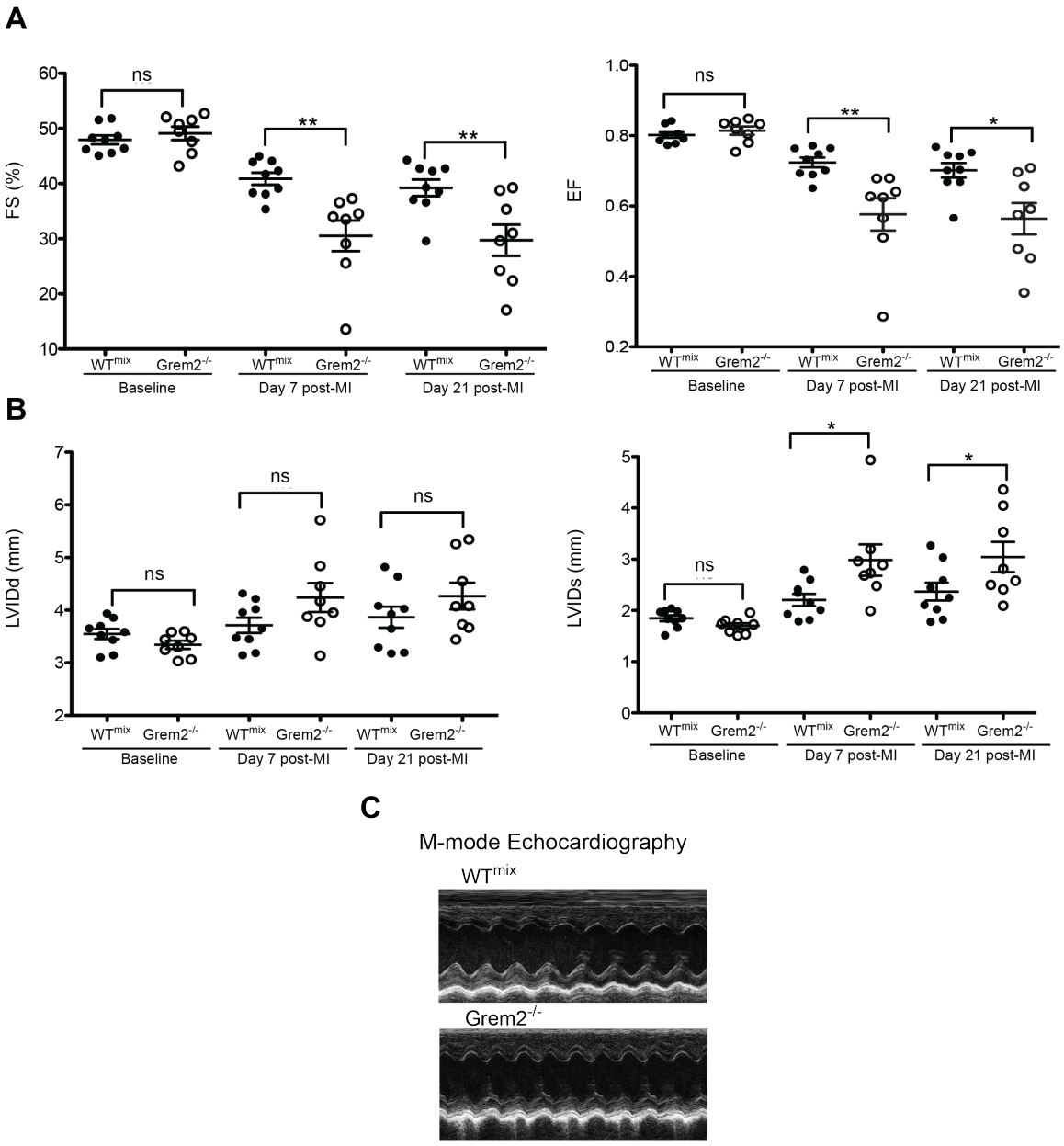

Figure 21. Loss of Grem2 leads to worse cardiac function after MI. *WT^{mix}* and *Grem2$^{-/-}$* mice (both in mixed C57BL/6 and 129/Sv background) underwent permanent ligation of the LAD artery and cardiac function was determined by M-mode echocardiography 21 days post-MI. **(A)** Fractional shortening (FS) and Ejection Fraction (EF) measurements at 21 days post-MI indicate cardiac function is worse in *Grem2$^{-/-}$* mice compared to *WT^{mix}*. **(B)** *Grem2$^{-/-}$* mice have specifically have higher systolic Left Ventricular Internal Diameter and not diastolic Left Ventricular Inter Diameter (LVIDd and LVIDs) parameters as compared to *WT^{mix}* controls 21 days post-MI. **(C)** Representative M-mode images from *WT^{mix}* and *Grem2$^{-/-}$* mice 21 days post-MI. ** P < 0.05; **P < 0.01*. Student's two-tailed unpaired *t*-test. *WT^{mix}* N=9, *Grem2$^{-/-}$* N=8. Bars represent means ± SEM.

Discussion

The mechanisms responsible for inducing the inflammatory response after MI have been well described, but those that regulate the magnitude or spread of inflammatory cells are less well understood (Frangogiannis, 2014). Our results suggest that Grem2 controls the magnitude but not the duration of the inflammatory response, likely due to the fact that lack of *Grem2* also triggers overexpression of cytokines and growth factors involved in the resolution of inflammation such as *Tgf1* and *Il-10*. The effects of Grem2 loss in increasing the inflammatory response correlate with ventricular function after MI, as evidenced by deteriorated systolic parameters in *Grem2*$^{-/-}$ mice as compared to *WT* littermate controls. This represents the first time Grem2 has been implicated in the adult cardiac repair program and in the regulation of a disease state such as inflammation.

The Hatzopoulos laboratory has previously shown that Grem2 is necessary for cardiac asymmetry and atrial development in zebrafish. However, it appears that Grem2 is dispensable for mouse development. This result is not without precedent among BMP signaling components. For example, single Bmp5, Bmp6, and Bmp7 knockout mice are viable, but double knockouts of either Bmp5/7 or Bmp6/7 are embryonic lethal due to cardiac developmental defects (Kingsley et al., 1992; Dudley et al., 1997; Kim et al., 2001; Solloway et al.,1998; Solloway et al., 1999). It is likely that, as with Bmp ligands, there is redundancy among BMP antagonists in cardiac development. Such redundancy may also happen in the adult heart.

Although Grem2 is the highest induced BMP antagonist induced after MI, the heart maintains expression of a number of BMP antagonists such as *Chordin, Sost*, *Twsg1* and *Dan*. There are also low levels of *Noggin* expression. Sost does not inhibit BMP2 and thus is unlikely to play a role in the inflammatory response, which is dominated by BMP2 expression. Dan, Chordin and Twsg1 are weaker antagonists than Grem2 and may not compensate for Grem2 in the peri-infarct area where Grem2 is prominently induced (Nolan et al., 2015; Zhang et al., 2008). It would be informative to generate double loss of function mice by crossing the *Grem2*$^{-/-}$ mice to mice with conditional inactivation of other BMP antagonists such as Grem1 or Noggin to directly test redundant functions during development or after injury.

Again, due to the global, constitutive nature of our knockout model, the possibility remains that some of the phenotypic effects observed could be caused by the system compensating for the lack of Grem2. This could be examined by removing the expression of Grem2 only during the inflammatory phase of recovery by utilizing a conditional knockout model. If the loss of Grem2 during the inflammatory response results in an increase in the magnitude of inflammation, then it is unlikely that other mechanisms are directly involved.

Although our findings suggest that Grem2 is necessary to control the magnitude of inflammation, it does not demonstrate whether it is sufficient. In order to determine if additional Grem2 has a beneficial effect on inflammation and the cardiac repair process, a gain of Grem2 function animal model should be utilized to determine if the inflammatory response is augmented, and if more

importantly, this leads to positive effects on cardiac functional recovery. The Hatzopoulos laboratory has generated a transgenic model of Grem2 overexpression, and the results of these studies are the topic of the subsequent chapter.

Acknowledgements

I thank members of the Cardiovascular Pathophysiology and Complications Core of the Mouse Metabolic Phenotyping Center, the Cell Imaging Shared Resource, the Translational Pathology Shared Resource, the Transgenic Mouse/ES Cell Resource, and the Molecular Cell Biology Resource at Vanderbilt University Medical Center for technical assistance. This work also utilized the core(s) of the Vanderbilt Diabetes Research and Training Center funded by grant 020593 from the National Institute of Diabetes and Digestive and Kidney Disease. I thank Lianli Ma, Lin Zhong, and Zhizhang Wang for performing mice surgeries and echocardiograms; Mark Magnuson and Jennifer Skelton for the design and generation of the Grem2 mouse lines; Vineeta Tanwar for her help with the initial mouse colony maintenance; Daniel Levic and Ela W. Knapik for help with histological analyses; and David T. Paik for assistance in providing mouse heart samples for histological analysis.

CHAPTER IV

GAIN OF GREM2 FUNCTION LEADS TO A DECREASE IN THE MAGNITUDE OF INFLAMMATION AND AN IMPROVEMENT IN CARDIAC FUNCTION

Introduction

BMP signaling antagonists have been implicated in the regulation of the inflammatory phenotype present in vascular disease states, such as atherosclerosis. Endogenous inhibitors such as Noggin, BMPER, and Grem1 and chemical inhibitors such as dorsomorphin have previously been demonstrated to inhibit the pro-inflammatory effect of BMP signaling on endothelial cells (Chen et al., 2004; Helbing et al., 2011; Pi et al., 2012; Simões Sato et al., 2014; Steinbicker et al., 2011; Sucosky et al., 2009). Despite the fact that such antagonists have extensively been studied in the context of disease, a relatively unstudied Bmp antagonist is Grem2, has not previously been implicated in disease states, with exception of atrial fibrillation (Tanwar et al., 2014).

In addition to inflammation, BMP antagonism has also been shown to exert beneficial effects on the cardiac repair process (Pachori et al., 2010; Sun et al., 2013). Since the data described in the previous chapter illustrated that Grem2 is necessary for the regulation of the magnitude inflammation, as evidenced by a Grem2 loss-of-function model, I wanted to determine if Grem2 was also sufficient for the regulation of the inflammatory process following an MI.

In order to test this, the Hatzopoulos laboratory generated a transgenic (TG) gain-of-function model for Grem2.

Materials and methods

Generation of genetically engineered Grem2 mice

The *MHC-Grem2* plasmid was generated by inserting the full-length *Grem2* cDNA into the *αMHC* (*Myh6*) gene promoter-polyA hGH cloning vector 1 (kindly provided by Dr. J. Robbins; (Subramaniam et al., 1991)). The *αMHC-Grem2* transgenic (TG^{Grem2}) mice were generated by pronuclear microinjection of the construct into fertilized oocytes at the TMESCSR. TG^{Grem2} mice and *WT* littermate controls were raised in C57BL/6 background.

Histological, molecular and flow cytometric analyses were conducted using male mice at 12-16 weeks of age fed with a normal chow diet.

Experimental MI and Grem2 administration

See CHAPTER II.

Grem2 protein for mouse administration was provided by the laboratory of Dr. Thomas Thompson at the University of Cincinnati and was synthesized, purified and measured activity as previously described (Kattamuri et al., 2012a; Nolan et al., 2013). *WT* mice were injected with 1 μg Grem2 protein per gram of body weight or vehicle (sterile 1X PBS) via intraperitoneal injection (IP) once per day at day 2, 3, and 4 following MI.

Echocardiography

See CHAPTER III.

RNA analysis by Reverse Transcription and quantitative Polymerase Chain Reaction (RT-qPCR)

See CHAPTER II. The sequences of gene-specific primers for this chapter have also been included in **Table 1**.

Flow Cytometry

See CHAPTER III.

Statistical Analysis

Statistical analysis was performed using GraphPad Prism software. Data are represented as the mean ± SEM. Student's two-tailed unpaired *t*-test was used for comparison between two groups, *one-way ANOVA* was used to compare multiple groups, and *two-way ANOVA* was used to compare gene induction in each mouse model over time. Dunnett's and Bonferroni's multiple comparisons test was used post-hoc. **P<0.05*, ***P<0.01*, ****P< 0.001, ****P<0.0001* were considered significant.

Results

Grem2 overexpression attenuates the inflammatory response after MI

To explore the possibility that Grem2 controls the extent of inflammation after MI, we generated a transgenic mouse line where Grem2 is postnatally overexpressed in adult cardiomyocytes under the control of regulatory elements from the *alpha-myosin heavy chain* (*MHC* or *Myh 6*) promoter that are active in the adult heart (TG^{Grem2}; **Figure 22A**; **Figure 23**; see also Methods). TG^{Grem2} mice did not exhibit differences in cardiac morphology and function as compared to *WT* counterparts (**Table 3**; **Figure 23**).

TG^{Grem2} and *WT* siblings underwent permanent LAD ligation and whole heart RNA was isolated at day 0, 1, 2, 3, 5, and 7 after MI. qPCR analysis showed that gain-of-Grem2-function led to a significant reduction in the induction levels of inflammatory gene markers such as *E-selectin* and *Vcam1* after MI with no changes in the induction of pro-inflammatory cytokines (**Figure 22B, Figure 16**). Flow cytometry of cardiac cells 5 days after MI, excluding cardiomyocytes, confirmed that reduced expression of pro-inflammatory markers led to a significant decrease in the number of $CD45^+$leukocytes, $Ly6C^+$ monocytes, and $F4/80^+$ macrophages within cardiac tissue (**Figure 22C**; original flow graphs are shown in **Figure 24**). Attenuation of inflammation correlated with reduced induction of genes encoding the anti-inflammatory *Il-10* cytokine and *Tgf1* (**Figure 22D**). These data indicate Grem2 overexpression is able to contain the magnitude of the inflammatory response after MI.

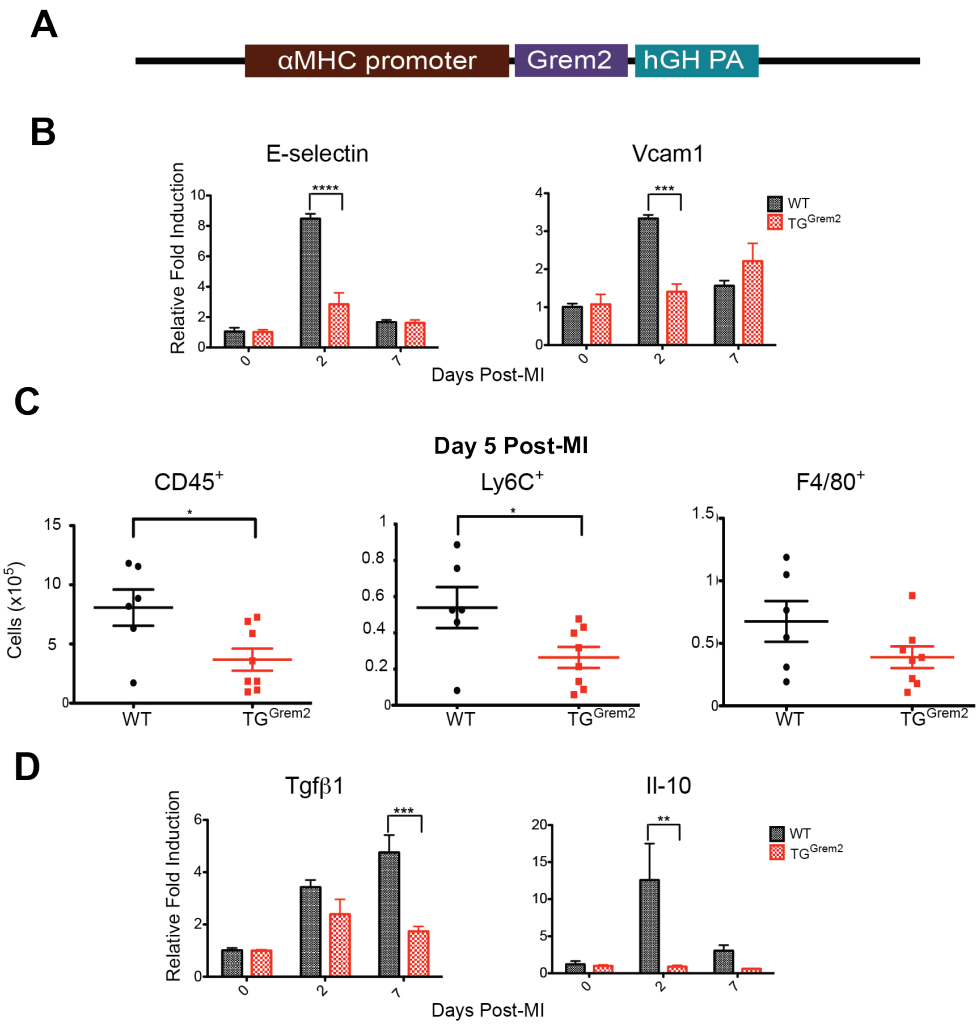

Figure 22. Grem2 overexpression attenuates inflammation after MI. (A) Schematic diagram of the DNA construct used to generate the *TG*^{Grem2} transgenic mice. The *Grem2* cDNA coding part was cloned behind a fragment of the *αMHC (Myh6)* gene promoter that specifically directs expression in adult cardiomyocytes. The construct includes the polyadenylation sequences of the human growth hormone gene (*hGH PA*). **(B)** qPCR analysis of whole heart RNA samples isolated from *WT* and *TG*^{Grem2} mice at days 0, 2, and 7 post-MI. Induction of endothelial cell-specific membrane proteins *E-selectin* and *Vcam1* is significantly attenuated in *TG*^{Grem2} hearts compared to *WT*. *** $P < 0.001$; **** $P < 0.0001$. Two-way ANOVA with Bonferroni multiple comparisons test. N=3 per group for all time points. All data are means ± SEM. **(C)** Flow cytometry analysis of single cell suspensions of non-cardiomyocyte cells isolated from whole hearts 5 days post-MI shows decreased number of CD45,$^{+}$ Ly6C^{+} and F4/80^{+} cells in *TG*^{Grem2} hearts compared to *WT*. * $P < 0.05$. Student's two-tailed unpaired *t*-test. *WT* N =6, *TG*^{Grem2} N = 8. Bars represent means ± SEM. **(D)** qPCR analysis of whole heart RNA samples isolated from *WT* and *TG*^{Grem2} mice at days 0, 2, and 7 post- MI shows lower fold induction of *Tgfβ1* and *Il-10* in *TG*^{Grem2} hearts compared to *WT*. ** $P < 0.01$; *** $P < 0.001$. Two-way ANOVA with Bonferroni multiple comparisons test. N=3 per group for all time points. All data are means ± SEM.

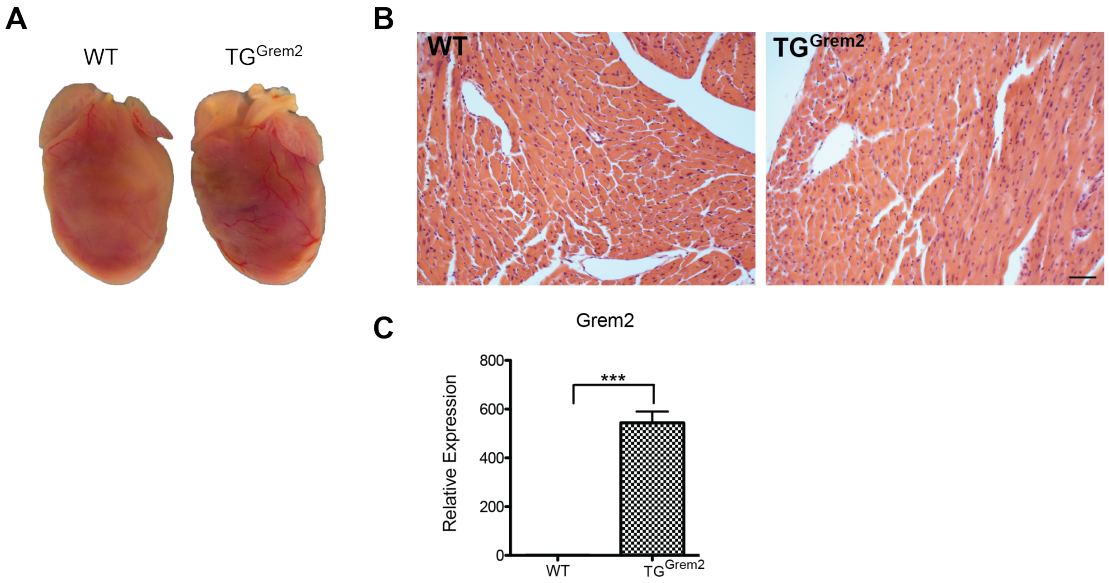

Figure 23. *TG^{Grem2}* hearts appear morphologically normal. (A) Whole mount images of 12-week old *WT* and *TG^{Grem2}* hearts show no differences in morphology and size between the two genotypes. **(B)** Hematoxylin & Eosin stained cardiac sections from the left ventricle of *WT* and *TG^{Grem2}* hearts show no apparent cellular and tissue abnormalities. Scale bar, 10 µm. **(C)** qPCR analysis of whole heart RNA samples isolated from *WT* and *TG^{Grem2}* mice shows a significant increase in *Grem2* expression in *TG^{Grem2}* compared to *WT*. **** P < 0.001*. Student's two-tailed unpaired *t*-test. N=3 for all groups. All data are means ± SEM.

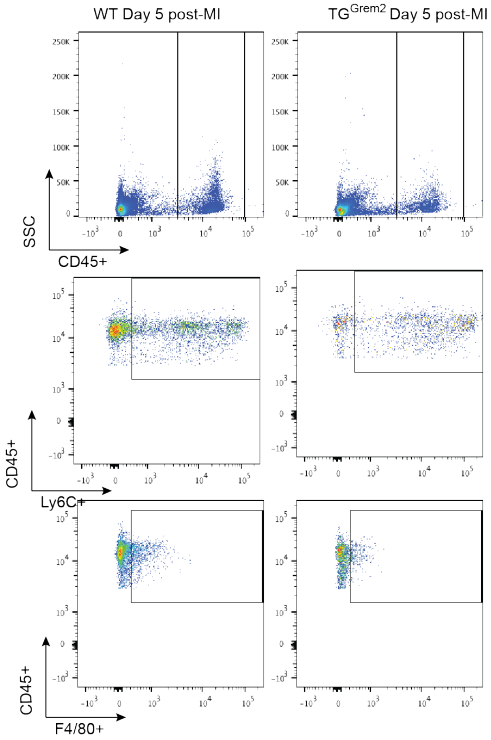

Figure 24. Flow cytometry of inflammatory cells in *WT* and *TG^{Grem2}* mouse hearts. Representative flow cytometry graphs flow of single cell suspensions from non-cardiomyocyte cells isolated from whole hearts at 5 days after MI. CD45^{+} cells represent leukocyte populations, Ly6C^{+} and F4/80^{+} cells are a subset of CD45^{+} cells. SSC=side scatter.

Grem2 promotes functional recovery after MI

The phenotypic analysis of TG^{Grem2} mice indicates that Grem2 levels are inversely related to the magnitude of inflammation after MI. Excessive inflammation has been linked to poor prognosis after MI both in animal models and human patients (Lefer et al., 1993; Simpson et al., 1988; Anzai et al., 1997; Gonzalez-Quesada and Frangogiannis, 2009; de Lemos et al., 2007; Christia and Frangogiannis, 2013). To determine the effects of Grem2 gain-of-function on cardiac recovery, we compared cardiac functional parameters among *WT* controls, TG^{Grem2} mice by M-mode echocardiography at various time points after MI (**Figure 25**).

Our data show that TG^{Grem2} mice have better preserved cardiac function compared to *WT* littermate controls of C57BL/6 background, as evidenced by higher fractional shortening (FS) and ejection fraction (EF) values 21 days after MI (**Fig. 25A**).

Functional recovery in TG^{Grem2} mice was due to preservation of both systolic and diastolic dimensions with lower overall values compared to *WT* control mice at day 21 after MI (**Figure 25B**). TG^{Grem2} mice have comparable ventricular dimensions and functional values to corresponding *WT* control mice at baseline (**Figure 25B**). These data indicate that Grem2 levels directly correlate with functional recovery after acute MI. Original images from M-mode echocardiography are shown in **Figure 25C**.

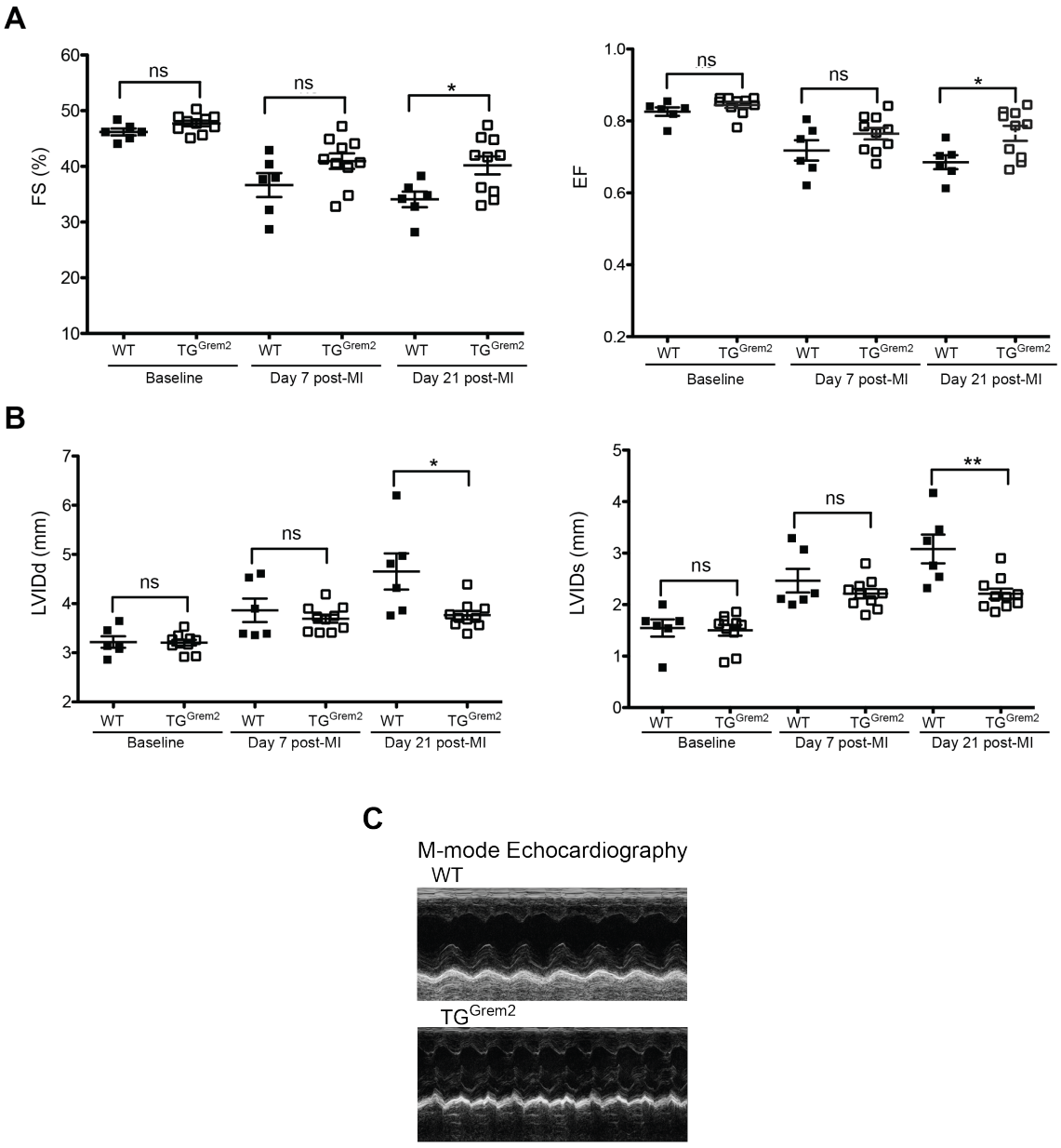

Figure 25. Grem2 improves cardiac function after MI. *WT* and *TG^{Grem2}* mice underwent permanent ligation of the LAD artery and cardiac function was determined by M-mode echocardiography 21 days post-MI. **(A)** Fractional shortening (FS) and Ejection Fraction (EF) measurements at 21 days post-MI indicate cardiac function is improved in *TG^{Grem2}* mice compared to their *WT* siblings. **(B)** Improvement of cardiac function in *TG^{Grem2}* mice is due to preservation of both diastolic and systolic Left Ventricular Internal Diameter (LVIDd and LVIDs) 21 days post-MI.**(C)** Representative M-mode images from *WT* and *TG^{Grem2}* mice 21 days post-MI. ** P < 0.05; **P < 0.01*. Student's two-tailed unpaired *t*-test. *WT* N=6, *TG^{Grem2}* N=10. Bars represent means ± SEM.

Systemic Grem2 administration attenuates inflammation after MI

The results obtained in TG^{Grem2} mice suggest that Grem2 is sufficient to attenuate cardiac tissue inflammation after ischemic injury. To test whether this activity is confined to a specific time window after MI and does not depend on structural or functional changes caused by permanent Grem2 overexpression in the heart of TG^{Grem2} mice, we injected *WT* mice intraperitoneally with Grem2 protein at day 2, 3, and 4 after MI, during the critical time window of the inflammatory phase, isolated hearts at day 5 after MI, prepared single cell suspensions of non-cardiomyocyte cells and performed flow cytometry using antibodies recognizing specific immune cell types. As shown in **Figure 26A**, there was a significant decrease in the leukocytes ($CD45^+$), monocytes ($Ly6C^+$), and macrophages ($F4/80^+$) as compared to saline-injected control mice (original flow graphs in **Figure 26B**). These results demonstrate that the anti-inflammatory phenotype in TG^{Grem2} after MI can be recapitulated by systemic administration of Grem2 protein during the inflammation phase of cardiac tissue repair. We were also able to confirm that Grem2 exerted direct effects in the hearts of as evidenced by a decrease in *Id2* gene induction 5 days post-MI (**Figure 26C**).

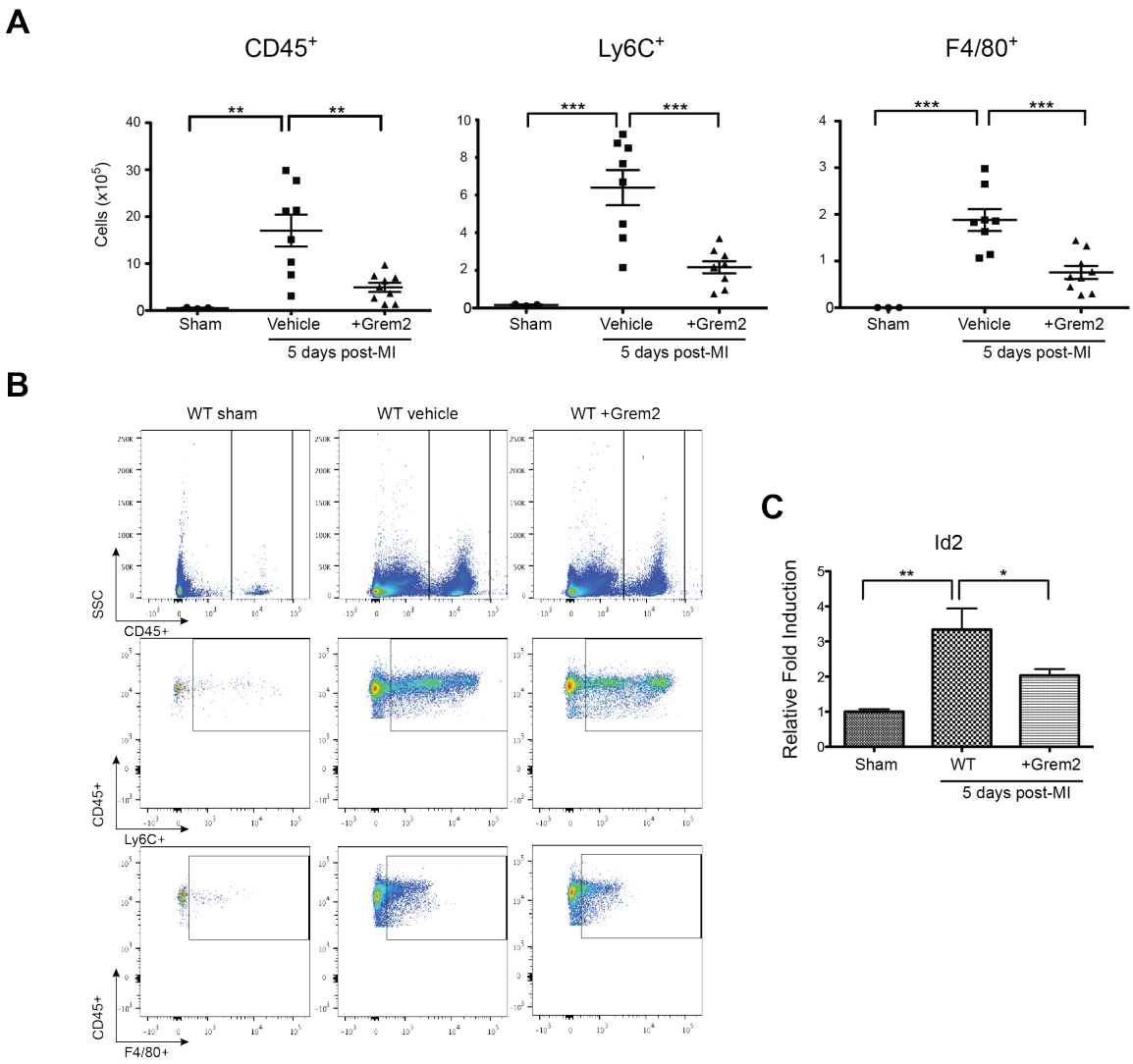

Figure 26. Systemic Grem2 protein administration attenuates inflammation after MI. (A) *WT* mice were injected once daily via IP with either Grem2 protein or vehicle (PBS) at day 2, 3, and 4 after MI. The number of $CD45^+$ leukocytes, and $Ly6C^+$ and $F/480^+$ cells in whole hearts was determined by flow cytometery at day 5 post-MI. Grem2 injected mice have decreased inflammatory cell infiltration compared to controls. ** $P < 0.01$; *** $P < 0.001$. One-way ANOVA with Bonferroni multiple comparisons test. Sham N = 3, Vehicle N=8, +Grem2 N=9. Bars represent means ± SEM. **(B)** Representative flow cytometry graphs of $CD45,^+$ $Ly6C^+$ and $F4/80^+$ cells conducted on whole heart single cell suspensions of non-cardiomyocyte cells 5 days after MI. SSC=side scatter. **(C)** *Id2* gene induction on whole hearts 5 days after MI. * $P < 0.05$; ** $P < 0.01$. One-way ANOVA with Bonferroni multiple comparisons test. N=3 for all time points. All data are means ± SEM.

Discussion

Gain of Grem2 function resulted in a decrease in cell adhesion molecule induction as well as inflammatory cell infiltration post-MI, phenotypes opposite to what was seen in the Grem2 loss of function animal. Taken together, the data

presented here demonstrate that Grem2 is both necessary and sufficient for the regulation of the inflammatory response following a myocardial infarction. The capability of Grem2 to augment the inflammatory response subsequently proved to be beneficial for functional cardiac recovery. Grem2 also appears to be playing a direct role on the inflammatory response, since the injection of Grem2 protein during the short time window that is the inflammatory response, lead to a decrease in inflammatory cell infiltrate. Altogether demonstrating that two independent methods of Grem2 delivery lead to an improved cardiac recovery.

Despite the fact that our data suggest Grem2 inhibits the magnitude of inflammation by decreasing the number of infiltrating inflammatory cells, the possibility remains that Grem2 reduces inflammation by increasing the induction of signals that actively lead to its resolution. Our current data, illustrating that the induction cytokines involved in activating the resolution of inflammation (*Tgfβ* and *Il-10)* is decreased in our gain of Grem2 function model, suggest that this is not the case. However, we did not assess the presence of reparative macrophages or regulatory T-cells. Future analysis to determine if Grem2 directly regulates the resolution of inflammation could include determining if Grem2 injection during the inflammatory phase changes the induction levels of the aforementioned resolution cytokines as well as determine if changes in Grem2 expression lead to changes in the presence of reparative macrophages or regulatory T-cells via flow cytometry.

The ability to treat mice with exogenous Grem2 protein several days following the MI, demonstrates that Grem2 has translational and therapeutic

potential. Most current therapies are administered within the first several hours after the MI (McMurray, 2010). Since Grem2 acts directly on decreasing the extent of the inflammatory phase of recovery while inflammation is occurring, it has the potential to offer a treatment plan that can continue after the first several hours following an acute cardiac injury. It remains to be seen however, what the long-term effects are of Grem2, for example if administration of Grem2 during inflammation leads to improved recovery during the later stages of repair. Further investigations into any long-term effects as well as the ability of Grem2 administration to improve cardiac functional recovery are ongoing, for example if the administration of Grem2 post-MI leads to an improved functional recovery 21 days post-MI.

Previous clinical trials testing whether blocking inflammation improves outcomes have so far produced mixed results. For example, inhibitors of the complement system, TNF, or integrins required for immune cell binding showed no significant improvement of infarct size and MI outcomes (Christia and Frangogiannis, 2013). Glucocorticoids actually had severe adverse effects, likely due to their interference with functions that are essential for healing (Roberts et al., 1976). On the other hand, inhibitors of the P-selectin antagonist inclacumab (Tardif et al., 2013), did show promising results, indicating that moderating inflammation can be beneficial for cardiac repair after MI. This work demonstrates a novel method of regulating the inflammatory phase without targeting direct components of the pathway. It should also be noted that the ability of Grem2 to modulate the inflammatory response could have vast

implications. Previous genome wide association studies (GWAS) have correlated Grem2 with the human response to the smallpox vaccine (Hindorff et al., 2009; Ovsyannikova et al., 2012). Therefore, our findings could be translatable to various inflammatory disease states besides the inflammatory response following an acute cardiac injury.

In order to generate a therapeutic target based on the function of Grem2, a comprehensive understanding of its mechanism of action is required. Although Grem2 is classically known to be a BMP antagonist, it contains a unique structure. Therefore it has the potential to have a novel mechanism of action. Previous work demonstrating the pro-inflammatory activity of BMP signaling has shown to act through the non-canonical activation of NFκB (Csiszar et al., 2006). Therefore further analysis is needed in order to determine if canonical BMP signaling is responsible for the pro-inflammatory phenotype and if Grem2 regulates canonical BMP signaling in the context of cardiac recovery. The role of canonical BMP signaling in cardiac repair is addressed in the subsequent chapter.

Acknowledgements

I thank members of the Cardiovascular Pathophysiology and Complications Core of the Mouse Metabolic Phenotyping Center, the Cell Imaging Shared Resource, the Translational Pathology Shared Resource, the Transgenic Mouse/ES Cell Resource, and the Molecular Cell Biology Resource at Vanderbilt University Medical Center for technical assistance. This work also

utilized the core(s) of the Vanderbilt Diabetes Research and Training Center funded by grant 020593 from the National Institute of Diabetes and Digestive and Kidney Disease. I thank Lianli Ma, Lin Zhong, and Zhizhang Wang for performing mice surgeries and echocardiograms; Mark Magnuson and Jennifer Skelton for generation of the Grem2 mouse lines; Vineeta Tanwar for her help with the initial mouse colony maintenance; Daniel Levic and Ela W. Knapik for help with histological analyses; and David T. Paik for assistance in providing mouse heart samples for histological analysis.

CHAPTER V

GREM2 REGULATES CANONICAL BMP SIGNALING POST-MI

Introduction

BMP signaling occurs through binding and activation of the type 1 and type 2 receptor complexes. During canonical signaling, receptor Smads (Smad1/5/8) become phosphorylated and then form a complex with co-Smads that then translocate to the nucleus and activate target gene transcription such as IDs. BMP signaling is known to be important for cardiac and vascular development and has also been implicated in vascular disease (Lowery and de Caestecker, 2010).

Previous work has implicated that BMP signaling is also induced following a cardiac injury. However, its role during cardiac repair is not entirely understood. Using gene expression and immunofluorescence analysis, we found that BMP signaling is activated in border zone cardiomyoctyes during the inflammatory phase of recovery. Due to the fact that I determined that a BMP signaling antagonist, Grem2, regulates the magnitude of inflammation following an MI (CHAPTERS III and IV) and since the Hatzopoulos laboratory has previously shown that Grem2 regulates canonical BMP signaling *in vivo* during development (Muller et al., 2013), I therefore wanted to determine if Grem2 regulates the canonical BMP signaling pathway in the context of cardiac repair.

We hypothesized that canonical BMP signaling is responsible for increasing the magnitude and spread of inflammation following a myocardial infarction.

Materials and methods

Generation of genetically engineered Grem2 mice

See CHAPTERS III and IV.

Experimental MI and administration of Grem2 protein and DMH1

See CHAPTER II.

For administration of DMH1 (Sigma), *Grem2*$^{-/-}$ mice were injected IP with 13 µg DMH1 (Helbing et al., 2011) per gram of body weight or vehicle (DMSO) once per day at 2, 3 and 4 days following MI as previously described (Hao et al., 2014).

RNA analysis by Reverse Transcription and quantitative Polymerase Chain Reaction (RT-qPCR)

See CHAPTER II. The sequences of gene-specific primers for this chapter have also been included in **Table 1**.

Immunofluorescence and immunohistochemistry analyses

See CHAPTER II.

Primary antibodies used for IF analysis were as follows: rabbit monoclonal anti-mouse p-Smad1/5/8 (Cell Signaling; 1:50, Cat. No. 9511), mouse

monoclonal anti-mouse MF20 (Developmental Studies Hybridoma Bank; 1:5, Cat. No. MF 20, RRID:AB_2147781), rabbit monoclonal anti-Id2 (Biocheck Can. No. BCH-3/#9-2-8) and rat monoclonal anti-mouse CD45 (BD Pharmingen; 1:100, Cat. No. 550539).

p-Smad1/5/8^{+} cardiomyocytes were quantified using ImageJ 1.46r (NIH) color thresholding, as a percentage of cells double positive for MF20 and p-Smad1/5/8 amongst all DAPI positive cells in the viewing field; at least 4 viewing fields were used for calculations. N=3 mice for each group.

Flow Cytometry

See CHAPTER III.

Statistical Analysis

Statistical analysis was performed using GraphPad Prism software. Data are represented as the mean ± SEM. Student's two-tailed unpaired *t*-test was used for comparison between two groups, *one-way ANOVA* was used to compare multiple groups, and *two-way ANOVA* was used to compare gene induction in each mouse model over time. Dunnett's and Bonferroni's multiple comparisons test was used post-hoc. **P<0.05*, ***P<0.01*, ****P< 0.001, ****P<0.0001* were considered significant.

Results

Changes in Grem2 expression leads to changes in BMP pathway component induction post-MI

Grem2$^{-/-}$, *TG*^{Grem2}, and their corresponding *WT* siblings underwent permanent LAD ligation and whole heart RNA was isolated at the indicated days after MI. qPCR analysis showed that changes in Grem2 expression led to changes in the induction of BMP ligands. Namely, the loss-of Grem2 function resulted in an increase in *Bmp2* and *Bmp4* induction, with no significant changes in *Bmp6* induction. However the gain-of Grem2 function significantly increased and decreased the induction of *Bmp4* and *Bmp6* respectively, with no change in the induction of *Bmp2* (**Figure 27A).**

Dynamic changes to BMP antagonist induction also occurred with changes in *Grem2* expression. The antagonists that exhibited a modest induction in *WT* mice post-MI were analyzed (*Dan* and *Noggin*). The expression level of *Grem2* directly correlated with the induction of *Dan.* However the loss-of Grem2 resulted in an increase in the induction of *Noggin* and gain-of Grem2 function did not affect *Noggin* levels (**Figure 27B**).

To assess if the level of *Grem2* expression affects the induction levels of BMP signaling target genes, *Id2* induction was analyzed since this was the only BMP target gene that exhibited a significant increase in *WT* mice post-MI. As expected, levels of *Grem2* expression inversely correlated with the induction of *Id2* at 7 days post-MI (**Figure 27C**). These results suggest that *Grem2* is acting as a canonical BMP signaling antagonists during this time.

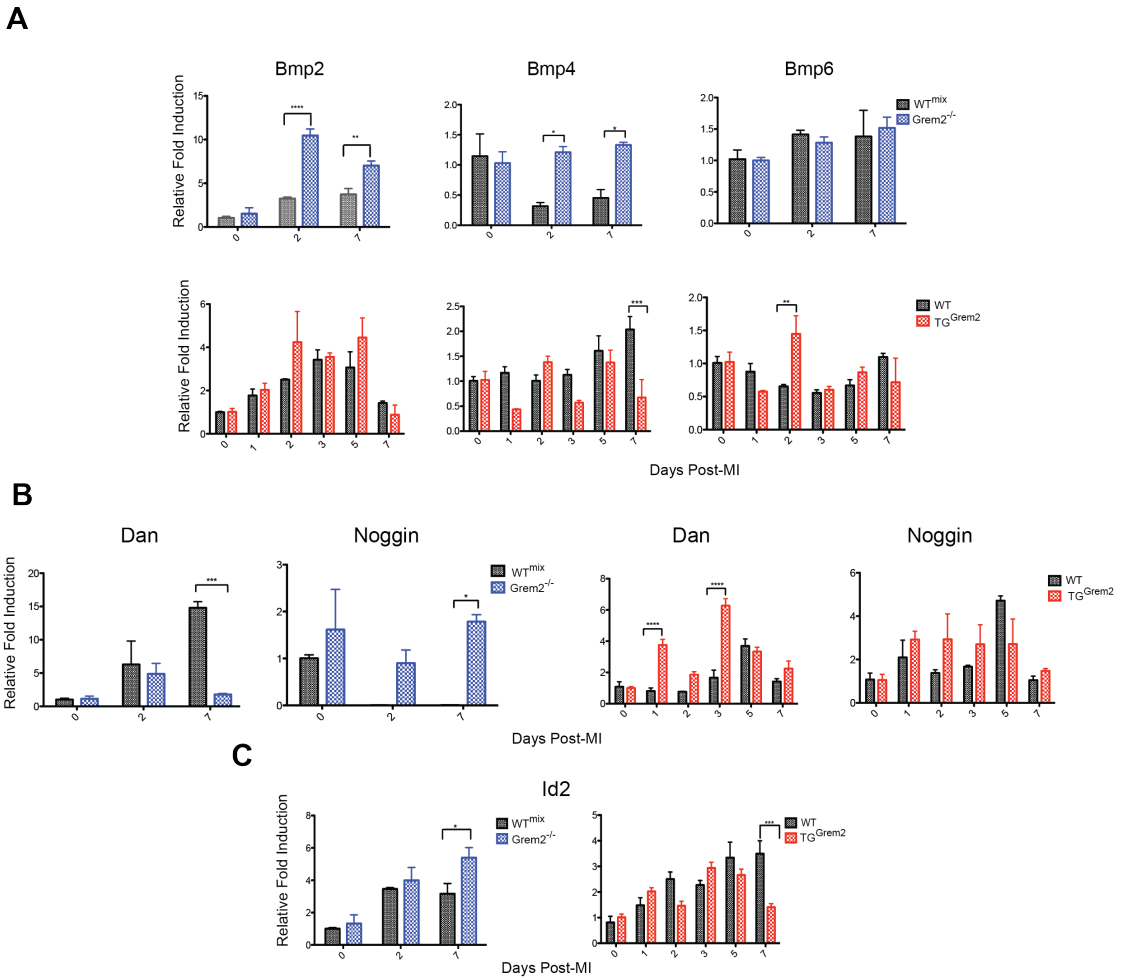

Figure 27. Dynamic changes in the expression of BMP pathway components occurs in both *Grem2* loss-of and gain-of function models. qPCR analysis of whole heart RNA samples isolated from *WT^{mix}*, *Grem2$^{-/-}$*, *WT,* and *TG^{Grem2}* mice at the indicated days post-MI. **(A)** Changes to the level of *Grem2* lead to changes in the induction of Bmp ligands, where the loss of *Grem2* lead to an increase in *Bmp2* and *Bmp4* induction and the gain of *Grem2* lead to a decrease and an increase in *Bmp4* and *Bmp6* respectively. **(B)** Changes to the level of *Grem2* lead to changes in the induction of Bmp antagonists, where *Dan* induction levels directly correlated with the level of *Grem2* and the loss of *Grem2* lead to an increase in *Noggin* induction. **(C)** *Grem2* levels are inversely correlated with the induction of the Bmp pathway target gene *Id2.* P < 0.05*; *** P < 0.01*; **** P< 0.001; ****P<0.0001*. Two-way ANOVA with Bonferroni multiple comparisons test. N=3 for all time points. All data are means ± SEM.

However, despite the fact that dynamic changes occur in these BMP pathway component genes, most genes do not exhibit effects that are dependent upon *Grem2* expression levels. Therefore it is difficult to make any conclusion that *Grem2* affects the expression of these genes, which is corroborated by their timing of peak induction in *WT* mice post-MI (CHAPTER II). It is more likely that

the changes observed are due to systemic changes that occur in order to compensate for the level of *Grem2*.

Grem2 regulates canonical BMP signaling in border zone cardiomyocytes

Grem2 is known to inhibit the canonical BMP signaling pathway by preventing BMP ligand-mediated phosphorylation of Smad1/5/8 and activation of target gene transcription (Nolan et al., 2013; Sudo et al., 2004). To test whether Grem2 regulates canonical BMP signaling in the heart, we analyzed cardiac tissue sections at day 7 after MI from *WT*, *Grem2*$^{-/-}$ and *TG*^{Grem2} mice. IF staining with antibodies recognizing expression of the target gene *Id2* showed that *Id2* is increased in the *Grem2*$^{-/-}$ animals compared to *WT* controls, however the increase in *Id2*$^{+}$ cells could be due the increase in the number of what are likely inflammatory cells in the infarct area (**Figure 28A**). However, despite the fact that the BMP target gene Id2 is present in infiltrating cells, leukocytes (CD45, red) do not show active canonical BMP signaling activity (p-Smad1/5/8, green), demonstrating that inflammatory cells are not the target cells of Grem2 (**Figure 28B**). IF staining with antibodies recognizing the phosphorylated, i.e., active form of Smad1/5/8, showed that intensity of p-Smad1/5/8 was increased in *Grem2*$^{-/-}$ mice and decreased in *TG*^{Grem2} hearts as compared to *WT*s (**Figure 28C,D**). However, unlike the early stages after MI (**Figure 10D**), we did not detect p-Smad1/5/8 in endothelial cells.

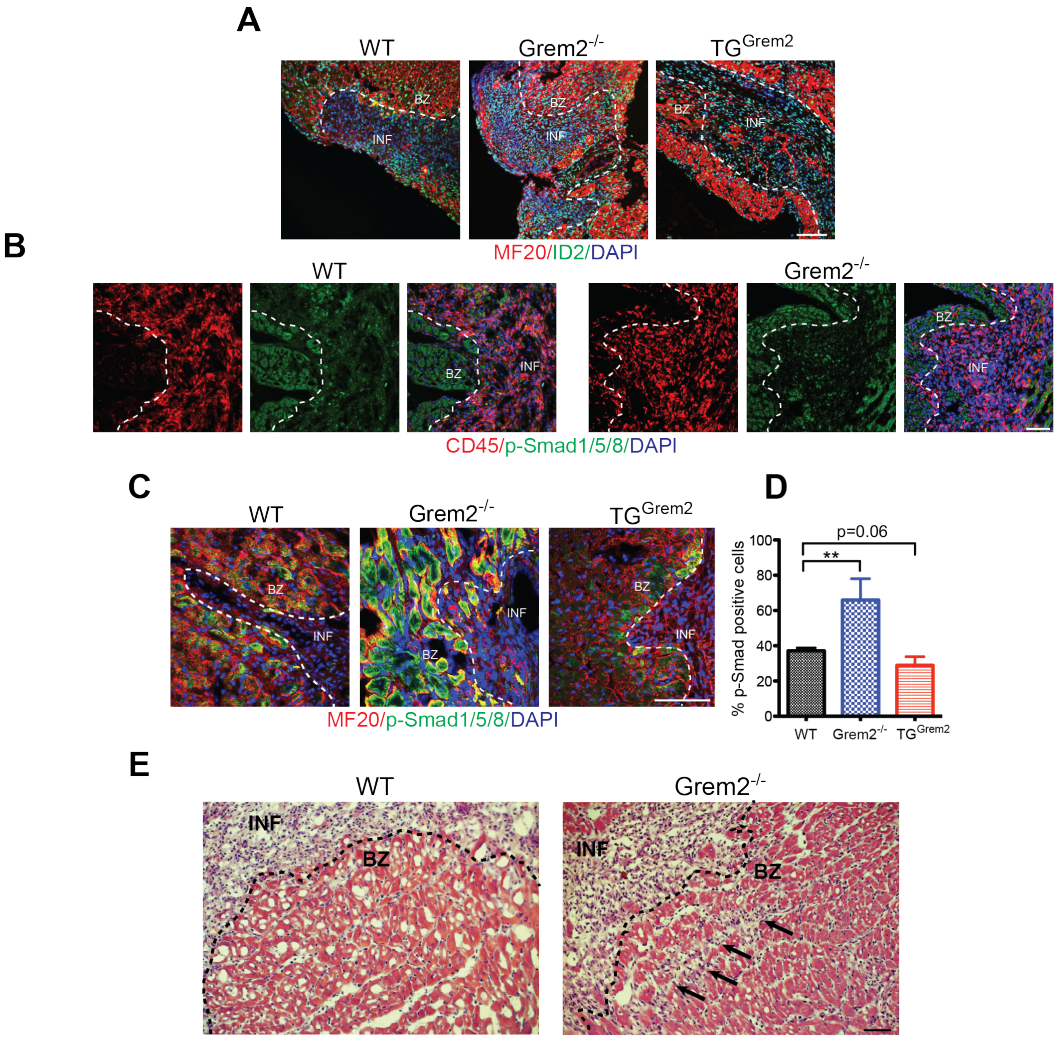

Figure 28. Grem2 regulates canonical BMP signaling in peri-infarct area cardiomyocytes. (A) IF analysis of cardiac tissue sections 7 days post-MI using antibodies recognizing Id2 (green) and Myosin Heavy Chain (MF20, red) shows that BMP signaling is increased*Grem2*$^{-/-}$ mice compared to *WT* counterparts. DAPI marks cellular nuclei. Scale bars, 100 μm. BZ=infarct border zone; INF=infarct. **(B)** IF analysis of cardiac tissue sections 5 days post-MI using antibodies recognizing p-Smad1/5/8 (green) and CD45, (red) shows that BMP signaling is not active in infiltrating inflammatory cells of *WT* and *Grem2*$^{-/-}$ hearts. DAPI marks cellular nuclei. Scale bars, 100 μm. BZ=infarct border zone; INF=infarct. **(C)** IF analysis of cardiac tissue sections 7 days post-MI using antibodies recognizing p-Smad1/5/8 (green) and Myosin Heavy Chain (MF20, red) shows activation of canonical BMP signaling in cardiomyocytes in the peri-infarct border zone. DAPI marks cellular nuclei. The number of p-Smad1/5/8+ cardiomyoctyes is increased in *Grem2*$^{-/-}$ mice and decreased in *TG*^{Grem2} mice. Scale bars, 100 μm. BZ=infarct border zone; INF=infarct. **(D)** Quantification of p-Smad1/5/8^{+} cells in the infarct border zone as percentage of total MF20^{+} cells per viewing area between *WT*, *Grem2*$^{-/-}$, and *TG*^{Grem2} mice. ** *P < 0.01*. Student's two-tailed unpaired *t*-test. N=3. All data are means ± SEM. **(E)** Hematoxylin/eosin staining 5 days post-MI shows that inflammatory cell infiltration (arrows) beyond the infarct border (dotted line) is greater in the *Grem2*$^{-/-}$ mice compared to *WT* counterparts. Scale bars, 10 μm. BZ=border zone, INF=infarct.

The p-Smad changes overlap with the Grem2 expression domain (Chapter II) in peri-infarct area cardiomyocytes, suggesting Grem2 acts as a barrier to limit the infiltration of inflammatory cells into neighboring, relatively

healthy cardiac tissue. In agreement with this notion, we observed inflammatory cells in the peri-infarct tissue past the infarct border zone in *Grem2*$^{-/-}$ hearts, whereas inflammatory cells were confined within the infarct area in *WT* controls (**Figure 28E**).

Inflammatory cell infiltration post-MI is regulated by canonical BMP signaling

To test whether the increased inflammatory cell infiltration is due to p-Smad1/5/8 mediated signaling, we injected *Grem2*$^{-/-}$ mice with the canonical BMP signaling chemical inhibitor DMH1 (Ao et al., 2012) and vehicle control (DMSO) on day 2, 3, and 4 after MI, which correspond to the peak days of inflammation. DMH1 is highly specific to canonical BMP signaling without known off-target effects, as tested in various mouse disease models (Owens et al., 2015; Ao et al., 2012; Hao et al., 2014; Sun et al., 2013). We found that DMH1 treatment rescued the pro-inflammatory phenotype in *Grem2*$^{-/-}$ mice. Flow cytometry analysis at day 5 after MI showed that treated *Grem2*$^{-/-}$ hearts had a dramatic decrease in infiltrated leukocytes ($CD45^+$), monocytes ($Ly6C^+$), and macrophages ($F4/80^+$) as compared to vehicle injected controls (**Figure 29**).

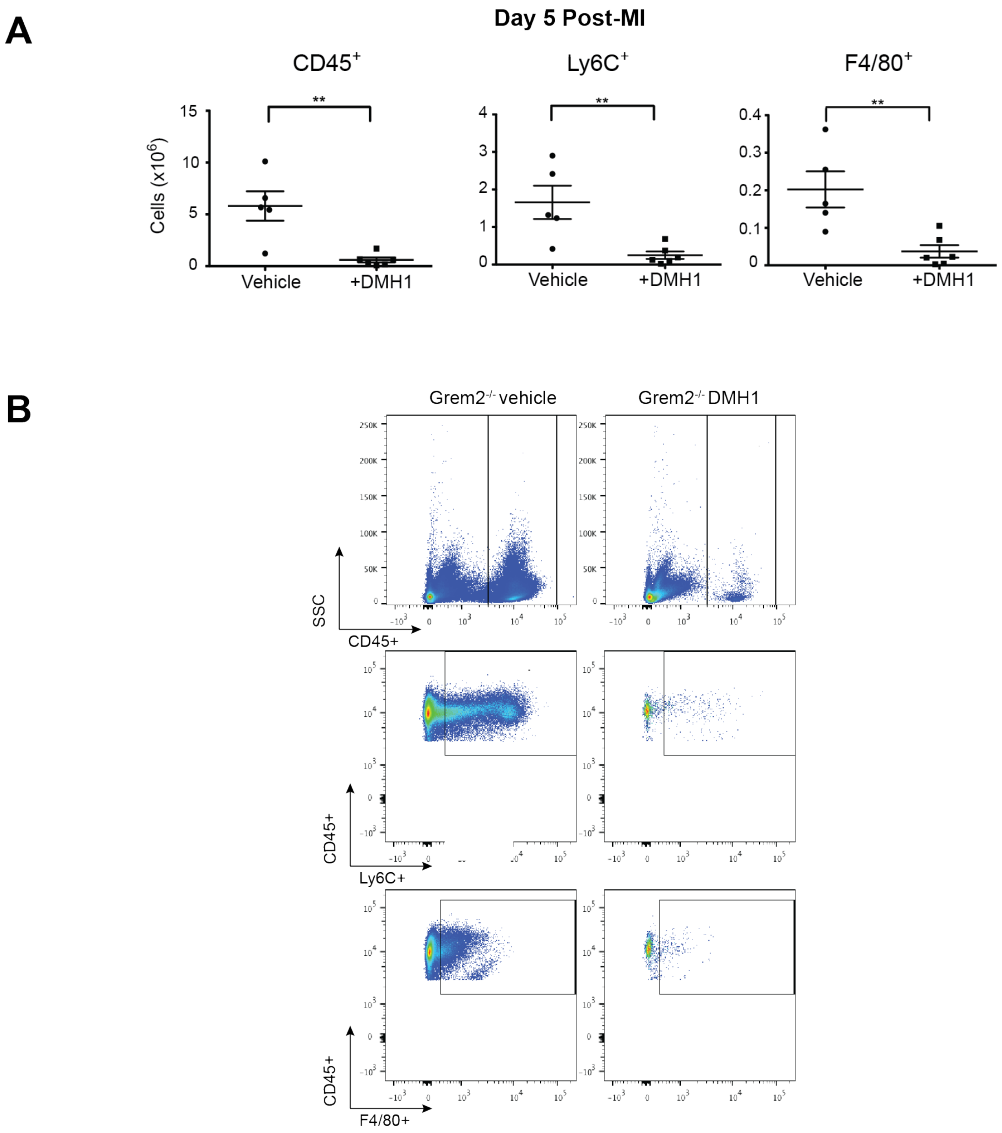

Figure 29. Flow cytometry of inflammatory cells in the heart of *Grem2*$^{-/-}$ mice treated with the canonical BMP signaling inhibitor DMH1. (A) *Grem2*$^{-/-}$ mice were injected once daily via IP with either the canonical BMP signaling inhibitor DMH1 or vehicle (DMSO) 2 days, 3 days, and 4 days post-MI. Number of total CD45,$^{+}$Ly6C^{+} and F/480^{+} cells in whole hearts at 5 days post-MI were determined by flow cytometry. DMH1 injected mice have a decreased inflammatory cell infiltration compared to vehicle controls. *** P < 0.01*. Student's two-tailed unpaired *t*-test. Vehicle N=5, +DMH1 N=6. Bars represent means ± SEM. **(B)** Representative flow cytometry graphs of CD45^{+}, Ly6C^{+} and F4/80^{+} cells conducted on whole heart single cell suspensions of non-cardiomyocyte cells 5 days after MI. Cells were isolated from *Grem2*$^{-/-}$ mice after administration on days 2, 3, and 4 after MI of the chemical compound DMH1, which specifically inhibits canonical, i.e., p-Smad-mediated BMP signaling. *Grem2*$^{-/-}$ mice injected with DMSO vehicle served as controls. SSC=side scatter.

Discussion

Our data indicate that BMP signaling plays an important role in the cardiac repair process after MI. Although it was known that BMP ligands cause cardiomyocyte apoptosis during the early stages of ischemia/reperfusion injury,

to our knowledge, ours is the first study to show that canonical BMP signaling activation after MI controls the magnitude of the inflammatory response. Specifically, our data indicate that in the absence of Grem2, increased p-Smad-mediated BMP signaling in the infarct border-zone is responsible for excessive infiltration of inflammatory cells. Canonical BMP signaling is also responsible for limiting inflammatory cell infiltrate, since canonical BMP inhibition rescues the loss-of-Grem2-phenotype. Taken together, inhibition of canonical BMP signaling is required to limit the extent and spread of the inflammatory response following an acute cardiac injury, and Grem2 may be critical in reducing and eventually stopping the recruitment of circulating leukocytes. Therefore, recognizing the role of BMP signaling and the mechanisms of its inhibition in cardiac tissue repair after MI may offer novel insights in the cardiac healing process and provide new ways to regulate inflammation in a physiological manner.

Due to the wide interest in regulating BMP signaling in bone fractures, osteoporosis and cancer (Gao et al., 2012; Hayashi et al., 2009; Khosla et al., 2008; Kua et al., 2012; Sneddon et al., 2006; Tang et al., 2013; Yan et al., 2014), a number of chemical compounds and peptides, to either promote or hinder BMP signaling, are being developed for clinical use (Cao et al., 2014; Sanvitale et al., 2013; Yu et al., 2008). Our findings may facilitate future repurposing of these new pharmacological resources for potential treatment of MI patients to expand current strategies that aim to restore circulation to infarcted areas with thrombolytics and percutaneous interventions.

Despite our current data demonstrating that Grem2 limits inflammation by inhibiting canonical BMP signaling post-MI, the possibility remains that other pathways could be regulated by changes in the expression of Grem2. Our previous work in mouse embryonic stem cells illustrated Grem2 treatment resulting in a counter activation of the non-canonical BMP signaling component, JNK (Tanwar et al., 2014), therefore Grem2 is capable of acting in ways that differ from its classical role as a canonical BMP antagonist. The ability of Grem2 to act in this way could lead to downstream effects on other pathways during the cardiac repair process, such as the JNK pathway, the Wnt pathway, and the TAK pathway, all of which have been implicated to be either regulated by Grem2 or BMP signaling as well as induced post-MI (Matsumoto-Ida et al., 2006; Pachori et al., 2010; Paik et al., 2015; Wu et al., 2015; Yamaguchi et al., 1999). Determining if Grem2 has an effect on the activation of these pathways during cardiac repair will be the topic of future investigations.

Besides determining that BMP signaling is involved in the regulating the inflammatory response post-MI, the context and exact mechanism of action remains to be elucidated. Since pro-inflammatory cell adhesion molecules bring circulating leukocytes into the site of injury, it is possible that Grem2 limits the magnitude of inflammation through inhibiting the pro-inflammatory effect of BMP2 in these cells. Molecular insight into how exactly Grem2 limits inflammation is the topic of the subsequent chapter.

Acknowledgements

I thank members of the Cardiovascular Pathophysiology and Complications Core of the Mouse Metabolic Phenotyping Center, the Cell Imaging Shared Resource, the Translational Pathology Shared Resource, the Transgenic Mouse/ES Cell Resource, and the Molecular Cell Biology Resource at Vanderbilt University Medical Center for technical assistance. This work also utilized the core(s) of the Vanderbilt Diabetes Research and Training Center funded by grant 020593 from the National Institute of Diabetes and Digestive and Kidney Disease. I thank Lianli Ma, and Lin Zhong for performing mice surgeries; Mark Magnuson and Jennifer Skelton for generation of the Grem2 mouse lines; Daniel Levic and Ela W. Knapik for help with histological analyses; and David T. Paik for assistance in providing mouse heart samples for histological analysis.

CHAPTER VI

GREM2 INHIBITS THE PRO-INFLAMMATORY EFFECT OF BMP2 ON ENDOTHELIAL CELLS

Introduction

BMP signaling has previously been shown to be pro-inflammatory in several vascular disease states (Simões Sato et al., 2014; Sorescu et al., 2003). The majority of this work provides evidence that BMP signaling exerts these pro-inflammatory effects on endothelial cells, specifically by increasing their expression of pro-inflammatory cell adhesion molecules (Csiszar et al., 2005, 2006; Sucosky et al., 2009). BMP signaling antagonists such as BMPER and Noggin are able to inhibit this effect (Helbing et al., 2011; Koga et al., 2013; Pi et al., 2012).

Work described in the previous chapters demonstrates that canonical BMP signaling is induced during the inflammatory phase of cardiac repair within border zone endothelial cells and later in border zone cardiomyocytes, and is responsible for increasing the magnitude of inflammation as evidenced by loss and gain of function models of the BMP antagonist Grem2 as well as through injection of the canonical BMP signaling inhibitor DMH1. Grem2 is also induced directly after the peak of BMP2 ligand induction. Therefore Grem2 exerts autocrine effects on these cardiomyocytes in order to limit inflammation. However BMP ligands and antagonists, including Grem2, are secreted proteins and are

likely to have paracrine effects on neighboring cell types. Therefore in order to gain a greater insight on the molecular interplay between BMP signaling, Grem2, and inflammation, we used a human endothelial cell line in order to delve into the activation of the inflammatory response through the induction of pro-inflammatory cell adhesion molecules present on these cell types.

Materials and methods

Cell culture

Human Microvascular Endothelial cells (HMECs) (Ades et al., 1992) were kindly provided by Dr. Sergey Ryzhov. Cells used for experiments were between the third and fourth passages and cultured in 199 media (Gibco 11150) containing 15% FBS, 10 U/ml Heparin (Sigma), and 30 µg/ml endothelial cell growth supplement (Biomedical Technologies). Cells were grown in full growth serum and then seeded in 12-well plates. Prior to growth factor addition, cells were incubated with serum starvation media (same as normal media with 1% FBS) over night. Cells were subsequently treated with rhTNF (R&D; 10 ng/ml), rhBMP2 (R&D; 100 ng/ml-250 ng/ml), Grem2 (100 ng/ml), and DMH1 (10µM) or the equivalent volume of vehicle solution (PBS or DMS0). After 4 hours, 24 hours, or 48 hours of treatment, cells were lysed for RNA extraction. Data is representative of at least two independent experiments.

For binding assays, HMEC cells were grown for three days until they reached monolayer confluency (3 x 10^4 cells/well within a 96-well plate). Calcein AM labeled (1 µM, 30 min) human monocytes (THP-1 cells) were added to the

HMEC monolayer at a concentration of 10 x 10^4 cells per well (EC:THP-1 ratio – 1:3) and incubated together for 30 minutes. After incubation, non-adherent THP-1 cells were aspirated off and the remaining cells were washed with PBS 5 times. The fluorescence intensity was measured using the Modulus microplate multimode reader. The number of adherent THP-1 cells was calculated from a calibration curve prepared using increasing concentrations (ranging from 0.1 to 100 x 10^3 cells) of THP-1 cells. 300 ng/ml of BMP2, 100 ng/ml of Grem2 and 100ng/ml of TNFα were used alone or combination for 24 hours.

RNA analysis by Reverse Transcription and quantitative Polymerase Chain Reaction (RT-qPCR)

See CHAPTER II. RNA was obtained from cells in culture using the RNeasy Mini Kit (Qiagen). The sequences of gene-specific primers for this chapter have also been included in **Table 1**.

Statistical Analysis

Statistical analysis was performed using GraphPad Prism software. Data are represented as the mean ± SEM. Student's two-tailed unpaired *t*-test was used for comparison between two groups, *one-way ANOVA* was used to compare multiple groups, and *two-way ANOVA* was used to compare gene induction in each mouse model over time. Dunnett's and Bonferroni's multiple comparisons test was used post-hoc. **P<0.05*, ***P<0.01*, ****P< 0.001, ****P<0.0001* were considered significant.

Results

Grem2 inhibits the pro-inflammatory effect of Bmp2 on endothelial cells

The data described above indicate that secretion of Grem2 protein by peri-infarct cardiomyocytes affects directly or indirectly the pro-inflammatory phenotype of cardiac endothelial cells and that canonical BMP signaling is induced in endothelial cells during the inflammatory phase. Further gene expression analysis at various time points after MI showed that *TN* is induced first, followed by *Bmp2* and then *Grem2* (**Figure 30A**). To investigate whether the sequential temporal induction patterns of the three genes after MI are linked; we tested the effects of TNFα, BMP2 and Grem2 on the human microvascular endothelial cell line HMEC-1. We found that TNFα induces expression of *E-SELECTIN* and *BMP2*, suggesting early pro-inflammatory cytokines contribute to the induction of the *Bmp2* gene after MI *in vivo* (**Figure 31** and **Figure 30B**). BMP2 in turn induces *E-SELECTIN* expression in endothelial cells as well as Grem2, suggesting BMP2 induces a negative regulatory loop to limit its own activity (**Figure 30C, D**).

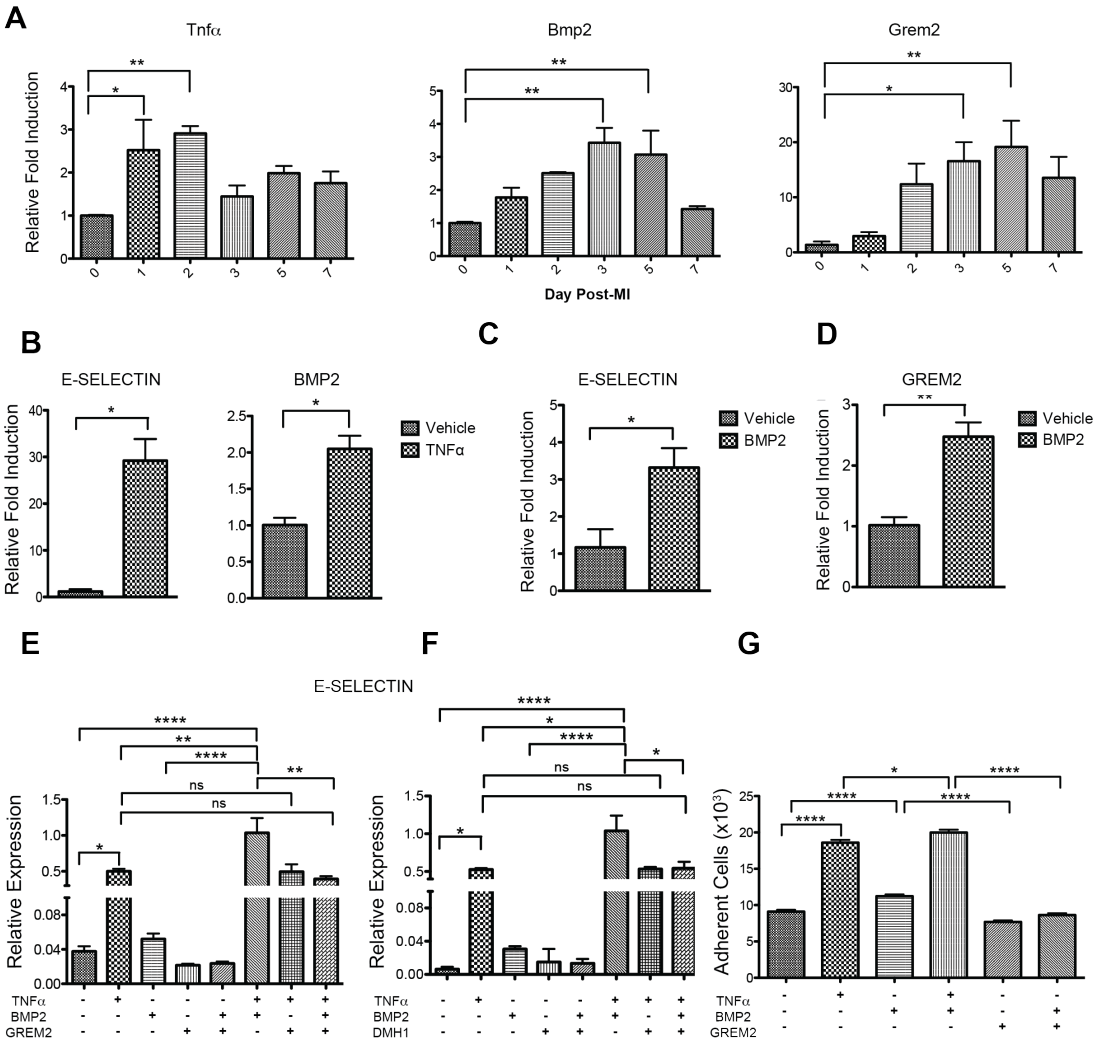

Figure 30. Grem2 inhibits the pro-inflammatory effect of BMP2 on endothelial cells. (A) qPCR analysis of whole heart RNA samples isolated from WT mice at days 0, 1, 2, 3, 5 and 7 post-MI shows sequential induction of Tnfα, Bmp2 and Grem2 during the cardiac repair process. ** P < 0.05; ** P < 0.01*. One-way ANOVA with Dunnett's multiple comparisons test. N=3 for all time points. All data are means ± SEM. **(B)** qPCR analysis of RNA samples isolated from Human Microvascular Endothelial Cells (HMEC) at 4 hours (left) and 24 hours (right) after TNFα treatment shows TNFα induces *E-SELECTIN* and *BMP2* expression. ** P < 0.05*. Student's two-tailed unpaired *t*-test. N=3 per group. All data are means ± SEM. **(C, D)** qPRC analysis shows BMP2 induces *E-SELECTIN* and *GREM2* in HMEC cells after 24 hours. ** P < 0.05;**P<0.01*. Student's two-tailed unpaired *t*-test. N=3 per group. All data are means ± SEM. **(E,F)** qPCR analysis of RNA sample isolated from HMEC 24 hours after treatment with TNFα, BMP2, Grem2 and DMH1 in different combinations as indicated. **(E)** TNFα and BMP2 together super induce expression of *E-SELECTIN*. Grem2 specifically inhibits the BMP2 effect, but has no effect on the *E-SELECTIN* induction by TNFα. **(F)** Canonical BMP signaling inhibitor DMH1 specifically inhibits the BMP2-induced *E-SELECTIN*. ns=not significant, ** P < 0.05; ** P < 0.01; **** P < 0.0001*. One-way ANOVA with Dunnett's multiple comparisons test. N=3 for all treatments. All data are means ± SEM. **(G)** Adhesion of human monocytes (THP-1 cells) to HMEC cells was measured after HMEC cells incubation with TNFα, BMP2, or in combination for 24 hours. TNFα and BMP2 induce binding of endothelial cells to monocytes. Grem2 specifically inhibits the BMP2 effect. ** P < 0.05; **** P < 0.0001*. One-way ANOVA with Bonferroni's multiple comparison test. N=36. All data are means ± SEM.

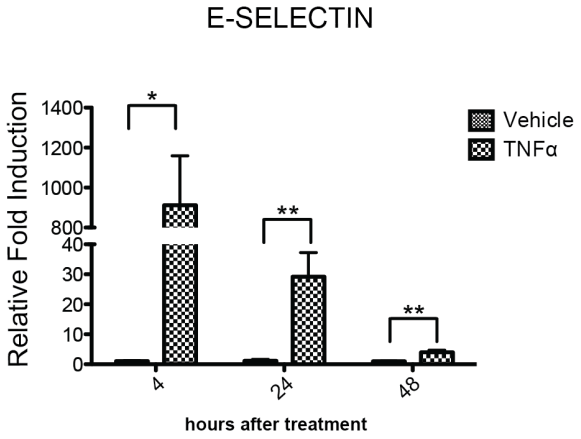

Figure 31. TNFα leads to early and transient *E-SELECTIN* induction. qPCR analysis of RNA samples isolated from Human Microvascular Endothelial Cells (HMEC) at 4, 24, and 48 hours after TNFα treatment shows TNFα induces *E-SELECTIN* expression at early time points (4, and 24 hours), but *E-SELECTIN* levels decline close to baseline at 48 hours. **P < 0.05*; *** P < 0.01*. Two-way ANOVA with Bonferroni multiple comparisons test. N=3 per group for all time points. All data are means ± SEM.

To determine whether: a) BMP2 acts synergistically with TNFαand, b) Grem2 blocks the pro-inflammatory effect of BMP2 on endothelial cells, we treated HMEC-1 with TNFα, BMP2 and Grem2 in different combinations (**Figure 30E, Figure 32**). When protein factors were added alone, both TNFαand BMP2 induced *E-SELECTIN* expression. Co-stimulation with TNFα and BMP2 led to *E-SELECTIN* induction levels higher than either factor alone, suggesting TNFα and BMP2 have a synergistic or additive effect. Grem2 did not affect the TNFα induction of *E-SELECTIN*, but completely inhibited the BMP2 effect. In similar fashion, co-incubation with TNFα, BMP2 and Grem2 specifically abrogated the BMP2 effect, reducing *E-SELECTIN* levels to those induced by TNFα treatment alone (**Figure 30E**). In accordance with its function as a canonical BMP signaling antagonist, Grem2 blocked induction of BMP signaling target *ID2*, whereas TNFα alone had no effect on *ID2* expression, although it reduced the

fold induction of *ID2* by BMP2 **(Figure 32**). Treating cells with the chemical inhibitor of canonical BMP signaling DMH1 showed similar effects as Grem2, indicating that that BMP2-induction of *E-SELECTIN* is due to activation of canonical BMP signaling (**Figure 30F**).

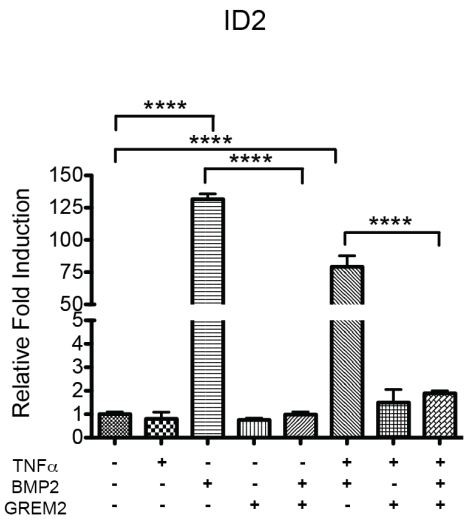

Figure 32. Grem2 inhibits canonical BMP signaling in endothelial cells. *ID2* induction in endothelial cells is completely inhibited by Grem2. TNFα has a moderate effect on BMP2-mediated *ID2* induction. ***** P < 0.0001*. One-way ANOVA with Dunnett's multiple comparisons test. N=3 for all treatments. All data are means ± SEM.

To test the functional significance of the modulation of pro-inflammatory gene expression in endothelial cells by Grem2, we performed cell adhesion assays of monocytes to endothelial cells *in vitro* in collaboration with Dr. Sergey Ryzhov. These assays showed that pre-incubation of endothelial cells with BMP2 increased adhesion of monocytes to endothelial cells and further enhanced the TNFα effect. Incubation with Grem2 abolished the BMP2 effect, but not that of TNFα (**Figure 30G**). In contrast, pre-incubation of monocytes with BMP2 and/or Grem2 had no effect on their adhesion to endothelial cells

(**Figure 33**). Moreover, immunofluorescence analysis of infarct areas with antibodies recognizing p-Smad1/5/8 and CD45 to determine canonical BMP signaling activity in infiltrating inflammatory cells showed no detectable p-Smad1/5/8 i.e., canonical BMP signaling in inflammatory cells, and this pattern did not change in the *Grem2*$^{-/-}$ mice (CHAPTER V, **Figure 28B**). These data further support the idea that the primary cellular targets of Grem2 are the endothelial cells.

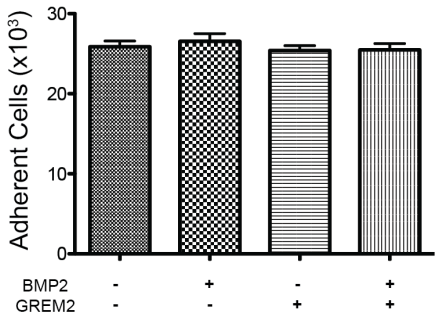

Figure 33. Grem2 acts specifically on endothelial cells. Incubation of human monocytes (THP-1 cells) with BMP2, Grem2, or in combination did not alter binding to endothelial cells (HMEC). N=12. All data are means ± SEM.

Discussion

In conclusion, we provide evidence to suggest that pro-inflammatory cytokines such as Tnfα induces *Bmp2* and Bmp2 further increases the pro-inflammatory phenotype of endothelial cells. BMP2 then induces the expression of its own antagonist, *Grem2* as a negative feedback loop, thereby inhibiting canonical BMP signaling and the positive effect of Bmp2 on inflammatory gene expression.

Histological analysis demonstrated that Grem2 as well as canonical BMP signaling components are produced in peri-infarct cardiomyocytes, however

canonical BMP signaling is also present in endothelial cells (CHAPTERS II and V). Therefore, Grem2 acts both in an autocrine fashion to inhibit p-Smad activation in cardiomyocytes, as well as in a paracrine fashion to suppress expression of the pro-inflammatory genes in adjacent endothelial cells.

This induction of Grem2 appears to be an integral part of an orchestrated sequence of events that regulates the inflammatory response. Our *in vitro* analyses suggest that this sequence starts with induction of Bmp2 by Tnfα, which is released shortly after cardiac tissue injury. Bmp2 then further increases the Tnfα effect in the induction of pro-inflammatory cell interaction membrane proteins in endothelial cells, as the Tnfα effects decrease. The pro- inflammatory action of Bmp2 is then blocked by Grem2, which itself is induced by Bmp2, thus forming a negative regulatory loop. This concept is supported by *in vivo* data, which show sequential induction of *Tnf*α, *Bmp2* and *Grem2* after MI, each approximately 24 hours apart. The *in vitro* assays that show BMP2 acts on endothelial cells to promote cell adhesion of monocytes, the consistent changes in the number of inflammatory cells across a wide spectrum of various immune cell types, and histological analyses showing minimal changes in BMP signaling in infiltrating leukocytes, all suggest that the main cellular target of Grem2 in the regulation of the inflammatory response in the heart are the endothelial cells. However, at present we cannot exclude that Grem2 may also affect the inflammatory cell differentiation, activation or mobilization prior to their recruitment in the infarct area.

We have previously shown that Grem2 promotes the cardiogenic potential of mouse ES cells (Tanwar et al., 2014). Interestingly, we found that Grem2 has distinct biological effects from other BMP antagonists such as Noggin, Cerberus-like 1 and Dan on cardiac differentiation of ES cells, suggesting a Grem2-specific and unique mechanism of BMP signaling regulation (Tanwar et al., 2014). While the mechanism for how Grem2 blocks BMP-ligand receptor interactions is unknown, it is likely that structural differences of the antagonists give rise to distinct binding strategies. We currently test whether the unique structural arrangement of Grem2 is also critical for its function in cardiac repair. Future biochemical analyses may identify critical structural motifs, which could be exploited to design molecules that would mimic the Grem2 biological effects in the attenuation of inflammation.

To summarize the data presented thus far, we have determined a mechanism whereby Grem2 limits the magnitude and spread of inflammation post-MI by inhibiting canonical BMP signaling, which in turn inhibits the pro-inflammatory effect of BMP2 in the context of cardiac repair following an acute injury. Our data also suggests that the magnitude of inflammation has a direct correlation to cardiac functional recovery. However, it is still unclear if Grem2 affects the cellular processes that occur during the later stages of recovery. Insight into the affect of Grem2 on cellular proliferation as well as fibrosis formation will help determine how Grem2 affects these stages and is the topic of the investigations in the following chapter.

Acknowledgements

I thank the Molecular Cell Biology Resource at Vanderbilt University Medical Center for technical assistance. I also thank Dr. Sergey Rhyzov for providing the HMEC cells as well as for conducting the cell adhesion assays.

CHAPTER VII

THE ROLE OF GREM2 DURING THE PROLIFERATIVE PHASE OF RECOVERY POST-MI

Introduction

The cardiac repair process that occurs following an acute injury such as a myocardial infarction consists of several defined phases, the inflammatory phase, the proliferative phase, and the remodeling phase. After inflammation clears cellular debris, granulation tissue begins to be deposited, consisting of reparative macrophages and proliferating endothelial cells as well as fibroblasts. It is due to these populations of proliferating cells gives that this stage of recovery is called the proliferative phase. After the granulation tissue is deposited, it eventually forms into a mature collagen based scar. It is the presence of this dense inflexible scar that leads to cardiac remodeling and heart failure (Boudoulas and Hatzopoulos, 2009; Frangogiannis, 2008; Virag and Murry, 2003).

The Hatzopoulos laboratory has previously determined that other cellular processes, namely endothelial to mesenchymal transition (EndMT), play an important part of the proliferative phase of recovery (Aisagbonhi et al., 2011), as well as found that the canonical Wnt pathway regulates post-infarct angiogenesis and fibrosis (Paik et al., 2015). Aside from Wnt signaling, Tgfβ has also been implicated in the regulation of epithelial to mesenchymal transition (EMT) and fibrosis post-MI (Shinde and Frangogiannis, 2014; Zeisberg et al., 2007). Due to the fact that Grem2 has previously been linked to Wnt signaling and since its

close paralog Grem1 has been shown to be pro-fibrotic through promoting Tgfβ, we wanted to determine if Grem2 plays a role during the proliferative phase of cardiac recovery (Im et al., 2007; Li et al., 2012; Rodrigues-Diez et al., 2012).

Materials and methods

Generation of genetically engineered Grem2 mice

See CHAPTERS III and IV.

Experimental MI

See CHAPTER II.

RNA analysis by Reverse Transcription and quantitative Polymerase Chain Reaction (RT-qPCR)

See CHAPTER II. The sequences of gene-specific primers for this chapter have also been included in **Table 1**.

Immunofluorescence analyses

See CHAPTER II.

Primary antibodies used for IF analysis were as follows: rat monoclonal anti-mouse CD31/PECAM1 (BD Pharmingen; 1:100, Cat. No. 553370), rabbit anti-mouse Ki67 (Abcam 1:100 Ab15580), and rabbit anti-mouse collagen I (Abcam 1:400 Ab292).

Ki67^{+} cells were quantified using ImageJ 1.46r (NIH) color thresholding, as a percentage of cells double positive for DAPI and Ki67 amongst all DAPI positive cells in the viewing field; at least 4 viewing fields were used for calculations.

Flow Cytometry

See CHAPTER III.

Statistical Analysis

Statistical analysis was performed using GraphPad Prism software. Data are represented as the mean ± SEM. Student's two-tailed unpaired *t*-test was used for comparison between two groups, *one-way ANOVA* was used to compare multiple groups, and *two-way ANOVA* was used to compare gene induction in each mouse model over time. Dunnett's and Bonferroni's multiple comparisons test was used post-hoc. **P<0.05*, ***P<0.01*, ****P< 0.001, ****P<0.0001* were considered significant.

Results

Gain of Grem2 function results in increased endothelial cell gene expression and proliferation post-MI

Granulation tissue formation is marked by endothelial cell proliferation that acts to re-vascularize the infarcted tissue. To determine if Grem2 affects this phase of recovery, *Grem2*$^{-/-}$, *TG*^{Grem2}, and their corresponding *WT* siblings

underwent permanent LAD ligation and whole heart RNA was isolated at the indicated days after MI. qPCR analysis showed that gain of Grem2 function led an increase in the induction of genes that are involved in blood vessel formation. Vascular markers such as *Angiopoietin 1 (Ang1)* and *Ve-cadherin,* exhibited higher levels of induction in TG^{Grem2} animals compared to their respective *WT* counterparts. Conversely, the phenotype seen in the $Grem2^{-/-}$ mice was modest and not statistically significant, demonstrating that Grem2 is not required for the induction of angiogenic genes post-MI. Therefore the overexpression of Grem2 specifically results in a positive effect on vascular formation (**Figure 34A**).

To determine if *Grem2* affects the proliferation of these cells, histological analysis using antibodies for Ki67, a marker of proliferation, and CD31, a marker for endothelial cells, was conducted in $Grem2^{-/-}$, TG^{Grem2}, and *WT* controls at day 5 post-MI. The overexpression of *Grem2* resulted in an increase in $Ki67^{+}$ endothelial cells in the infarct border zone, whereas the loss of Grem2 did not result in a significant change in the number of proliferating cells (**Figure 34B, C**). Taken together with the data mentioned above, Grem2 is not necessary for the induction of the vascular gene program or proliferation of endothelial cell populations, but its overexpression promotes vascular integrity post-MI.

Flow cytometry of cardiac cells 5 days after MI, excluding cardiomyocytes, was used to determine if changes seen in gene programs and proliferation resulted in changes to the number of cells present in cardiac tissue at this time point post-MI. $Grem2^{-/-}$, TG^{Grem2}, and *WT* controls did not exhibit a significantly different amount in the number of $CD31^{+}$ endothelial cells (**Figure 34D**).

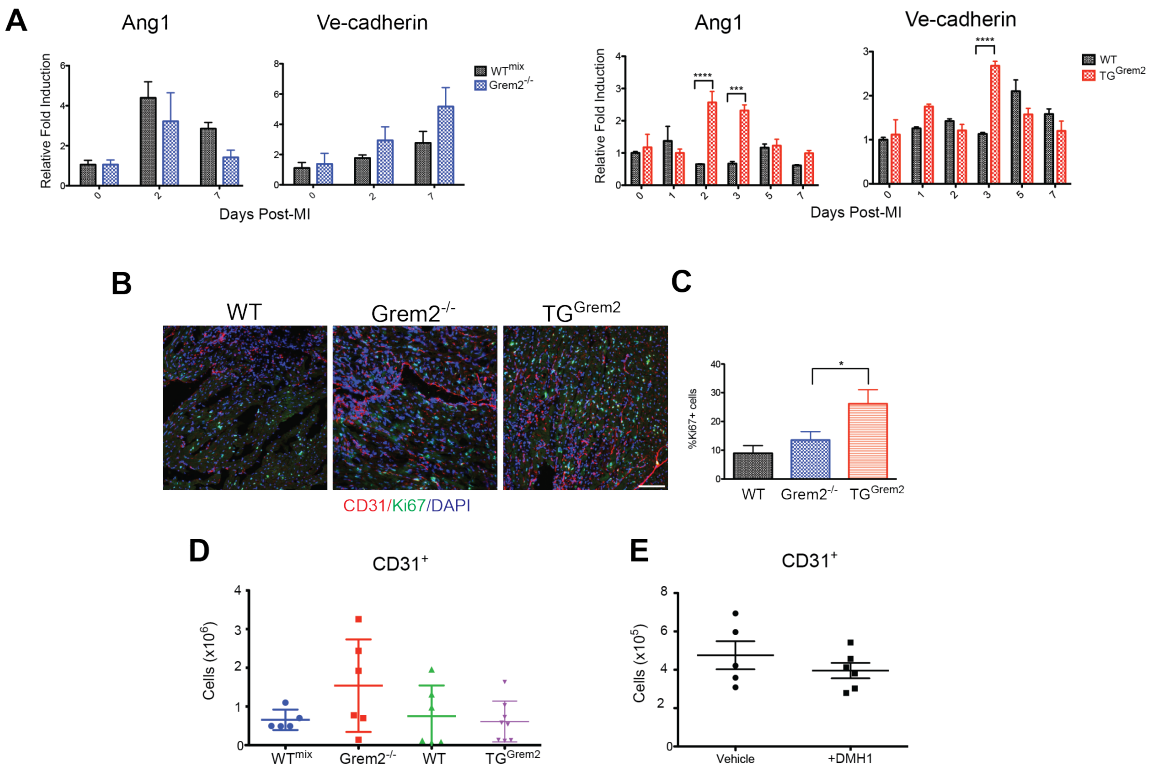

Figure 34. Grem2 alters the proliferative phase of cardiac recovery. (A) qPCR analysis of whole heart RNA samples isolated from *WT*^{mix}, *Grem2*$^{-/-}$, *WT,* and *TG*^{Grem2} mice at the indicated days post-MI shows that *Grem2* gain of function results in an increased induction of endothelial genes. *** *P< 0.001;* ****P<0.0001.* Two-way ANOVA with Bonferroni multiple comparisons test. N=3 for all time points. All data are means ± SEM. Abbreviations: *Ang1: Angiopoietin 1*. **(B)** IF analysis of cardiac tissue sections 5 days post-MI using antibodies recognizing Ki67 (green) and endothelial cells (CD31, red) shows proliferation occuring in areas close to the peri-infarct border zone. DAPI marks cellular nuclei. Scale bars, 100 μm. BZ=infarct border zone; INF=infarct. **(C)** Quantification of Ki67^{+} cells in the infarct border zone as percentage of total DAPI^{+} nuclei per viewing area between *WT*, *Grem2*$^{-/-}$, and *TG*^{Grem2} mice. The number of Ki67+ cells is increased in in *TG*^{Grem2} mice. * *P < 0.05*. Student's two-tailed unpaired *t*-test. N=3. All data are means ± SEM. **(D)** Flow cytometry analysis of single cell suspensions of non-cardiomyocyte cells isolated from whole hearts shows no significant difference in the number of CD31^{+} endothelial cells at 5 days post-MI in *Grem2*$^{-/-}$ or *TG*^{Grem2} mice compared to *WT*s. One-way ANOVA with Bonferroni multiple comparisons test. *WT*^{mix} N=5, *Grem2*$^{-/-}$ N=6; *WT* N=6; *TG*^{Grem2} N=8. Bars represent means ± SEM. **(E)** *Grem2*$^{-/-}$ mice were injected once daily via IP with either the canonical BMP signaling inhibitor DMH1 or vehicle (DMSO) 2 days, 3 days, and 4 days post-MI. Number of total CD31^{+} endothelial cells in whole hearts at 5 days post-MI were determined by flow cytometry. DMH1 injected mice have no change in the absolute numbers of these populations compared to vehicle controls. Student's two-tailed unpaired *t*-test. Vehicle N=5, +DMH1 N=6. Bars represent means ± SEM.

However, the possibility remained that BMP signaling could be responsible for regulating the level of cells present post-MI. To test whether the number of endothelial cell populations is correlated with p-Smad1/5/8 mediated signaling, we injected *Grem2*$^{-/-}$ mice with the canonical BMP signaling chemical inhibitor DMH1 (Ao et al., 2012) and vehicle control (DMSO) on day 2, 3, and 4 after MI. DMH1 is highly specific to canonical BMP signaling without known off-target

effects, as tested in various mouse disease models (Owens et al., 2015; Ao et al., 2012; Hao et al., 2014; Sun et al., 2013). We found that DMH1 treatment did not change the number of endothelial cells present in *Grem2*$^{-/-}$ mice (**Figure 34E**). Therefore, our current data demonstrates a positive role for Grem2 in vascular biology. However, it is not necessary nor results in changes to the actual vasculature of the heart post-MI.

The Wnt pathway is induced during the proliferative phase of recovery and is affected by Grem2 expression levels

Work previously published by our laboratory demonstrates that canonical Wnt signaling is induced during the proliferative phase of cardiac recovery (Aisagbonhi et al., 2011). Using qPCR analysis, we subsequently determined that a particular canonical Wnt ligand, *Wnt10b* demonstrates a peak induction that follows the induction of known components of this phase of repair such as *Tgfβ1* (**Figure 35A,** from Paik et al., 2015). Other Wnt ligands were analyzed via qPCR, however *Wnt4* was the only ligand found to be robustly induced post-MI (**Figure 35B**).

Since the overexpression of *Wnt10b* conferred positive effects on the recovery process through the induction of angiogenesis (Paik et al., 2015), we investigated if changes in the expression of *Grem2* resulted in changes to the induction of Wnt pathway components. *Grem2*$^{+/-}$, *Grem2*$^{-/-}$, *TG*^{Grem2}, and *WT* mice underwent permanent LAD ligation and whole heart RNA was isolated at the indicated days post-MI. qPCR analysis showed that changes in *Grem2*

expression were directly correlated with levels of *Wnt4* induction (**Figure 35B**). To further explore the effect of Grem2 on Wnt signaling activation, the induction level of the canonical Wnt target gene *Axin2* post-MI was analyzed in *Grem2*$^{-/-}$, *TG*^{Grem2}, and their corresponding *WT* siblings. Interestingly, the loss-of Grem2 did not affect *Axin2* induction levels, and the gain-of Grem2 function resulted in a complete lack of *Axin2* induction (**Figure 35C**). Taken together, these data demonstrate that Grem2 directly affects the induction levels of Wnt ligands, however it appears to have a negative effect on the activation of canonical Wnt signaling.

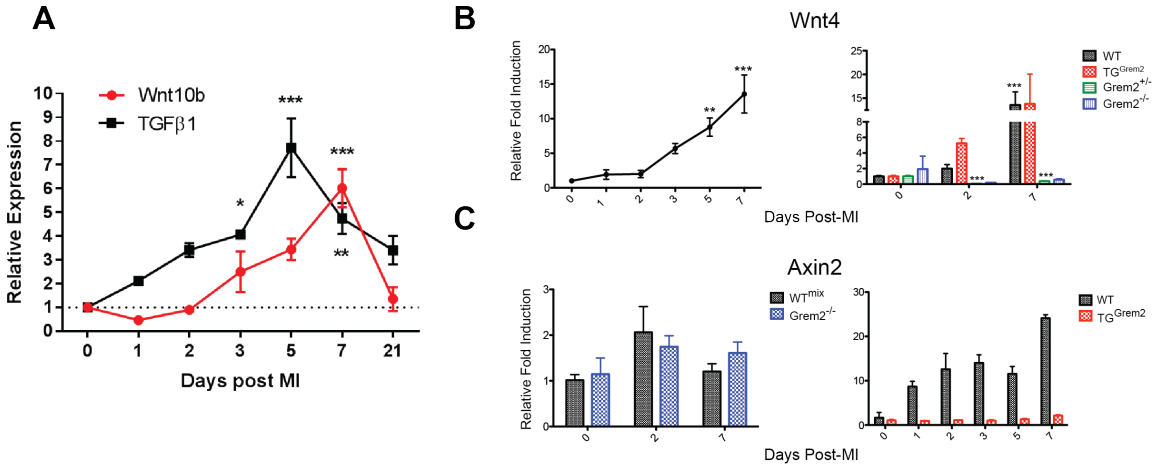

Figure 35. Wnt pathway gene induction during cardiac recovery. (A) qPCR analysis demonstrates that canonical Wnt pathway genes such as *Wnt10b* are induced after the onset of genes involved in granulation tissue formation, such as *Tgfβ1*. One-way ANOVA with Dunnett's multiple comparisons test. qPCR analysis of whole heart RNA samples isolated from *WT*^{mix}, *Grem2*$^{-/-}$, *WT,* and *TG*^{Grem2} mice at the indicated days post-MI. **(B)** Wnt pathway genes such as *Wnt4* and *Axin2* are induced during the prolierative phase of recovery. *Wnt4* induction directly correlates with Grem2 expression levels. However the opposite is true for Wnt target genes such as *Axin2* **(C)**.* *P < 0.05*; ** *P < 0.01*; *** *P< 0.001*. Two-way ANOVA with Bonferroni multiple comparisons test. N=3 for all time points. All data are means ± SEM. Panel **(A)** adapted from Paik et al *Circulation Research* 2015.

Grem2 does not affect scar formation post-MI

EndMT gene induction such as *Vimentin* was assessed via qPCR and was not affected by the overexpression of *Grem2*. The loss of *Grem2* function however, resulted in the significant increased induction of *Vimentin* post-MI

(**Figure 36A**). Genes that represent the mesenchymal or fibrotic pathway such as *Fsp-1* and α*Sma* exhibited dynamic changes in each of the *Grem2* models. *Fsp-1* was increased in both the loss-of and gain-of function models, the cause of which likely differs in each model (**Figure 36B**). The enhanced inflammatory response in the loss-of-function model could lead to an increase in the induction of pro-fibrotic genes. However, Grem2 may also itself be pro-fibrotic, due to the fact that the literature suggests its close paralog Grem1*,* is pro-fibrotic in the heart as well as in other disease states. Therefore, an increase in *Grem2* expression would lead to an increase in the induction of fibroblasts (Koli et al., 2006; Li et al., 2012; Mueller et al., 2013; Rodrigues-Diez et al., 2012)(kidney paper, EMT paper). Conversely, the induction levels of the myofibroblast marker α*Sma* exhibited an inverse correlation with the expression levels of *Grem2* (**Figure 36C**). Therefore the induction of a myofibroblast gene program may be directly affected by the extent of the inflammatory response post-MI.

Flow cytometry as described above, was used to determine if Grem2 regulated the number of fibroblasts present in cardiac tissue post-MI. *Grem2*$^{-/-}$*,* *TG*^{Grem2}*,* and *WT* controls did not contain different amounts of CD140a^{+} fibroblasts (**Figure 36D**). The inhibition of canonical BMP signaling via DMH1 treatment also did not change the number of fibroblasts present in *Grem2*$^{-/-}$ mice (**Figure 36D**). Therefore, neither Grem2 nor the inhibition of canonical BMP signaling changes the number of fibroblasts present in the heart post-MI, despite the changes seen at the gene induction level.

Due to the effect of Grem2 on the inflammatory phase of recovery as well as its effect on fibroblast gene induction, molecular and histological analysis was conducted in order to measure scar component gene induction, scar morphology, and scar size. *Grem2*$^{-/-}$, *TG*^{Grem2}, and *WT* mice underwent permanent LAD ligation and whole heart RNA was isolated at the indicated days post-MI. qPCR analysis showed that both the loss-of and gain-of Grem2 function resulted in an increased induction of *pro-Collagen Ia1 (Collagen I)* at days 7 and 3 post-MI respectively (**Figure 36E**).

Immunofluorescence using antibodies for Collagen I and CD31 was conducted in *Grem2*$^{-/-}$, *TG*^{Grem2}, and *WT* controls 7 days post-MI to determine if the changes at the RNA level can be appreciated at the histological level. Collagen I intensity and density is overall comparable between the groups (**Figure 36F**). The lack of any obvious difference in collagen intensity at day 7 post-MI could be an artifact from the timing of the analysis, since the scar is only beginning to mature at this time. In order to obtain greater insight into any possible changes in scar formation caused by Grem2, tissue sections from *Grem2*$^{-/-}$, *TG*^{Grem2}, and *WT* mice were analyzed using Masson's Trichrome staining at 21 days post-MI, when the scar is thought to be mature. The overall size of the scar was relatively comparable among all mouse groups, despite an obvious increase in cardiac hypertrophy in *Grem2*$^{-/-}$ hearts (**Figure 36G**). Taking a closer look at the morphology of the scar, it did appear that the scar in *Grem2*$^{-/-}$ mice is more loosely compact compared to *WT* counterparts and could be a

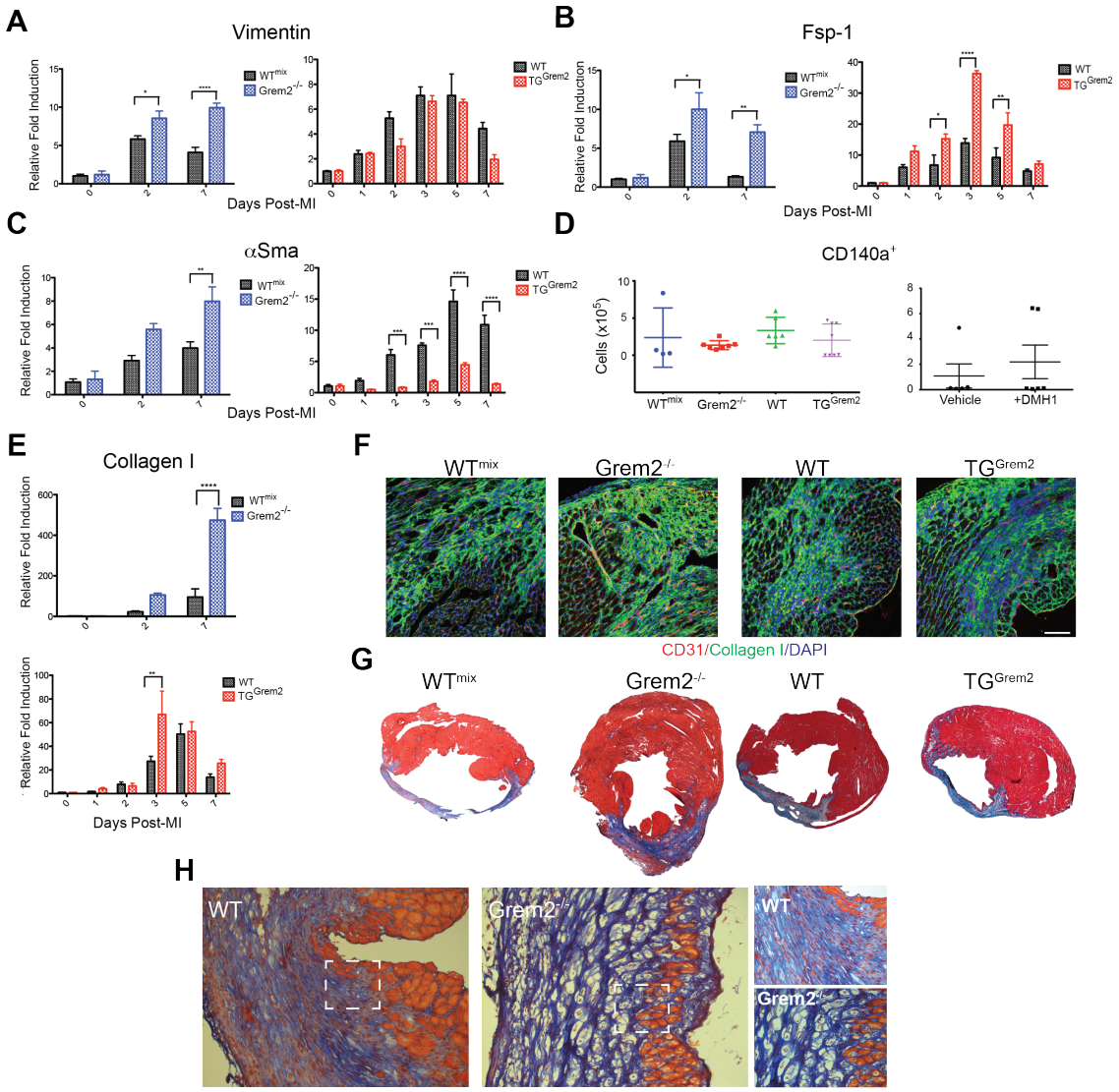

Figure 36. The fibrotic response of cardiac recovery is affected by *Grem2* expression levels. **(A-C)** qPCR analysis of whole heart RNA samples isolated from *WT*^{mix}, *Grem2*$^{-/-}$, *WT,* and *TG*^{Grem2} mice at the indicated days post-MI. **P<0.05; ** P < 0.01; *** P< 0.001; ****P<0.0001*. Two-way ANOVA with Bonferroni multiple comparisons test. N=3 for all time points. All data are means ± SEM. Abbreviation: *Fsp-1: Fibroblast specific protein-1*. **(D)** Flow cytometry analysis shows no significant difference in the number of CD140a^{+} fibroblast cells at 5 days post-MI in *Grem2*$^{-/-}$ or *TG*^{Grem2} mice compared to *WT*s or in DMH1 treated *Grem2*$^{-/-}$ mice compared to vehicle controls. One-way ANOVA with Bonferroni multiple comparisons test. *WT*^{mix} N=5, *Grem2*$^{-/-}$ N=6; *WT* N=6; *TG*^{Grem2} N=8. Student's two-tailed unpaired *t*-test. Vehicle N=5, +DMH1 N=6. Bars represent means ± SEM. **(E)** qPCR analysis of whole heart RNA samples isolated from *WT*^{mix}, *Grem2*$^{-/-}$, *WT,* and *TG*^{Grem2} mice at the indicated days post-MI shows that changes to *Grem2* expression lead to an increase in the induction of *Collagen* . *** P < 0.01*; *****P<0.0001*. Two-way ANOVA with Bonferroni multiple comparisons test. N=3 for all time points. All data are means ± SEM. **(F)** IF analysis of cardiac tissue sections 7 days post-MI using antibodies recognizing Collagen (green) and CD31 (red) indicates that there are no major differences in Collagen intensity between groups. DAPI marks cellular nuclei. Scale bars, 100 μm. **(G)** Masson's trichrome staining on heart sections 21 days post-MI indicates that the scar size is largely comparable between groups. **(H)** Masson's trichrome stain demonstrates a difference in scar morphology between *Grem2*$^{-/-}$ and *WT* mice. An inset marked in the dotted white box is provided on the right. Scale bars, 10 μm.

result of the overactive inflammatory response (**Figure 36H**). Therefore, current data suggest that Grem2 does not regulate scar size post-MI.

Grem2 affects cardiac remodeling

Following the proliferative phase of repair is cardiac remodeling. The extent of remodeling is primarily determined by the extent of the inflammatory and/or proliferative phases of recovery. Furthermore, there is a set of genes that are considered to be indicative of cardiac remodeling. In order to determine if Grem2 affects the cardiac remodeling gene program, we assessed the induction of gene such as *Mmp9*, *Nppa, Nppb,* and *β-MHC* in *Grem2*$^{-/-}$, *TG*^{Grem2}, and their *WT* counterparts at 0, 7, and 21 days post-MI (de Lemos et al., 2001; Omland et al., 1996). The genes demonstrated the same trend in both *Grem2* loss of- and gain of- function models. However, the direction of the trend was not consistent, meaning that the induction of certain genes was increased whereas others were decreased (**Figure 37**). Therefore, it is clear that Grem2 plays a role in cardiac remodeling; the nature of its role however requires further investigation.

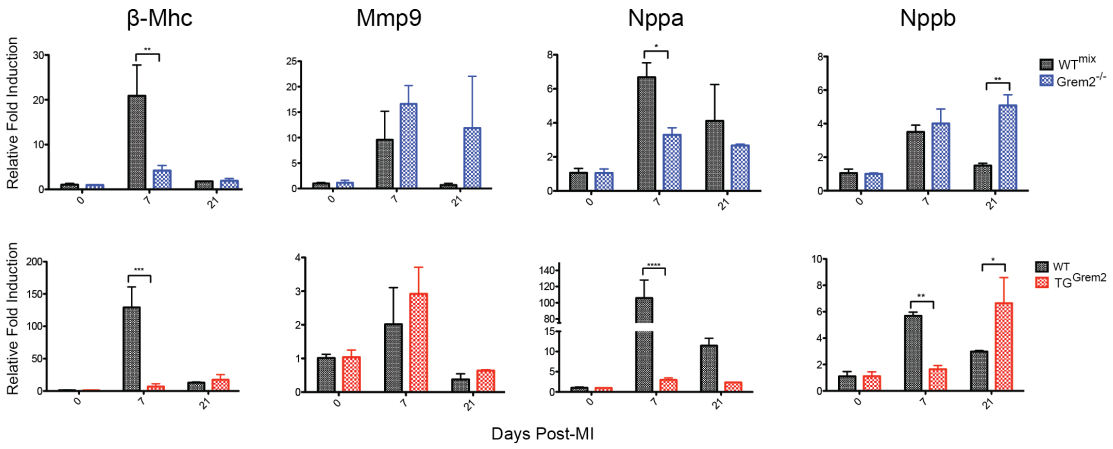

Figure 37. The cardiac remodeling gene program is affected by *Grem2* expression levels. qPCR analysis of whole heart RNA samples isolated from *WT*^{mix}, *Grem2*$^{-/-}$, *WT,* and *TG*^{Grem2} mice at days 0, 2, 7 and 21 post-MI shows that changes to the level of *Grem2* lead to changes in the induction of genes that are part of the cardiac remodeling gene program. ** P < 0.05*; *** P < 0.01*; **** P< 0.001; ****P<0.0001.* Two-way ANOVA with Bonferroni multiple comparisons test. N=3 for all time points. All data are means ± SEM. Abbreviations: *β-Mhc: β-myosin heavy chain; Mmp9: matrix metalloproteinase 9; Nppa: natriuretic peptide a; Nppb: natriuetic peptide b.*

Discussion

In conclusion, Grem2 promotes the proliferation of endothelial cells as well as the induction of pro-angiogenic gene programs. However, Grem2 expression does not appear to be required for the proliferative phase of recovery since the loss- of-function model did not exhibit dramatic phenotypic changes, nor were there changes to the actual number of endothelial cells present in cardiac tissue at day 5 post-MI. This is likely due to the fact that canonical BMP signaling is not responsible for regulating the presence of endothelial cells as demonstrated by the data obtained through the injection of DMH1. Therefore, Grem2 could be activating alternative pathways during the proliferative phase of repair, such as the JNK pathway, as we have previously demonstrated to occur during cardiac development (Tanwar et al., 2014).

Subsequently, the fibrotic phase of repair exhibited a similar trend, where Grem2 promoted the expression of genes such as *Fsp-1,* however the number of actual fibroblasts were not changed by levels of Grem2 or through chemical inhibition of canonical BMP signaling. The scar size is also comparable between all experimental groups, and although changes in Grem2 expression led to changes in the cardiac remodeling gene program, it is unclear whether Grem2 plays a positive or negative role during this phase of repair.

Despite the dramatic changes seen during inflammation as a result of changes in *Grem2* expression, the changes observed during the proliferative or remodeling phases do not correlate with the level of Grem2. Taken together, these data suggest that the phenotype seen in cardiac function post-MI (shown in

Chapters III and IV) is specifically due to the effect of Grem2 on the inflammatory phase of repair. This result is somewhat surprising, since the current belief in the field is that the extent of injury that occurs during the early phases of cardiac recovery, directly affects all the subsequent stages.

It is important to note that there are several limitations present in the current analysis. Conducting flow cytometry for endothelial cells and fibroblasts at day 5, may not be instructive, since that time point corresponds to the initiation of the proliferative phase of recovery. Flow cytometry analysis at a later time point following myocardial infarction could be more informative for determining if Grem2 regulates cell populations present during later stages of cardiac repair.

Due to the constitutive nature of the Grem2 gain of- and loss of- function animals, it is difficult to discern direct effects of Grem2 expression on the proliferative and remodeling phases of cardiac repair. Therefore, future experimentation including Grem2 treatment specifically during these phases in lieu of treatment during the inflammatory phase would be beneficial in discerning the specific role of Grem2. The same is true for determining the role of canonical BMP signaling through injection of DMH1.

In order to gain further mechanistic insight, *in vitro* models could ascertain the function of Grem2 during the proliferative and fibrotic stages of cardiac recovery. Fibroblast and endothelial cells treated with Grem2 would provide information regarding the molecular pathways and specific phenotypes Grem2 alters in these cell populations. Namely, Grem2 treatment could be used to determine if it promotes proliferation, processes such as EndMT, and if it

promotes or inhibits the production of collagen in fibroblasts. Such studies would also be instrumental in determining the target cell of Grem2 during the phases of cardiac repair following the inflammatory phase as well as determine if Grem2 affects molecular pathways other than those regulated by BMP signaling, as addressed in the next chapter.

Acknowledgements

I thank members of the Cardiovascular Pathophysiology and Complications Core of the Mouse Metabolic Phenotyping Center, the Cell Imaging Shared Resource, the Translational Pathology Shared Resource, the Transgenic Mouse/ES Cell Resource, and the Molecular Cell Biology Resource at Vanderbilt University Medical Center for technical assistance. This work also utilized the core(s) of the Vanderbilt Diabetes Research and Training Center funded by grant 020593 from the National Institute of Diabetes and Digestive and Kidney Disease. I thank Lianli Ma and Lin Zhong for performing mice surgeries; Mark Magnuson and Jennifer Skelton for generation of the Grem2 mouse lines; Vineeta Tanwar for her help with the initial mouse colony maintenance; Daniel Levic and Ela W. Knapik for help with histological analyses; and David T. Paik for assistance in providing mouse heart samples for histological analysis.

CHAPTER VIII

HIGH THROUGHPUT SEQUENCING ANALYSIS IN THE CONTEXT OF THE LOSS OF GREM2

Introduction

Grem2, also known as protein related to Dan and Cerberus is a member of the DAN family of BMP signaling antagonists. Initially discovered just over a fifteen years ago (Pearce et al., 1999) most published work to date describes its mechanism of action to be through its role as a BMP antagonist (Ideno et al., 2009; Kriebitz et al., 2009; Sudo et al., 2004). However, Grem2 is a relatively unstudied protein and dimerizes in a head to tail dimer confirmation, making its structure unique among other BMP antagonists (Nolan et al., 2013). Due to this unique tertiary structure, it remains possible that Grem2 has pleiotropic effects on previously undetermined pathways. Therefore, an unbiased methodology is required to broaden the scope of investigation in order to determine if there are any novel associations, interactions, or pathways affected by the loss of Grem2 function.

RNA-seq analysis is a shotgun approach for measuring levels of genes expression, assessing the entire transcriptome of cells or tissues (Wang et al., 2009). To conduct a thorough and extensive analysis of any possible Grem2 pathway interaction, we used this method of high-throughput sequencing on whole hearts isolated from *Grem2*$^{-/-}$ mice and *WT* counterparts both without injury

as well as day 7 post-MI, so that data can be collected pertaining to both the inflammatory and fibrotic response that occurs during cardiac repair.

Materials and methods

Generation of genetically engineered Grem2 mice

See CHAPTERS III and IV.

Experimental MI

See CHAPTER II.

RNA isolation from whole murine hearts

Whole hearts were dissected at the indicated time points after MI, perfused to remove blood cells and RNA was obtained using TriZol Reagent according to the manufacturer's instruction (Life Technologies).

High throughput sequencing

Sequencing was performed at Paired-End 75 base pair on the Illumina HiSeq 3000, where 45 million PF reads per sample. The initial gene association alignment data was done on CLC workbench using gene ontology. An N=2 were used for the following: *WT* day 0, *Grem2*$^{-/-}$ day 0, *WT* day 7, and *Grem2*$^{-/-}$ day 7. WebGestalt Go enrichment analysis based on Entrez gene protein coding references was then conducted based on genes annotated using gene ontology gene symbols that had a 2-fold up-regulation post-MI and a p-value <0.05.

Pathways and genes that were induced in *WT* mice post-MI, *Grem2*$^{-/-}$ mice post-MI, and those that were uniquely induced in *Grem2*$^{-/-}$ mice were analyzed.

Results

Using the Kallisto database, we found a short list of 12 genes that showed >2-fold differences between *Grem2*$^{-/-}$ mice and their *WT* counterparts at baseline. The majority of the genes (included in **Table 4**) encode ribosomal or mitochondrial proteins. The lack of significant molecular differences between *WT* and *Grem2*$^{-/-}$ mice suggest no gross cardiac abnormalities exist at baseline. Initial pathway analysis results for genes induced post-MI are provided, where processes that are significantly induced are shown in red and first represent those pathways that are induced in *WT* mice post-MI (**Figure 38A**). Although the analysis separates genes into different categories based on biological processes, molecular function, and cellular components, the genes that are significantly induced 2-fold largely overlap. Within the immune system category, several TLRs and chemokine receptors are present, such as *Tlr6, 7,8,9, Ccr1, 2,3,* and *Cxcr1, 2,3.* Chemokine ligands such as *Ccl2, 3, Cx3cl1* as well as cytokines *Tnf, Il-6,* and *Il-1β* were also induced. Endothelial cell adhesion molecules *Icam1* and *E-selectin* also came up in this analysis, and other genes such as *Tgfβ1, Timp1, myeloperoxidase, and thrombospondin* not surprisingly exhibited significant changes in *WT* mice post-MI. The positive regulation of biological and cell processes categories included *angiopoietin-like 4, Mmp9, Bmp2, Wnt4, Snai1 and 2, Twist1, Vimentin, Col1a1* and *angiotensin converting enzyme*, thereby

representing genes involved in EndMT and fibrosis. The heparin, carbohydrate derivative, and glycosaminoglycan categories were unique in *WT* mice post-MI, and contained several *thrombospondin* isoforms, *Sfrp1*, and *latency binding protein 2*, overall demonstrating Tgfβ and Wnt pathway regulation. Taken together, the data from *WT* mice post-MI confirms what has been known about molecular pathways induced during cardiac repair.

Pathways significantly changed in *Grem2*$^{-/-}$ mice post-MI are shown in **Figure 38B**. There are several categories that overlap with those present during normal cardiac repair, such as the immune system process and response. Within these several TLRs, chemokine receptors, chemokine ligands, and cytokines that were also present in *WT* mice such as *Tlr6, 8,9, Ccr1, 2,3, Cxcr2, Cx3cl1* and *Il-6* were also present in *Grem2*$^{-/-}$ mice post-MI. Of note, as seen by our qPCR analysis, *E-selectin* and *Tgfβ1* were also shown to be upregulated in this analysis. Overlap within the positive regulation of biological processes category was seen through the presence of *Snail1, Twist1, thrombospondin, Vimentin,* and *Col1a1.* The cation binding, catalytic activity, hydrolase activity, actin binding, and cell surface categories were uniquely altered in the case of the loss of Grem2 function. The genes within these categories include *activated leukocyte cell adhesion molecule (Alcam), XIAP associated factor 1 (Xaf1), immunoresponsive gene 1 (Irg1), alpha-fetoprotein (Afp), secretory leukocyte peptidase inhibitor (Slpi), lymphocyte specific 1 (Lsp1),* and *CD8a.* These data demonstrate that, genes that are induced in *Grem2*$^{-/-}$ mice post-MI include genes involved in cell adhesion, proteins specific to leukocytes and lymphocytes, and

interestingly, a factor associated with XIAP, a known non-canonical downstream target of BMP signaling (Yamaguchi et al., 1999). The results confirm our current phenotypic data, where Grem2 appears to regulate the inflammatory response post-MI.

Finally, the genes that are uniquely induced in *Grem2*$^{-/-}$ mice post-MI were isolated for their own analysis, the results of which are shown in **Figure 38C**. The genes that were uniquely present during the loss of Grem2 within the immune system process include *thymocyte antigen-1 (Thy1), Vcam1, lymphocyte cell tyrosine kinase (Lck),* and *cell adhesion molecule-1 (Cadm1).* Of note, other genes that were specifically altered in *Grem2*$^{-/-}$ mice include *cytotoxic T lymphocyte-associated protein 2α (Ctla2α), Cd4, Il-2 inducible T cell kinase (Itk), lymphotoxin B (Ltb), cannabinoid receptor 2 macrophage (Cnr2), chymase 1 mast cell (Cma1), Ly6E,* and *T-cell interacting activating receptor myeloid cells (Tarm1),* all of which fall under the unique pathway categories leukocyte activation, lymphocyte activation, and T cell activation. Therefore, the changes to the inflammatory response post-MI from the loss of Grem2 could possibly be through the regulation of genes present within inflammatory cell populations themselves. However, endothelial cell genes such as *endothelial cell surface expressed chemotaxis and apoptosis regulator (Ecscr)* and adhesion genes such as *Alcam, Cadm1,* and *Vcam1* are also uniquely induced, corroborating with out previous data, where the regulation of the inflammatory response occurs at the level of inflammatory cell attachment and adhesion.

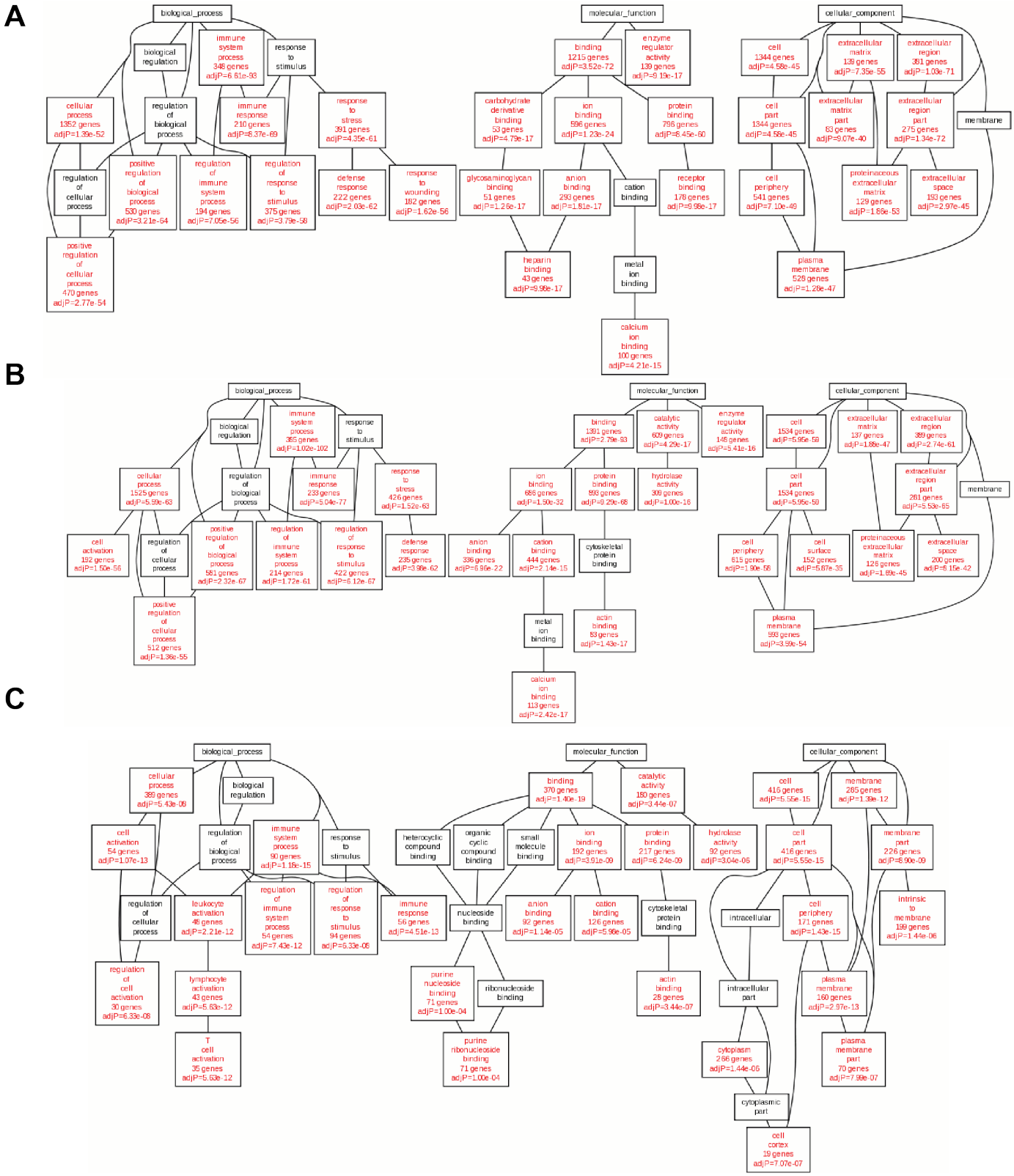

Figure 38. High throughput sequencing pathway analysis. (A) Pathway analysis on gene induction in *WT* mice 7 days post-MI. **(B)** Pathway analysis on gene induction in *Grem2*$^{-/-}$ mice 7 days post-MI. **(C)** Pathway analysis on genes specifically induced in *Grem2*$^{-/-}$ mice 7 days post-MI. Red indicates *P<0.05.* N=2 per group.

Discussion

High-throughout sequencing analysis such as RNA-seq provides the capability of determining pathway associations of *Grem2* in an unbiased manner. To date, we have aligned our results to a mouse genome database and generated pathway analysis charts to see overall, the pathways that are significantly affected by the loss of *Grem2*. Our current data confirm our previous work with more targeted approaches using qPCR, where the loss of Grem2 resulted in profound changes to genes involved in inflammation and cell adhesion. Furthermore, this analysis provided new gene targets, such as those that are involved in leukocyte and lymphocyte biology. The next step in this analysis, will be to analyze the reads per kilo base per million mapped reads or RPKM values for genes present in both *WT* mice post-MI and *Grem2*$^{-/-}$ mice post-MI to determine if expression levels differ in the two models as well as conduct an analysis of genes that are uniquely present in *WT* mice post-MI as was done for the *Grem2*$^{-/-}$ mice. This will provide important information regarding pathways that directly correlate with the level of Grem2 expression. Future experiments confirming the results seen here, such as conducting qPCR for genes of interest will also be required.

The advantage of conducting RNA-seq analysis is that it provides a breadth of information that could never be obtained at the targeted level. In contrast, the information that can be obtained from such an analysis is limited by the alignment database utilized. Current work focuses on using different alignment programs such as Tophat2 and the previously mentioned Kallisto in

order to confirm that the results being observed are not artifacts from the alignment. Furthermore, there is a large amount of data that was not discussed in this chapter that requires further analysis. The data presented here has been focused on pathways that are related to inflammatory response, however it would be interesting to investigate changes in other molecular pathways.

Despite the fact that an unbiased approach such as high-throughput sequencing has confirmed the work described in previous chapters, it remains to be seen how the unique structure of Grem2 could confer to unique pathway associations. The results from this analysis could therefore be used to initiate a new hypothesis and series of experiments to move the research into new directions. It is important to note that due to the plethora of data provided, there is still a lot to be done in order to gain further insight into the implications of the analysis. Consequently, this analysis will serve as a starting point for future work.

Acknowledgements

I thank members of the Cardiovascular Pathophysiology and Complications Core of the Mouse Metabolic Phenotyping Center, the VANTAGE Core, the Transgenic Mouse/ES Cell Resource, and the Molecular Cell Biology Resource at Vanderbilt University Medical Center for technical assistance. This work also utilized the core(s) of the Vanderbilt Diabetes Research and Training Center funded by grant 020593 from the National Institute of Diabetes and Digestive and Kidney Disease. I thank Lianli Ma, Lin Zhong for performing mice

surgeries; Mark Magnuson and Jennifer Skelton for generation of the Grem2 mouse lines; and Vineeta Tanwar for her help with the initial mouse colony maintenance.

CHAPTER IX

SUMMARY AND CONCLUSION

Summary

In conclusion, our data support the following model of cardiac tissue repair: induction of pro-inflammatory cytokines such as Tnfα after MI initiates a transient inflammatory response, which is sustained by subsequent induction of Bmp2 by Tnfα. Bmp2 increases the magnitude of inflammation through induction of pro-inflammatory cell adhesion membrane proteins in endothelial cells. Grem2 is then induced as part of a negative feedback loop to inhibit Bmp2's pro-inflammatory activity and act as a barrier of inflammation at the infarct border zone (**Figure 39A, B**). To determine if Grem2 also plays a role during the later phases of recovery such as the proliferative and pro-fibrotic phases or to see if it has a direct role on cardiac remodeling, we conducted gene induction, histological, and flow cytometric analysis. Our current data demonstrate that Grem2 may have complex roles in these processes. In order to gain further insight into the role of Grem2 in the recovery process after MI, we conducted RNA-seq analysis on our loss of function model 7 days post-MI. Current high-throughput sequencing data suggest that the loss of Grem2 leads to a specific up-regulation of certain immune processes as well as provides novel pathway associations that can be used to initiate future investigations.

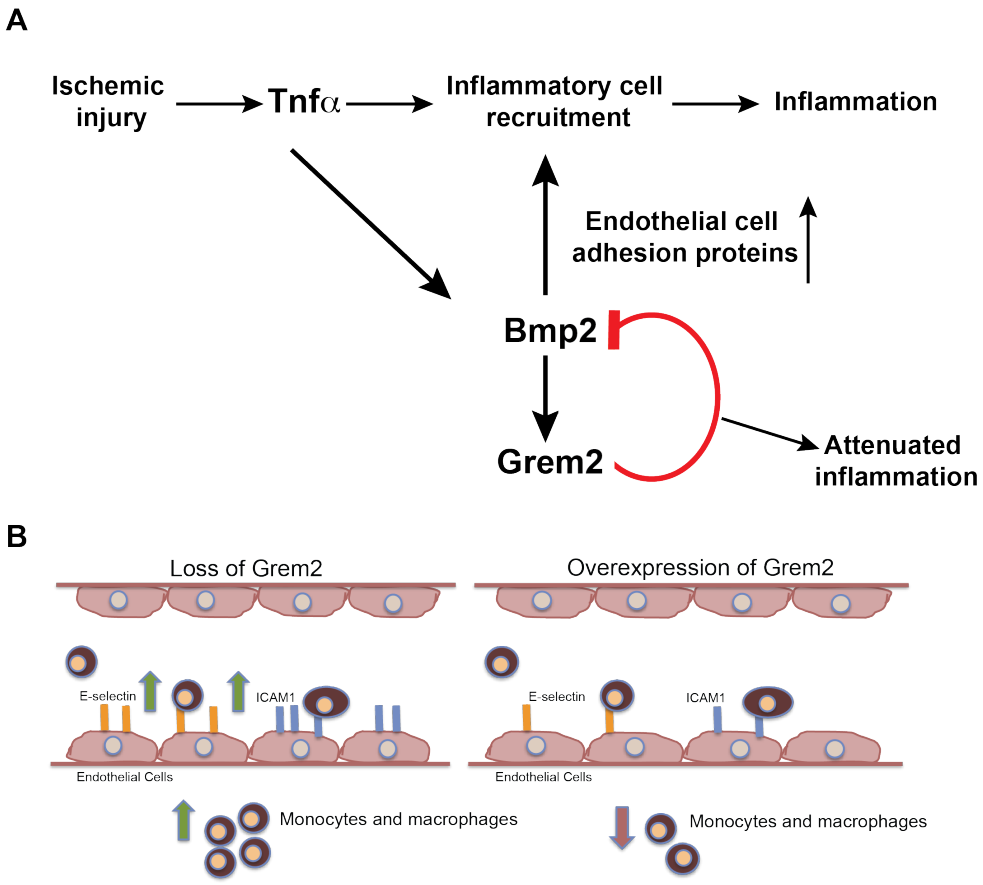

Figure 39. Model. (A) Model of the role of Grem2 during the inflammatory phase after MI. Cardiomyocyte cell death after ischemic injury causes immediate induction of TNFα, which directly stimulates expression of chemokines and endothelial membrane proteins to initiate inflammatory cell recruitment. TNFα also induces the expression of Bmp2 that further augments the pro-inflammatory phenotype of endothelial cells. Bmp2 in turn induces its own negative modulator Grem2 that inhibits the Bmp2-mediated inflammatory effects. **(B)** Schematic representation of the inflammatory phenotype in each *Grem2* model.

Implications

Here we provide evidence for a new mechanism that regulates the magnitude and extent of the inflammatory response after myocardial infarction. Specifically, we show that the BMP antagonist Grem2 is robustly and transiently induced after myocardial infarction during the late inflammatory phase and early proliferative phase of granulation tissue formation. Genetic loss and gain of function approaches revealed that Grem2 a) controls the magnitude of the

inflammatory cell infiltration and, b) acts as a molecular barrier to limit infiltration of inflammatory cells in the relatively healthy cardiac tissue adjacent to the infarct border zone. Consistent with this model, our data indicate that Grem2 administration during the inflammatory phase of cardiac tissue repair decreases the number of inflammatory cells recruited to the infarct site after MI. Our results further demonstrate that the anti-inflammatory effects of Grem2 depend, at least in part, on suppression of canonical BMP signaling through inhibition of Smad1/5/8 phosphorylation within ventricular tissue at the infarct border zone. In agreement with this notion, administration of DMH1, a chemical inhibitor of canonical BMP signaling, rescued the inflammatory phenotype in *Grem2*$^{-/-}$ mice.

The long history of either negative effects or no effects from using anti-inflammatory treatments is due to targeting direct inflammatory mediators, however the success of the cyclosporine trial demonstrates that there is promise in utilizing inflammation as a therapeutic target (Piot et al., 2008a). However, the benefits of cyclosporine use after MI could not be replicated in a larger clinical trial (Cung et al., 2015). Here, we show that targeting a mediator of inflammation may prove to be more successful than targeting direct players in the inflammatory process.

Limitations and Future directions

Mouse models

The major limitations with this work involve the mouse models themselves and the model of myocardial infarction. The mouse models described here

included the loss-of function or gene knock out mouse model which is constitutive and global and the gain- of function TG model, which is tissue specific but also constitutive. This makes discerning specific roles of Grem2 during the dynamic process of cardiac tissue repair, difficult. Although we were able to test the effects of Grem2 directly by injecting mice with purified protein during the inflammatory phase of repair demonstrating that it plays a role during this process, the ability to determine how changes that occur during the inflammatory phase affects the later stages of recovery, including cardiac remodeling, requires further investigation. Future experiments utilizing our loss-of-function mouse model, gain-of-function mouse model, or injection models for long-term studies (>21 days post-MI) in order to observe any long-term affects due to changes in *Grem2* expression are therefore required. Bone marrow transplantation studies would also be informative in determining the possible global effects of Grem2 loss-of-function on cells involved in the inflammatory phase of repair.

Despite the fact the repair process following a myocardial infarction consists of distinct phases, these are actually intertwined, where a larger inflammatory response usually leads to a larger fibrotic response, thereby causing extensive cardiac remodeling. Therefore, whether or not Grem2 has direct affects on these later stages of recovery or if the changes that occur are simply a result of the role of Grem2 on limiting the inflammatory phase is yet to be confirmed. Future experiments utilizing inducible cell-specific knock-out models, would be useful in both confirming the cellular source of Grem2 in the

context of cardiac repair as well as well as tease apart roles of Grem2 during early versus late phases of cardiac repair.

The model of myocardial infarction in the studies described here was a permanent ligation model, where the LAD coronary artery is permanently ligated or closed. Since the mice that undergo the procedure are young and without the co-morbidities usually associated with a myocardial infarction in human patients, they are able to survive the surgery. Therefore the model is more akin to those that suffer a massive heart attack resulting from a major artery being blocked and that do not survive. However another model exists that is more similar to the clinic, and that is the ischemia/reperfusion (I/R) model. In this model the LAD coronary artery is also ligated, but after several minutes re-opened, allowing blood to flow through. Utilization of such a model would also provide information regarding infarct size in our experimental groups. We did not use this model in our studies due to the fact that the re-oxygenation of cells leads to a more complex inflammatory response, the infarct size in a permanent ligation model is more reproducible, and because mice tolerate permanent ligation better than I/R.

In lieu of these limitations, future experiments could include injecting mice with Grem2 at a later stage of the recovery process, i.e. days 5-7 post-MI, to determine if there are changes to cell populations, gene expression analysis, or functional recovery. Based on the data described in CHAPTER VII however it is unlikely that Grem2 will have a dramatic effect. Future experiments could also include the use of 60 minute I/R instead of permanent ligation as a model of MI in order determine if the inflammatory phenotype is due to changes to infarct size

as well as determine if the changes to inflammation seen post-MI are also present during the recovery process of this type of injury.

Due to the fact that the work described here illustrates a positive role for Grem2 in cardiac tissue repair, and previous work in the lab demonstrates a positive role for Wnt10b in cardiac repair (Paik et al., 2015), it would be beneficial to test the repair process when both BMP and Wnt pathways are favorably modulated. It is possible that the overexpression of *Grem2* to limit the inflammatory response, when combined with *Wnt10b* overexpression to induce arteriogenesis and limits fibrosis as was previously described, will further optimize recovery.

Although therapeutic potential was illustrated through the administration of proteins following a myocardial infarction as described in previous chapters, this was done through IP. Despite the fact that our data indicated that these proteins do in fact reach the heart, it is still unclear if we are reaching maximal efficiency. To address this issue, more optimal delivery methods and evaluation of protein bioavailability will need to be tested.

Molecular Mechanisms

Our data thus far have demonstrated that BMP2 increases the pro-inflammatory activity of TNFα through activation of canonical BMP signaling. However, previous reports have demonstrated that BMP2 is able to activate non-canonical BMP signaling and NFκB signaling (Csiszar et al., 2005, 2006; Helbing et al., 2011). Therefore, there is a need for future experiments aimed at testing if

BMP activates NFκB in the context of cardiac repair. These could include injecting *Grem2*$^{-/-}$ mice with an NFκB inhibitor in order to see what phenotypes are rescued, conducting histological analysis in order to measure levels of nuclear NFκB in each of the different mouse models, and western blot analysis with tissue isolated post-MI to measure levels of P-Smad1/5/8 and NFκB signaling components. The molecular mechanism could also be investigated using endothelial cell *in vitro* models, and include conducting BRE-luc and NFκB-luc analysis and western blot analyses after treatment with exogenous TNFα, BMP2, and the two together.

Due to the unique structure of Grem2 as well as the limited number of studies conducted on the molecular action of Grem2, it remains possible that Grem2 could have a unique binding capacity with BMP ligands, which could also lead to a unique mode of BMP antagonism. The Hatzopoulos laboratory has previously shown that Grem2 promotes the activation of non-canonical BMP signaling components such as JNK in cardiomyocytes derived from mouse embryonic stem cells (Tanwar et al., 2014). Whether Grem2 activates non-canonical BMP signaling during cardiac tissue repair is yet to be determined. Future experiments could explore if JNK activation occurs after experimental MI and if changes to Grem2 expression lead to changes in this activation. Through collaborative efforts, we have access to several mutant proteins that contain a point mutation within the binding domain of Grem2. Therefore, future analysis could be conducted in order to assess the ability of these proteins to not only

inhibit canonical versus non-canonical BMP signaling in our system, but if binding of Grem2 to the BMP2 ligand is required for its anti-inflammatory activity.

Our current analysis also does not reveal if Grem2 activity is dependent upon certain BMP receptors or ligands. Future research could be aimed at determining the molecular basis for the biochemical and biological activities of Grem2.

The constitutive nature of the Grem2 loss of function mouse model is a weakness in the context of cardiac repair. However the fact that *Grem2*$^{-/-}$ is global and the mice are viable is in fact beneficial for the use of investigations into a wide range of disease states.

Conclusions

Cardiovascular diseases remain to be the number one cause of death in both men and women around the world despite the many advances that have been made in the field. An acute cardiac injury such as a heart attack or myocardial infarction contributes to the onset of heart failure, a disease with a survival rate lower than any cancer (Braunwald, 2015; McMurray, 2010). Current therapies such as angiotensin converting enzyme (ACE) inhibitors and Beta-blockers are aimed at regaining blood flow as well as decreasing workload on the damaged heart. However, it is important to note that most of these treatments also have some sort of anti-inflammatory effect, underscoring the importance of regulating the inflammatory phase of recovery (McMurray, 2010). One of the major hindrances in the field is that not much is known about the molecules that

help generate a barrier and limit the magnitude of the inflammatory response. We have data to suggest that we have in fact identified one such molecule. Utilizing unique mouse models, we have been able to determine a novel role of a relatively unstudied protein in the context of cardiac repair. Therefore Grem2 has demonstrated to be a molecule with great therapeutic potential.

TABLES

Table 1. Primer Sequences used in qPCR analyses and *Grem2*$^{-/-}$ mouse genotyping

Mouse primers qPCR:

Ang-1	5’	CCACCATGCTTGAGATAGGAACC
	3’	CTGTGAGTAGGCTCGGTTCCC
Anp(Nppa)	5’	TTTCAAGAACCTCGTAGACCACCTG
	3’	AAGCTGTTGCAGCCTAGTCCACTCT
Axin2	5’	CCAGAAGATCACAAAGAGCCAAAGA
	3’	CTCAGTCGATCCTCTCCACTTTGC
Bmp2	5’	GCTGTCTTCTAGTGTTGCTGCTT
	3’	GGGACAGAACTTAAATTGAAGAAGA
Bmp4	5’	ATGATTCCTGGTAACCGAATGCTG
	3’	CTTCGTGATGGAAACTCCTC
Bmp6	5’	AACGCCCTGTCCAATGACG
	3’	ACTCTTGCGGTTCAAGGAGTG
Bmp7	5’	ACGGACAGGGCTTCTCCTAC
	3’	ATGGTGGTATCGAGGGTGGAA
Bmp10	5’	AAATTCGCCACAGACCGGAC
	3’	GGTGAGGGATAGACACATTGAAG
Bmpr2	5’	CTCAGAATCAAGAACGGCTGTG
	3’	CAACTGGACGCTGATCCAAGG
Bnp (Nppb)	5’	ATGCATCTCCTGAAGGTGCTG
	3’	GTGCTGCCTTGAGACCGAA
β-mhc	5’	CCAACTATGCTGGAGCTGGATG
	3’	CTTCTTGAACTCCATTCTGGAGAG
Chordin	5’	CTAGGAAATGGCTCCCTTATCTATC
	3’	TGTAAGTGACAATGTGTATCCAAGG
Pro-Collagen Ia1	5’	GCTAACGTGGTTCGTGACCGTG
	3’	GGTCAGCTGGATAGCGACATC
Dand5	5’	CTGTCCTTTGTTCAGGTGATCTC
	3’	CCGAGGGGAGGCTAATTGG
Dan	5’	CTAGGACAATGCTTCAGTTACAGC
	3’	CTTCAGATCTCCATGACAACCAG
E-selectin	5’	GAGCACAGCTTGGTACTACAATGC
	3’	GGTGGCACTTGCAGGTGTAAC
Fsp-1	5’	TCAGGCAAAGAGGGTGACAAG
	3’	AGGCAGCTCCCTGGTCAGT
Gapdh	5’	CTCACTCAAGATTGTCAGCAATG
	3’	GAGGGAGATGCTCAGTGTTGG
Grem1	5’	GGAA/TTCTGCAAGCCCAAGAAGTTCACCAC
	3’	CGGGA/TCCTCTGTCCCGTTTGCCATCAC
Grem2(1)	5’	CCTGTCATTCACAGAGAGGA
	3’	CATTCGAGCTCTACGATGAC
Icam1	5’	GGAGACGCAGAGGACCTTAACAG
	3’	CATCTCCTGTTTGACAGACTTCACC

Id2	5’	CGACCCGATGAGTCTGCTCTACAAC
	3’	GTGTTCTCCTGGTGAAATGGCTGATAAC
Il-8	5’	CACCTCAAGAACATCCAGAGCT
	3’	CAAGCAGAACTGAACTACCATCG
Il-10	5’	GACCAGCTGGACAACATACTGC
	3’	CCAGCAGACTCAATACACACTGC
Il-1β	5’	TTTGACCTGGGCTGTCCTGATG
	3’	CATATGGGTCCGACAGCACGAG
Mcp-1 (Ccl-2)	5’	ACCTGCTGCTACTCATTCACC
	3’	CACTGTCACACTGGTCACTCC
Mmp9	5’	CCCGCTGTATAGCTACCTCGAGGGC
	3’	AGCGTTGCAGGCAGGGCTGG
Noggin	5’	GCCAGCACTATCTACACATCC
	3’	GCGTCTCGTTCAGATCCTTCTC
αSma	5’	CCACGAAACCACCTATAACAGCATC
	3’	GTCGTATTCCTGTTTGCTGATCCAC
Sost	5’	AGCCTTCAGGAATGATGCCAC
	3’	CTTTGGCGTCATAGGGATGGT
Tgfβ1	5’	AGATTAAAATCAAGTGTGGAGCAAC
	3’	GTCCTTCCTAAAGTCAATGTACAGC
Tnfα	5’	CTACTGAACTTCGGGGTGATCGGTCC
	3’	CCTTCATCTTCCTCCTTATCTCTCATGCC
Twsg1	5’	TCTAGCCTCCCTGACGTTCC
	3’	CACATACCGACACAGTCGC
Vcam1	5’	AGAGAAACCATTTATTGTTGACATCTCCC
	3’	CAAGTGGCCCACTCATTTTAATTACTGG
Ve-cadherin	5’	CACTATCACAGTGATTACCTTGCTG
	3’	GTCATAATCGATGTCAGAGTCGG
Vimentin	5’	GGTACAAGTCCAAGTTTGCTGACCT
	3’	CATTGAGCAGATCTTGGTATTCACG
Wnt4	5’	CTCCTGCGAGGTAAAGACGTG
	3’	AGTATCTTTTGGGGTAGGTGGTG
Wnt10b	5’	AGAAGTTCTCTCGGGATTTCTTG
	3’	CAAAGTAAACCAGCTCTCCAG

Human primers:

BMP2	5’	ACCCGCTGTCTTCTAGCGT
	3’	TTTCAGGCCGAACATGCTGAG
E-SELECTIN	5’	GCTGGACTCTCCCTCCTGACATTAGC
	3’	CATAAAGGCATCTGGCATAGTAGGCAAG
GAPDH	5’	AAGGTGAAGGTCGGAGTCAAC
	3’	GGGGTCATTGATGGCAACAATA
GREM2	5’	ATCCCCTCGCCTTACAAGGA
	3’	TCTTGCACCAGTCACTCTTGA
ID2	5’	GCATCCCCCAGAACAAGAAGGTGAG
	3’	CGCTTATTCAGCCACACAGTGCTTTG

Genotyping Primers:

Primer 1	5’	CTGTGCAGCAGAGAAAGCTG
Primer 2	3’	TGGCAATGTACCTCATCTCA
Primer 3	3’	CTGTCCATCTGCACGAGACT
Primer 4	5’	TCTGGTACCCACGAGGACAAGC
Primer 5	5’	GTCTGAGTAGGTGTCATTCTA
Primer 6	3’	CACAGATCACTCGATGCTCT

1. Suzuki D et al. (2012). BMP2 differentially regulates the expression of Gremlin1 and Gremlin2, the negative regulators of BMP function, during osteoblast differentiation. *Calcif. Tissue. Int.* **91**, 88–96.

	Body Weight (g)	LV Mass (mg)	HR (bpm)	
WT	26.0 ± 0.2	87.1 ± 10.0	513.8 ± 78.7	
Grem2$^{-/-}$	26.0 ± 2.0	78.7 ± 13.0	627.0 ± 59.4	
P Value	ns	ns	p<0.01	

	IVS;d (mm)	IVS;s (mm)	LVPW;d (mm)	LVPW;s (mm)
WT	0.9 ± 0.07	1.3 ± 0.1	0.8 ± 0.1	1.2 ± 0.1
Grem2$^{-/-}$	1.0 ± 0.1	1.3 ± 0.1	0.8 ± 0.1	1.2 ± 0.1
P Value	ns	ns	ns	ns

	LVID;d (mm)	LVID;s (mm)	LV vol;d (µl)	LV vol;s (µl)
WT	3.5 ± 0.1	1.8 ± 0.1	53.1 ± 3.3	10.6 ± 0.8
Grem2$^{-/-}$	3.3 ± 0.1	1.7 ± 0.1	45.8 ± 2.5	8.5 ± 0.7
P Value	ns	ns	ns	ns

	EF	FS (%)	SV (µL)	CO (ml/min)
WT	0.8 ± 0.01	48.0 ± 0.8	41.8 ± 7.9	21.0 ± 2.3
Grem2$^{-/-}$	0.8 ± 0.01	49.1 ± 1.2	36.6 ± 5.3	23.0 ± 2.6
P Value	ns	ns	ns	ns

Table 2. Physiological and cardiac functional parameters of *Grem2*$^{-/-}$ mice and *WT* siblings. Body weight, left ventricle (LV) mass, heart rates, LV wall and cavity dimensions, including calculated functional parameters (measured by echocardiography), are comparable in *WT*^{mix} and *Grem2*$^{-/-}$ adult mice at baseline, with the exception of heart rate. HR=heart rate; IVS=interventricular septum; LVPW=Left Ventricle Posterior Wall; LVID=Left Ventricle Internal Dimension; vol=volume, EF=ejection fraction, FS=fractional shortening; SV=stroke volume; CO=cardiac output; d=dystole; s=systole.ns=not significant. Student's two-tailed unpaired *t*-test. *WT* N=9, *Grem2*$^{-/-}$ N=8. All data represent means ± S.D.

	Body Weight (g)	LV Mass (mg)	HR (bpm)	
WT	24.5 ± 0.4	75.6 ± 10.4	619.3 ± 26.8	
TG^{Grem2}	24.3 ± 0.5	60.7 ± 6.6	645.6 ± 35.9	
P Value	ns	ns	ns	
	IVS;d (mm)	**IVS;s (mm)**	**LVPW;d (mm)**	**LVPW;s (mm)**
WT	0.9 ± 0.08	1.1 ± 0.06	0.8 ± 0.07	1.2 ± 0.03
TG^{Grem2}	0.8 ± 0.04	1.1 ± 0.04	0.8 ± 0.04	1.1 ± 0.1
P Value	ns	ns	ns	ns
	LVID;d (mm)	**LVID;s (mm)**	**LV vol;d (µl)**	**LV vol;s (µl)**
WT	3.2 ± 0.1	1.5 ± 0.2	40.6 ± 4.2	7.7 ± 1.4
TG^{Grem2}	3.2 ± 0.1	1.5 ± 0.1	37.7 ± 2.1	7.2 ± 0.6
P Value	ns	ns	ns	ns
	EF	**FS (%)**	**SV (µL)**	**CO (ml/min)**
WT	0.8 ± 0.01	46.2 ± 0.6	33.6 ± 7.2	20.7 ± 3.8
TG^{Grem2}	0.8 ± 0.01	47 .7 ± 0.5	29.0 ± 5.1	18.8 ± 2.9
P Value	ns	ns	ns	ns

Table 3. Physiological and cardiac functional parameters of *TG^{Grem2}* mice and *WT* siblings. Body weight, left ventricle (LV) mass, heart rates, LV wall and cavity dimensions, including calculated functional parameters (measured by echocardiography), are comparable in *WT* and *TG^{Grem2}* adult mice at baseline. HR=heart rate; IVS=interventricular septum; LVPW=Left Ventricle Posterior Wall; LVID=LeftVentricle Internal Dimension; vol=volume, EF=ejection fraction, FS=fractionalshortening; SV=stroke volume; CO=cardiac output; d=dystole; s=systole. ns=not significant. Student's two-tailed unpaired *t*-test. Body weight, LV mass, HR, IVSd, IVSs, LBPWd, LVPWs, LVvold, LVvols, SV, CO N=4 per group; LVIDd, LVIDs, EF, FS *WT* N=6, *TG^{Grem2}* N=10. All data representmeans ± S.D.

Definition	Symbol	fold-Grem2KO_vs_WT
histone cluster 1, H4m [Source:MGI Symbol;Acc:MGI:2448441]	Hist1h4m	-8.404752002
ribosomal protein S3A2 [Source:MGI Symbol;Acc:MGI:3642853]	Rps3a2	-8.268432785
ribosomal protein S3A3 [Source:MGI Symbol;Acc:MGI:3643406]	Rps3a3	-3.430341307
glycerophosphodiester phosphodiesterase domain containing 3 [Source:MGI Symbol;Acc:MGI:1915866]	Gdpd3	-2.932662122
immunoglobulin kappa joining 4 [Source:MGI Symbol;Acc:MGI:1316692]	Igkj4	-2.411175729
histone cluster 1, H4i [Source:MGI Symbol;Acc:MGI:2448432]	Hist1h4i	2.010354801
myomesin 1 [Source:MGI Symbol;Acc:MGI:1341430]	Myom1	2.086813383
solute carrier family 27 (fatty acid transporter), member 2 [Source:MGI Symbol;Acc:MGI:1347099]	Slc27a2	2.152859496
ribosomal protein L21, pseudogene 15 [Source:MGI Symbol;Acc:MGI:3705426]	Rpl21-ps15	2.827529748
tropomyosin 3, related sequence 7 [Source:MGI Symbol;Acc:MGI:99705]	Tpm3-rs7	2.942246171
chemokine (C-X-C motif) ligand 14 [Source:MGI Symbol;Acc:MGI:1888514]	Cxcl14	3.990014607
PAXIP1 associated glutamate rich protein 1B [Source:MGI Symbol;Acc:MGI:5141883]	Pagr1b	5.912658163

Table 4. RNA-seq analysis comparing *WT* and *Grem2*$^{-/-}$ mice at baseline.

APPENDIX

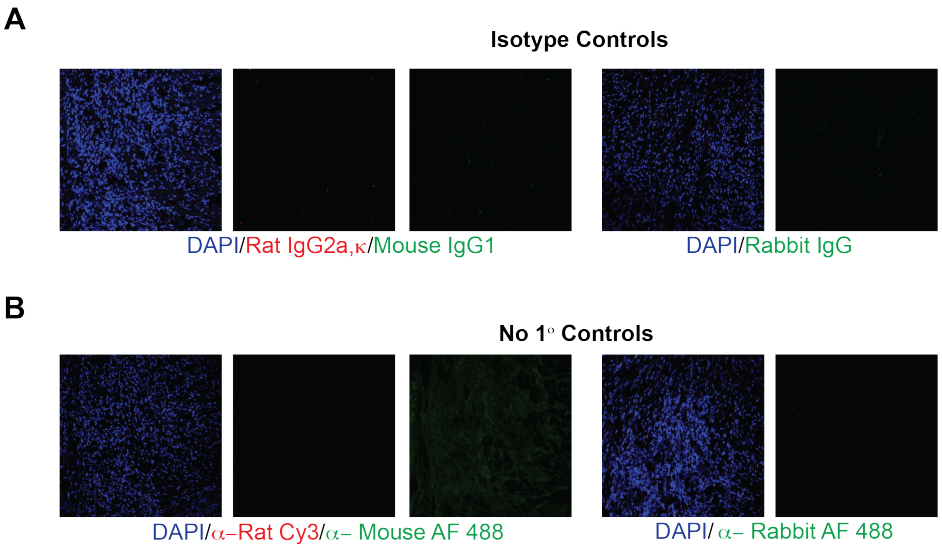

Appendix Figure 1. Control antibody analysis for immunofluorescence staining. (A) IF using non-immune immunoglobulins (isotype controls) of same species and same concentration as the corresponding primary antibodies used on cardiac tissue sections post-MI. Rat and mouse isotypes controls are shown in combination (left) and the rabbit isotype control is shownindependently (right). **(B)** IF staining with respective secondary antibody-only of the sections in the absence of primary antibodies.

REFERENCES

Ades, E.W., Candal, F.J., Swerlick, R.A., George, V.G., Summers, S., Bosse, D.C., and Lawley, T.J. (1992). HMEC-1: establishment of an immortalized human microvascular endothelial cell line. *J. Invest. Dermatol*. **99,** 683–690.

Aisagbonhi, O., Rai, M., Ryzhov, S., Atria, N., Feoktistov, I., and Hatzopoulos, A.K. (2011). Experimental myocardial infarction triggers canonical Wnt signaling and endothelial-to-mesenchymal transition. *Dis. Model. Mech*. **4**, 469–483.

Akira, S., and Takeda, K. (2004). Toll-like receptor signalling. *Nat. Rev. Immunol*. **4,** 499–511.

Anzai, T., Yoshikawa, T., Shiraki, H., Asakura, Y., Akaishi, M., Mitamura, H., and Ogawa, S. (1997). C-reactive protein as a predictor of infarct expansion and cardiac rupture after a first Q-wave acute myocardial infarction. *Circulation* **96**, 778–784.

Ao, A., Hao, J., Hopkins, C.R., and Hong, C.C. (2012). DMH1, a novel BMP small molecule inhibitor, increases cardiomyocyte progenitors and promotes cardiac differentiation in mouse embryonic stem cells. *PloS One* **7**, e41627.

Armstrong, P.W., Granger, C.B., Adams, P.X., Hamm, C., Holmes, D., O'Neill, W.W., Todaro, T.G., Vahanian, A., and Van de Werf, F. (2007). Pexelizumab for acute ST-elevation myocardial infarction in patients undergoing primary percutaneous coronary intervention: a randomized controlled trial. *JAMA* **297**, 43–51.

Avsian-Kretchmer, O., and Hsueh, A.J.W. (2004). Comparative genomic analysis of the eight-membered ring cystine knot-containing bone morphogenetic protein antagonists. *Mol. Endocrinol*. **18**, 1–12.

Baran, K.W., Nguyen, M., McKendall, G.R., Lambrew, C.T., Dykstra, G., Palmeri, S.T., Gibbons, R.J., Borzak, S., Sobel, B.E., Gourlay, S.G., et al. (2001). Double-blind, randomized trial of an anti-CD18 antibody in conjunction with recombinant tissue plasminogen activator for acute myocardial infarction: limitation of myocardial infarction following thrombolysis in acute myocardial infarction (LIMIT AMI) study. *Circulation* **104**, 2778–2783.

Beck, H., Semisch, M., Culmsee, C., Plesnila, N., and Hatzopoulos, A.K. (2008). Egr-1 regulates expression of the glial scar component phosphacan in astrocytes after experimental stroke. *Am. J. Pathol*. **173**, 77–92.

Boudoulas, K.D., and Hatzopoulos, A.K. (2009). Cardiac repair and regeneration: the Rubik's cube of cell therapy for heart disease. *Dis. Model. Mech*. **2**, 344–358.

Bragdon, B., Moseychuk, O., Saldanha, S., King, D., Julian, J., and Nohe, A. (2011). Bone morphogenetic proteins: a critical review. *Cell Signal*. **23**, 609–620.

Braunwald, E. (2015). The war against heart failure: the Lancet lecture. *Lancet* **385**, 812–824.

Cahill, E., Costello, C.M., Rowan, S.C., Harkin, S., Howell, K., Leonard, M.O., Southwood, M., Cummins, E.P., Fitzpatrick, S.F., Taylor, C.T., et al. (2012). Gremlin plays a key role in the pathogenesis of pulmonary hypertension. *Circulation* **125**, 920–930.

Cao, Y., Wang, C., Zhang, X., Xing, G., Lu, K., Gu, Y., He, F., and Zhang, L. (2014). Selective small molecule compounds increase BMP-2 responsiveness by inhibiting Smurf1-mediated Smad1/5 degradation. *Sci. Rep*. **4**, 4965.

Chang, S.-A., Lee, E.J., Kang, H.-J., Zhang, S.-Y., Kim, J.-H., Li, L., Youn, S.-W., Lee, C.-S., Kim, K.-H., Won, J.-Y., et al. (2008). Impact of myocardial infarct proteins and oscillating pressure on the differentiation of mesenchymal stem cells: effect of acute myocardial infarction on stem cell differentiation. *Stem Cells* **26**, 1901–1912.

Chen, B., Blair, D.G., Plisov, S., Vasiliev, G., Perantoni, A.O., Chen, Q., Athanasiou, M., Wu, J.Y., Oppenheim, J.J., and Yang, D. (2004). Cutting edge: bone morphogenetic protein antagonists Drm/Gremlin and Dan interact with Slits and act as negative regulators of monocyte chemotaxis. *J. Immunol*. **173**, 5914–5917.

Chocron, S., Verhoeven, M.C., Rentzsch, F., Hammerschmidt, M., and Bakkers, J. (2007). Zebrafish Bmp4 regulates left-right asymmetry at two distinct developmental time points. *Dev. Biol*. **305**, 577–588.

Choi, M., Stottmann, R.W., Yang, Y.-P., Meyers, E.N., and Klingensmith, J. (2007). The bone morphogenetic protein antagonist noggin regulates mammalian cardiac morphogenesis. *Circ. Res*. **100**, 220–228.

Christia, P., and Frangogiannis, N.G. (2013). Targeting inflammatory pathways in myocardial infarction. Eur. *JCI* **43**, 986–995.

Csiszar, A., Smith, K.E., Koller, A., Kaley, G., Edwards, J.G., and Ungvari, Z. (2005). Regulation of bone morphogenetic protein-2 expression in endothelial cells: role of nuclear factor-kappaB activation by tumor necrosis factor-alpha, H2O2, and high intravascular pressure. *Circulation* **111**, 2364–2372.

Csiszar, A., Ahmad, M., Smith, K.E., Labinskyy, N., Gao, Q., Kaley, G., Edwards, J.G., Wolin, M.S., and Ungvari, Z. (2006). Bone morphogenetic protein-2 induces proinflammatory endothelial phenotype. *Am. J. Pathol*. **168**, 629–638.

de Lemos, J.A., Morrow, D.A., Blazing, M.A., Jarolim, P., Wiviott, S.D., Sabatine, M.S., Califf, R.M., and Braunwald, E. (2007). Serial measurement of monocyte chemoattractant protein-1 after acute coronary syndromes: results from the A to Z trial. *J. Am. Coll. Cardiol*. **50**, 2117–2124.

Derwall, M., Malhotra, R., Lai, C.S., Beppu, Y., Aikawa, E., Seehra, J.S., Zapol, W.M., Bloch, K.D., and Yu, P.B. (2012). Inhibition of bone morphogenetic protein signaling reduces vascular calcification and atherosclerosis. *Arterioscler. Thromb. Vasc. Biol.* **32**, 613–622.

Dudley, A.T., Lyons, K.M., and Robertson, E.J. (1995). A requirement for bone morphogenetic protein-7 during development of the mammalian kidney and eye. *Genes Dev.* **9**, 2795–2807.

Dudley AT, Robertson EJ. (1997). Overlapping expression domains of bone morphogenetic protein family members potentially account for limited tissue defects in BMP7 deficient embryos. *Dev Dyn*. **208**, 349–362.

Entman, M.L., Youker, K., Shoji, T., Kukielka, G., Shappell, S.B., Taylor, A.A., and Smith, C.W. (1992). Neutrophil induced oxidative injury of cardiac myocytes. A compartmented system requiring CD11b/CD18-ICAM-1 adherence. *JCI* **90**, 1335–1345.

Euler-Taimor, G., and Heger, J. (2006). The complex pattern of SMAD signaling in the cardiovascular system. *Cardiovasc. Res.* **69**, 15–25.

Faxon, D.P., Gibbons, R.J., Chronos, N.A.F., Gurbel, P.A., Sheehan, F., and HALT-MI Investigators (2002). The effect of blockade of the CD11/CD18 integrin receptor on infarct size in patients with acute myocardial infarction treated with direct angioplasty: the results of the HALT-MI study. *J. Am. Coll. Cardiol*. **40**, 1199–1204.

Feng, J.Q., Xing, L., Zhang, J.-H., Zhao, M., Horn, D., Chan, J., Boyce, B.F., Harris, S.E., Mundy, G.R., and Chen, D. (2003). NF-kappaB specifically activates BMP-2 gene expression in growth plate chondrocytes in vivo and in a chondrocyte cell line in vitro. *J. Biol. Chem*. **278**, 29130–29135.

Frangogiannis, N.G. (2008). The immune system and cardiac repair. *Pharmacol. Res.* **58**, 88–111.

Frangogiannis, N.G. (2012). Regulation of the inflammatory response in cardiac repair. *Circ. Res*. **110**, 159–173.

Frangogiannis, N.G. (2014). The inflammatory response in myocardial injury, repair, and remodelling. *Nat. Rev. Cardiol*. **11**, 255–265.

Fukui, N., Ikeda, Y., Ohnuki, T., Hikita, A., Tanaka, S., Yamane, S., Suzuki, R., Sandell, L.J., and Ochi, T. (2006). Pro-inflammatory cytokine tumor necrosis

factor-alpha induces bone morphogenetic protein-2 in chondrocytes via mRNA stabilization and transcriptional up-regulation. *J. Biol. Chem*. **281**, 27229–27241.

Furtado, M.B., Solloway, M.J., Jones, V.J., Costa, M.W., Biben, C., Wolstein, O., Preis, J.I., Sparrow, D.B., Saga, Y., Dunwoodie, S.L., et al. (2008). BMP/SMAD1 signaling sets a threshold for the left/right pathway in lateral plate mesoderm and limits availability of SMAD4. *Genes Dev*. **22**, 3037–3049.

Gao, H., Chakraborty, G., Lee-Lim, A.P., Mo, Q., Decker, M., Vonica, A., Shen, R., Brogi, E., Brivanlou, A.H., and Giancotti, F.G. (2012). The BMP inhibitor Coco reactivates breast cancer cells at lung metastatic sites. *Cell* **150**, 764–779.

Gonzalez-Quesada, C., and Frangogiannis, N.G. (2009). Monocyte chemoattractant protein-1/CCL2 as a biomarker in acute coronary syndromes. *Curr. Atheroscler. Rep*. **11**, 131–138.

Granger, C.B., Mahaffey, K.W., Weaver, W.D., Theroux, P., Hochman, J.S., Filloon, T.G., Rollins, S., Todaro, T.G., Nicolau, J.C., Ruzyllo, W., et al. (2003). Pexelizumab, an anti-C5 complement antibody, as adjunctive therapy to primary percutaneous coronary intervention in acute myocardial infarction: the COMplement inhibition in Myocardial infarction treated with Angioplasty (COMMA) trial. *Circulation* **108**, 1184–1190.

Groppe, J., Greenwald, J., Wiater, E., Rodriguez-Leon, J., Economides, A.N., Kwiatkowski, W., Affolter, M., Vale, W.W., Izpisua Belmonte, J.C., and Choe, S. (2002). Structural basis of BMP signalling inhibition by the cystine knot protein Noggin. *Nature* **420**, 636–642.

Gullestad, L., Orn, S., Dickstein, K., Eek, C., Edvardsen, T., Aakhus, S., Askevold, E.T., Michelsen, A., Bendz, B., Skårdal, R., et al. (2013). Intravenous immunoglobulin does not reduce left ventricular remodeling in patients with myocardial dysfunction during hospitalization after acute myocardial infarction. *Int. J. Cardiol.* **168**, 212–218.

Hammerschmidt, M., Serbedzija, G.N., and McMahon, A.P. (1996). Genetic analysis of dorsoventral pattern formation in the zebrafish: requirement of a BMP-like ventralizing activity and its dorsal repressor. *Genes Dev.* **10**, 2452–2461.

Hao, J., Lee, R., Chang, A., Fan, J., Labib, C., Parsa, C., Orlando, R., Andresen, B., and Huang, Y. (2014). DMH1, a small molecule inhibitor of BMP type i receptors, suppresses growth and invasion of lung cancer. *PloS One* **9**, e90748.

Hayashi, K., Yamaguchi, T., Yano, S., Kanazawa, I., Yamauchi, M., Yamamoto, M., and Sugimoto, T. (2009). BMP/Wnt antagonists are upregulated by dexamethasone in osteoblasts and reversed by alendronate and PTH: potential therapeutic targets for glucocorticoid-induced osteoporosis. *Biochem. Biophys. Res. Commun.* **379**, 261–266.

Helbing, T., Rothweiler, R., Ketterer, E., Goetz, L., Heinke, J., Grundmann, S., Duerschmied, D., Patterson, C., Bode, C., and Moser, M. (2011). BMP activity controlled by BMPER regulates the proinflammatory phenotype of endothelium. *Blood* **118**, 5040–5049.

Hinck, A.P. (2012). Structural studies of the TGF-βs and their receptors - insights into evolution of the TGF-β superfamily. *FEBS* **586**, 1860–1870.

Hindorff, L.A., Sethupathy, P., Junkins, H.A., Ramos, E.M., Mehta, J.P., Collins, F.S., and Manolio, T.A. (2009). Potential etiologic and functional implications of genome-wide association loci for human diseases and traits. *Proc. Natl. Acad. Sci*. **106**, 9362–9367.

Hulsmans, M., Sam, F., and Nahrendorf, M. (2016). Monocyte and macrophage contributions to cardiac remodeling. *J. Mol. Cell. Cardiol*. **93**, 149–155.

Ideno, H., Takanabe, R., Shimada, A., Imaizumi, K., Araki, R., Abe, M., and Nifuji, A. (2009). Protein related to DAN and cerberus (PRDC) inhibits osteoblastic differentiation and its suppression promotes osteogenesis in vitro. *Exp. Cell Res.* **315**, 474–484.

Im, J., Kim, H., Kim, S., and Jho, E.-H. (2007). Wnt/beta-catenin signaling regulates expression of PRDC, an antagonist of the BMP-4 signaling pathway. *Biochem. Biophys. Res. Commun.* **354**, 296–301.

Itoh, G., Tamura, J., Suzuki, M., Suzuki, Y., Ikeda, H., Koike, M., Nomura, M., Jie, T., and Ito, K. (1995). DNA fragmentation of human infarcted myocardial cells demonstrated by the nick end labeling method and DNA agarose gel electrophoresis. *Am. J. Pathol*. **146**, 1325–1331.

Jain, R., Li, D., Gupta, M., Manderfield, L.J., Ifkovits, J.L., Wang, Q., Liu, F., Liu, Y., Poleshko, A., Padmanabhan, A., et al. (2015). HEART DEVELOPMENT. Integration of Bmp and Wnt signaling by Hopx specifies commitment of cardiomyoblasts. *Science* **348**, aaa6071.

Jones, C.M., Lyons, K.M., and Hogan, B.L. (1991). Involvement of Bone Morphogenetic Protein-4 (BMP-4) and Vgr-1 in morphogenesis and neurogenesis in the mouse. *Development* **111**, 531–542.

Kain, V., Prabhu, S.D., and Halade, G.V. (2014). Inflammation revisited: inflammation versus resolution of inflammation following myocardial infarction. *Basic Res. Cardiol.* **109**, 444.

Kattamuri, C., Luedeke, D.M., Nolan, K., Rankin, S.A., Greis, K.D., Zorn, A.M., and Thompson, T.B. (2012a). Members of the DAN family are BMP antagonists that form highly stable noncovalent dimers. *J. Mol. Biol.* **424**, 313–327.

Kattamuri, C., Luedeke, D.M., and Thompson, T.B. (2012b). Expression and purification of recombinant protein related to DAN and cerberus (PRDC). *Protein Expr. Purif.* **82**, 389–395.

Kattman, S.J., Witty, A.D., Gagliardi, M., Dubois, N.C., Niapour, M., Hotta, A., Ellis, J., and Keller, G. (2011). Stage-specific optimization of activin/nodal and BMP signaling promotes cardiac differentiation of mouse and human pluripotent stem cell lines. *Cell Stem Cell* **8**, 228–240.

Khosla, S., Westendorf, J.J., and Oursler, M.J. (2008). Building bone to reverse osteoporosis and repair fractures. *JCI* **118**, 421–428.

Kingsley DM, Bland AE, Grubber JM, Marker PC, Russell LB, Copeland NG, Jenkins NA. (1992). The mouse short ear skeletal morphogenesis locus is associated with defects in a bone morphogenetic member of the TGF beta superfamily. *Cell* **71**, 399–410.

Kim, R.Y., Robertson, E.J., and Solloway, M.J. (2001). Bmp6 and Bmp7 are required for cushion formation and septation in the developing mouse heart. *Dev. Biol.* **235**, 449–466.

Koga, M., Engberding, N., Dikalova, A.E., Chang, K.H., Seidel-Rogol, B., Long, J.S., Lassègue, B., Jo, H., and Griendling, K.K. (2013). The bone morphogenic protein inhibitor, noggin, reduces glycemia and vascular inflammation in db/db mice. *Am. J. Physiol. Heart Circ. Physiol*. **305**, H747-755.

Koli, K., Myllärniemi, M., Vuorinen, K., Salmenkivi, K., Ryynänen, M.J., Kinnula, V.L., and Keski-Oja, J. (2006). Bone morphogenetic protein-4 inhibitor gremlin is overexpressed in idiopathic pulmonary fibrosis. *Am. J. Pathol*. **169**, 61–71.

Konstantinidis, K., Whelan, R.S., and Kitsis, R.N. (2012). Mechanisms of cell death in heart disease. *Arterioscler. Thromb. Vasc. Biol*. **32**, 1552–1562.

Kriebitz, N.N., Kiecker, C., McCormick, L., Lumsden, A., Graham, A., and Bell, E. (2009). PRDC regulates placode neurogenesis in chick by modulating BMP signalling. *Dev. Biol.* **336**, 280–292.

Krishnamurthy, P., Rajasingh, J., Lambers, E., Qin, G., Losordo, D.W., and Kishore, R. (2009). IL-10 inhibits inflammation and attenuates left ventricular remodeling after myocardial infarction via activation of STAT3 and suppression of HuR. *Circ. Res*. **104**, e9-18.

Kruithof, B.P.T., van Wijk, B., Somi, S., Kruithof-de Julio, M., Pérez Pomares, J.M., Weesie, F., Wessels, A., Moorman, A.F.M., and van den Hoff, M.J.B. (2006). BMP and FGF regulate the differentiation of multipotential pericardial mesoderm into the myocardial or epicardial lineage. *Dev. Biol.* **295**, 507–522.

Kua, H.-Y., Liu, H., Leong, W.F., Li, L., Jia, D., Ma, G., Hu, Y., Wang, X., Chau, J.F.L., Chen, Y.-G., et al. (2012). c-Abl promotes osteoblast expansion by differentially regulating canonical and non-canonical BMP pathways and p16INK4a expression. *Nat. Cell Biol.* **14**, 727–737.

Lappin, D.W.P., McMahon, R., Murphy, M., and Brady, H.R. (2002). Gremlin: an example of the re-emergence of developmental programmes in diabetic nephropathy. *Nephrol. Dial. Transplant*. **17 Suppl 9**, 65–67.

Lefer, D.J., Shandelya, S.M., Serrano, C.V., Becker, L.C., Kuppusamy, P., and Zweier, J.L. (1993). Cardioprotective actions of a monoclonal antibody against CD-18 in myocardial ischemia-reperfusion injury. *Circulation* **88**, 1779–1787.

de Lemos, J.A., Morrow, D.A., Bentley, J.H., Omland, T., Sabatine, M.S., McCabe, C.H., Hall, C., Cannon, C.P., and Braunwald, E. (2001). The prognostic value of B-type natriuretic peptide in patients with acute coronary syndromes. *NEJM* **345**, 1014–1021.

Lenhart, K.F., Lin, S.-Y., Titus, T.A., Postlethwait, J.H., and Burdine, R.D. (2011). Two additional midline barriers function with midline lefty1 expression to maintain asymmetric Nodal signaling during left-right axis specification in zebrafish. *Development* **138**, 4405–4410.

Li, Y., Wang, Z., Wang, S., Zhao, J., Zhang, J., and Huang, Y. (2012). Gremlin-mediated decrease in bone morphogenetic protein signaling promotes aristolochic acid-induced epithelial-to-mesenchymal transition (EMT) in HK-2 cells. *Toxicology* **297**, 68–75.

Liu, W., Selever, J., Wang, D., Lu, M.-F., Moses, K.A., Schwartz, R.J., and Martin, J.F. (2004). Bmp4 signaling is required for outflow-tract septation and branchial-arch artery remodeling*. Proc. Natl. Acad. Sci.* **101**, 4489–4494.

Livak, K.J., and Schmittgen, T.D. (2001). Analysis of relative gene expression data using real-time quantitative PCR and the 2(-Delta Delta C(T)) Method. *Methods* **25**, 402–408.

Lowery, J.W., and de Caestecker, M.P. (2010). BMP signaling in vascular development and disease. *Cytokine Growth Factor Rev.* **21**, 287–298.

Lu, M.M., Yang, H., Zhang, L., Shu, W., Blair, D.G., and Morrisey, E.E. (2001). The bone morphogenic protein antagonist gremlin regulates proximal-distal patterning of the lung. *Dev. Dyn*. **222**, 667–680.

Luo, G., Hofmann, C., Bronckers, A.L., Sohocki, M., Bradley, A., and Karsenty, G. (1995). BMP-7 is an inducer of nephrogenesis, and is also required for eye development and skeletal patterning. *Genes Dev*. **9**, 2808–2820.

da Luz, P.L., Forrester, J.S., Wyatt, H.L., Diamond, G.A., Chag, M., and Swan, H.J. (1976). Myocardial reperfusion in acute experimental ischemia. Beneficial effects of prior treatment with steroids. *Circulation* **53**, 847–852.

Ma, L., Lu, M.-F., Schwartz, R.J., and Martin, J.F. (2005). Bmp2 is essential for cardiac cushion epithelial-mesenchymal transition and myocardial patterning. *Development* **132**, 5601–5611.

Ma, Y., Yabluchanskiy, A., and Lindsey, M.L. (2013). Neutrophil roles in left ventricular remodeling following myocardial infarction. *Fibrogenesis Tissue Repair* **6**, 11.

Mann, D.L., McMurray, J.J.V., Packer, M., Swedberg, K., Borer, J.S., Colucci, W.S., Djian, J., Drexler, H., Feldman, A., Kober, L., et al. (2004). Targeted anticytokine therapy in patients with chronic heart failure: results of the Randomized Etanercept Worldwide Evaluation (RENEWAL). *Circulation* **109**, 1594–1602.

Marques, S.R., and Yelon, D. (2009). Differential requirement for BMP signaling in atrial and ventricular lineages establishes cardiac chamber proportionality. *Dev. Biol.* **328**, 472–482.

Matsumoto-Ida, M., Takimoto, Y., Aoyama, T., Akao, M., Takeda, T., and Kita, T. (2006). Activation of TGF-beta1-TAK1-p38 MAPK pathway in spared cardiomyocytes is involved in left ventricular remodeling after myocardial infarction in rats. *Am. J. Physiol. Heart Circ. Physiol.* **290**, H709-715.

Mayeur, C., Lohmeyer, L.K., Leyton, P., Kao, S.M., Pappas, A.E., Kolodziej, S.A., Spagnolli, E., Yu, B., Galdos, R.L., Yu, P.B., et al. (2014). The type I BMP receptor Alk3 is required for the induction of hepatic hepcidin gene expression by interleukin-6. *Blood* **123**, 2261–2268.

McCulley, D.J., Kang, J.-O., Martin, J.F., and Black, B.L. (2008). BMP4 is required in the anterior heart field and its derivatives for endocardial cushion remodeling, outflow tract septation, and semilunar valve development. *Dev. Dyn*. **237**, 3200–3209.

McMurray, J.J.V. (2010). Clinical practice. Systolic heart failure. *NEJM* **362**, 228–238.

Minabe-Saegusa, C., Saegusa, H., Tsukahara, M., and Noguchi, S. (1998). Sequence and expression of a novel mouse gene PRDC (protein related to DAN and cerberus) identified by a gene trap approach. *Dev. Growth Differ.* **40**, 343–353.

Miyazono, K., Maeda, S., and Imamura, T. (2005). BMP receptor signaling: transcriptional targets, regulation of signals, and signaling cross-talk. *Cytokine Growth Factor Rev.* **16**, 251–263.

Miyazono, K., Kamiya, Y., and Morikawa, M. (2010). Bone morphogenetic protein receptors and signal transduction. *J. Biochem*. **147**, 35–51.

Morrell, N.W., Bloch, D.B., Ten Dijke, P., Goumans, M.-J.T.H., Hata, A., Smith, J., Yu, P.B., and Bloch, K.D. (2015). Targeting BMP signalling in cardiovascular disease and anaemia. *Nat. Rev. Cardiol.* **13,** 106-120.

Mozaffarian, D., Benjamin, E.J., Go, A.S., Arnett, D.K., Blaha, M.J., Cushman, M., de Ferranti, S., Després, J.-P., Fullerton, H.J., Howard, V.J., et al. (2015). Heart disease and stroke statistics--2015 update: a report from the American Heart Association. *Circulation* **131**, e29-322.

Mueller, K.A.L., Tavlaki, E., Schneider, M., Jorbenadze, R., Geisler, T., Kandolf, R., Gawaz, M., Mueller, I.I., and Zuern, C.S. (2013). Gremlin-1 identifies fibrosis and predicts adverse outcome in patients with heart failure undergoing endomyocardial biopsy. *J. Card. Fail*. **19**, 678–684.

Müller, I.I., Knapik, E.W., and Hatzopoulos, A.K. (2006). Expression of the protein related to Dan and Cerberus gene--prdc--During eye, pharyngeal arch, somite, and swim bladder development in zebrafish. *Dev. Dyn.* **235**, 2881–2888.

Müller, I.I., Melville, D.B., Tanwar, V., Rybski, W.M., Mukherjee, A., Shoemaker, M.B., Wang, W.-D., Schoenhard, J.A., Roden, D.M., Darbar, D., et al. (2013). Functional modeling in zebrafish demonstrates that the atrial-fibrillation-associated gene GREM2 regulates cardiac laterality, cardiomyocyte differentiation and atrial rhythm. *Dis. Model. Mech*. **6**, 332–341.

Nahrendorf M, Swirski FK, Aikawa E, Stangenberg L, Wurdinger T, Figueiredo J-L, Libby P, Weissleder R, Pittet MJ. (2007). The healing myocardium sequentially mobilizes two monocyte subsets with divergent and complementary functions. *J Exp Med*. **204**, 3037–3047.

Nolan, K., and Thompson, T.B. (2014). The DAN family: modulators of TGF-β signaling and beyond. *Protein Sci.* **23**, 999–1012.

Nolan, K., Kattamuri, C., Luedeke, D.M., Deng, X., Jagpal, A., Zhang, F., Linhardt, R.J., Kenny, A.P., Zorn, A.M., and Thompson, T.B. (2013). Structure of Protein Related to Dan and Cerberus: Insights into the Mechanism of Bone Morphogenetic Protein Antagonism. *Structure* **21**, 1417–1429.

Omland, T., Aakvaag, A., Bonarjee, V.V., Caidahl, K., Lie, R.T., Nilsen, D.W., Sundsfjord, J.A., and Dickstein, K. (1996). Plasma brain natriuretic peptide as an indicator of left ventricular systolic function and long-term survival after acute myocardial infarction. Comparison with plasma atrial natriuretic peptide and N-terminal proatrial natriuretic peptide. *Circulation* **93**, 1963–1969.

Ørn, S., Manhenke, C., Ueland, T., Damås, J.K., Mollnes, T.E., Edvardsen, T., Aukrust, P., and Dickstein, K. (2009). C-reactive protein, infarct size,

microvascular obstruction, and left-ventricular remodelling following acute myocardial infarction. *Eur. Heart J.* **30**, 1180–1186.

Ortega-Gómez, A., Perretti, M., and Soehnlein, O. (2013). Resolution of inflammation: an integrated view. *EMBO Mol. Med*. **5**, 661–674.

Ovsyannikova, I.G., Kennedy, R.B., O'Byrne, M., Jacobson, R.M., Pankratz, V.S., and Poland, G.A. (2012). Genome-wide association study of antibody response to smallpox vaccine. *Vaccine* **30**, 4182–4189.

Owens, P., Pickup, M.W., Novitskiy, S.V., Giltnane, J.M., Gorska, A.E., Hopkins, C.R., Hong, C.C., and Moses, H.L. (2015). Inhibition of BMP signaling suppresses metastasis in mammary cancer. *Oncogene* **34**, 2437–2449.

Pachori, A.S., Custer, L., Hansen, D., Clapp, S., Kemppa, E., and Klingensmith, J. (2010). Bone morphogenetic protein 4 mediates myocardial ischemic injury through JNK-dependent signaling pathway. *J. Mol. Cell. Cardiol*. **48**, 1255–1265.

Paik, D.T., Rai, M., Ryzhov, S., Sanders, L.N., Aisagbonhi, O., Funke, M.J., Feoktistov, I., and Hatzopoulos, A.K. (2015). Wnt10b Gain-of-Function Improves Cardiac Repair by Arteriole Formation and Attenuation of Fibrosis. *Circ. Res.* **117**, 804–816.

de Pater, E., Ciampricotti, M., Priller, F., Veerkamp, J., Strate, I., Smith, K., Lagendijk, A.K., Schilling, T.F., Herzog, W., Abdelilah-Seyfried, S., et al. (2012). Bmp signaling exerts opposite effects on cardiac differentiation. *Circ. Res.* **110**, 578–587.

Pearce, J.J., Penny, G., and Rossant, J. (1999). A mouse cerberus/Dan-related gene family. *Dev. Biol.* **209**, 98–110.

Pi, X., Lockyer, P., Dyer, L.A., Schisler, J.C., Russell, B., Carey, S., Sweet, D.T., Chen, Z., Tzima, E., Willis, M.S., et al. (2012). Bmper inhibits endothelial expression of inflammatory adhesion molecules and protects against atherosclerosis. *Arterioscler. Thromb. Vasc. Biol.* **32**, 2214–2222.

Piot, C., Croisille, P., Staat, P., Thibault, H., Rioufol, G., Mewton, N., Elbelghiti, R., Cung, T.T., Bonnefoy, E., Angoulvant, D., et al. (2008). Effect of cyclosporine on reperfusion injury in acute myocardial infarction. *NEJM* **359**, 473–481.

Ramel, M.-C., and Hill, C.S. (2012). Spatial regulation of BMP activity. *FEBS* **586**, 1929–1941.

Reimer, K.A., and Jennings, R.B. (1979). The "wavefront phenomenon" of myocardial ischemic cell death. II. Transmural progression of necrosis within the framework of ischemic bed size (myocardium at risk) and collateral flow. *Lab. Investig. J. Tech. Methods Pathol.* **40**, 633–644.

Roberts, R., DeMello, V., and Sobel, B.E. (1976). Deleterious effects of methylprednisolone in patients with myocardial infarction. *Circulation* **53**, I204-206.

Rodrigues-Diez, R., Lavoz, C., Carvajal, G., Rayego-Mateos, S., Rodrigues Diez, R.R., Ortiz, A., Egido, J., Mezzano, S., and Ruiz-Ortega, M. (2012). Gremlin is a downstream profibrotic mediator of transforming growth factor-beta in cultured renal cells. *Nephron Exp. Nephrol.* **122**, 62–74.

Saeed, O., Otsuka, F., Polavarapu, R., Karmali, V., Weiss, D., Davis, T., Rostad, B., Pachura, K., Adams, L., Elliott, J., et al. (2012). Pharmacological suppression of hepcidin increases macrophage cholesterol efflux and reduces foam cell formation and atherosclerosis. *Arterioscler. Thromb. Vasc. Biol.* **32**, 299–307.

Sanvitale, C.E., Kerr, G., Chaikuad, A., Ramel, M.-C., Mohedas, A.H., Reichert, S., Wang, Y., Triffitt, J.T., Cuny, G.D., Yu, P.B., et al. (2013). A new class of small molecule inhibitor of BMP signaling. *PloS One* **8**, e62721.

Saxena, A., Russo, I., and Frangogiannis, N.G. (2016). Inflammation as a therapeutic target in myocardial infarction: learning from past failures to meet future challenges. *Transl. Res. J. Lab. Clin. Med.* **167**, 152-166.

Schlange, T., Arnold, H.-H., and Brand, T. (2002). BMP2 is a positive regulator of Nodal signaling during left-right axis formation in the chicken embryo. *Development* **129**, 3421–3429.

Shinde, A.V., and Frangogiannis, N.G. (2014). Fibroblasts in myocardial infarction: a role in inflammation and repair. *J. Mol. Cell. Cardiol*. **70**, 74–82.

Sieber, C., Kopf, J., Hiepen, C., and Knaus, P. (2009). Recent advances in BMP receptor signaling. *Cytokine Growth Factor Rev*. **20**, 343–355.

Simões Sato, A.Y., Bub, G.L., and Campos, A.H. (2014). BMP-2 and -4 produced by vascular smooth muscle cells from atherosclerotic lesions induce monocyte chemotaxis through direct BMPRII activation. *Atherosclerosis* **235**, 45–55.

Simpson, P.J., Todd, R.F., Fantone, J.C., Mickelson, J.K., Griffin, J.D., and Lucchesi, B.R. (1988). Reduction of experimental canine myocardial reperfusion injury by a monoclonal antibody (anti-Mo1, anti-CD11b) that inhibits leukocyte adhesion. *JCI* **81**, 624–629.

Sneddon, J.B., Zhen, H.H., Montgomery, K., van de Rijn, M., Tward, A.D., West, R., Gladstone, H., Chang, H.Y., Morganroth, G.S., Oro, A.E., et al. (2006). Bone morphogenetic protein antagonist gremlin 1 is widely expressed by cancer-associated stromal cells and can promote tumor cell proliferation. *Proc. Natl. Acad. Sci.* **103**, 14842–14847.

Solloway MJ, Dudley AT, Bikoff EK, Lyons KM, Hogan BL, Robertson EJ. (1998). Mice lacking Bmp6 function. *Dev Genet*. **22**, 321–339.

Solloway, M.J., and Robertson, E.J. (1999). Early embryonic lethality in Bmp5;Bmp7 double mutant mice suggests functional redundancy within the 60A subgroup. *Development* **126**, 1753–1768.

Sorescu, G.P., Sykes, M., Weiss, D., Platt, M.O., Saha, A., Hwang, J., Boyd, N., Boo, Y.C., Vega, J.D., Taylor, W.R., et al. (2003). Bone morphogenic protein 4 produced in endothelial cells by oscillatory shear stress stimulates an inflammatory response. *J. Biol. Chem.* **278**, 31128–31135.

Steinbicker, A.U., Sachidanandan, C., Vonner, A.J., Yusuf, R.Z., Deng, D.Y., Lai, C.S., Rauwerdink, K.M., Winn, J.C., Saez, B., Cook, C.M., et al. (2011). Inhibition of bone morphogenetic protein signaling attenuates anemia associated with inflammation. *Blood* **117**, 4915–4923.

Subramaniam, A., Jones, W.K., Gulick, J., Wert, S., Neumann, J., and Robbins, J. (1991). Tissue-specific regulation of the alpha-myosin heavy chain gene promoter in transgenic mice. *J. Biol. Chem*. **266**, 24613–24620.

Sucosky, P., Balachandran, K., Elhammali, A., Jo, H., and Yoganathan, A.P. (2009). Altered shear stress stimulates upregulation of endothelial VCAM-1 and ICAM-1 in a BMP-4- and TGF-beta1-dependent pathway. *Arterioscler. Thromb. Vasc. Biol.* **29**, 254–260.

Sudo, S., Avsian-Kretchmer, O., Wang, L.S., and Hsueh, A.J.W. (2004). Protein related to DAN and cerberus is a bone morphogenetic protein antagonist that participates in ovarian paracrine regulation. *J. Biol. Chem*. **279**, 23134–23141.

Sun, B., Huo, R., Sheng, Y., Li, Y., Xie, X., Chen, C., Liu, H.-B., Li, N., Li, C.-B., Guo, W.-T., et al. (2013). Bone morphogenetic protein-4 mediates cardiac hypertrophy, apoptosis, and fibrosis in experimentally pathological cardiac hypertrophy. *Hypertension* **61**, 352–360.

Swirski FK, Nahrendorf M, Etzrodt M, Wildgruber M, Cortez-Retamozo V, Panizzi P, Figueiredo J-L, Kohler RH, Chudnovskiy A, Waterman P, Aikawa E, Mempel TR, Libby P, Weissleder R, Pittet MJ. (2009). Identification of splenic reservoir monocytes and their deployment to inflammatory sites. *Science* **325**, 612–616.

Chia S, Nagurney JT, Brown DFM, Raffel OC, Bamberg F, Senatore F, Wackers FJT, Jang I-K. (2009). Association of leukocyte and neutrophil counts with infarct size, left ventricular function and outcomes after percutaneous coronary intervention for ST-elevation myocardial infarction. *Am J Cardiol*. **103**, 333–337.

Tang, Y., Xie, H., Chen, J., Geng, L., Chen, H., Li, X., Hou, Y., Lu, L., Shi, S., Zeng, X., et al. (2013). Activated NF-κB in bone marrow mesenchymal stem cells

from systemic lupus erythematosus patients inhibits osteogenic differentiation through downregulating Smad signaling. *Stem Cells Dev.* **22**, 668–678.

Tanwar, V., Bylund, J.B., Hu, J., Yan, J., Walthall, J.M., Mukherjee, A., Heaton, W.H., Wang, W.-D., Potet, F., Rai, M., et al. (2014). Gremlin 2 promotes differentiation of embryonic stem cells to atrial fate by activation of the JNK signaling pathway. *Stem Cells* **32**, 1774–1788.

Tardif, J.-C., Tanguay, J.-F., Wright, S.S., Duchatelle, V., Petroni, T., Grégoire, J.C., Ibrahim, R., Heinonen, T.M., Robb, S., Bertrand, O.F., et al. (2013). Effects of the P-selectin antagonist inclacumab on myocardial damage after percutaneous coronary intervention for non-ST-segment elevation myocardial infarction: results of the SELECT-ACS trial. *J. Am. Coll. Cardiol*. **61**, 2048–2055.

Timmers, L., Pasterkamp, G., de Hoog, V.C., Arslan, F., Appelman, Y., and de Kleijn, D.P.V. (2012). The innate immune response in reperfused myocardium. *Cardiovasc. Res*. **94**, 276–283.

Umulis, D., O'Connor, M.B., and Blair, S.S. (2009). The extracellular regulation of bone morphogenetic protein signaling. *Development* **136**, 3715–3728.

Virag, J.I., and Murry, C.E. (2003). Myofibroblast and endothelial cell proliferation during murine myocardial infarct repair. *Am. J. Pathol*. **163**, 2433–2440.

Walsh, D.W., Godson, C., Brazil, D.P., and Martin, F. (2010). Extracellular BMP-antagonist regulation in development and disease: tied up in knots. *Trends Cell Biol.* **20**, 244–256.

Wang, Y.-X., Qian, L.-X., Liu, D., Yao, L.-L., Jiang, Q., Yu, Z., Gui, Y.-H., Zhong, T.P., and Song, H.-Y. (2007). Bone morphogenetic protein-2 acts upstream of myocyte-specific enhancer factor 2a to control embryonic cardiac contractility. *Cardiovasc. Res.* **74**, 290–303.

Wang, Z., Gerstein, M., and Snyder, M. (2009). RNA-Seq: a revolutionary tool for transcriptomics. *Nat. Rev. Genet*. **10**, 57–63.

Weaver, M., Yingling, J.M., Dunn, N.R., Bellusci, S., and Hogan, B.L. (1999). Bmp signaling regulates proximal-distal differentiation of endoderm in mouse lung development. *Development* **126**, 4005–4015.

Weinberger, T., and Schulz, C. (2015). Myocardial infarction: a critical role of macrophages in cardiac remodeling. *Front. Physiol*. **6**, 107.

Weirather, J., Hofmann, U.D.W., Beyersdorf, N., Ramos, G.C., Vogel, B., Frey, A., Ertl, G., Kerkau, T., and Frantz, S. (2014). Foxp3+ CD4+ T cells improve healing after myocardial infarction by modulating monocyte/macrophage differentiation. *Circ. Res.* **115**, 55–67.

van Wijk, B., Moorman, A.F.M., and van den Hoff, M.J.B. (2007). Role of bone morphogenetic proteins in cardiac differentiation. *Cardiovasc. Res.* **74**, 244–255.

Winnier, G., Blessing, M., Labosky, P.A., and Hogan, B.L. (1995). Bone morphogenetic protein-4 is required for mesoderm formation and patterning in the mouse. *Genes Dev.* **9**, 2105–2116.

Wozney, J.M., Rosen, V., Celeste, A.J., Mitsock, L.M., Whitters, M.J., Kriz, R.W., Hewick, R.M., and Wang, E.A. (1988). Novel regulators of bone formation: molecular clones and activities. *Science* **242**, 1528–1534.

Wu, Q., Tang, S.-G., and Yuan, Z.-M. (2015). Gremlin 2 inhibits adipocyte differentiation through activation of Wnt/β-catenin signaling. *Mol. Med. Rep*. **12**, 5891–5896.

Wu, X., Sagave, J., Rutkovskiy, A., Haugen, F., Baysa, A., Nygård, S., Czibik, G., Dahl, C.P., Gullestad, L., Vaage, J., et al. (2014). Expression of bone morphogenetic protein 4 and its receptors in the remodeling heart. *Life Sci*. **97**, 145–154.

Yadin, D., Knaus, P., and Mueller, T.D. (2016). Structural insights into BMP receptors: Specificity, activation and inhibition. *Cytokine Growth Factor Rev*. **27**, 13-34.

Yamaguchi, K., Nagai, S., Ninomiya-Tsuji, J., Nishita, M., Tamai, K., Irie, K., Ueno, N., Nishida, E., Shibuya, H., and Matsumoto, K. (1999). XIAP, a cellular member of the inhibitor of apoptosis protein family, links the receptors to TAB1-TAK1 in the BMP signaling pathway. *EMBO* **18**, 179–187.

Yan, K., Wu, Q., Yan, D.H., Lee, C.H., Rahim, N., Tritschler, I., DeVecchio, J., Kalady, M.F., Hjelmeland, A.B., and Rich, J.N. (2014). Glioma cancer stem cells secrete Gremlin1 to promote their maintenance within the tumor hierarchy. *Genes Dev.* **28**, 1085–1100.

Yan, X., Anzai, A., Katsumata, Y., Matsuhashi, T., Ito, K., Endo, J., Yamamoto, T., Takeshima, A., Shinmura, K., Shen, W., et al. (2013). Temporal dynamics of cardiac immune cell accumulation following acute myocardial infarction. *J. Mol. Cell. Cardiol*. **62**, 24–35.

Yanagita, M. (2005). BMP antagonists: their roles in development and involvement in pathophysiology. *Cytokine Growth Factor Rev*. **16**, 309–317.

Yu, P.B., Hong, C.C., Sachidanandan, C., Babitt, J.L., Deng, D.Y., Hoyng, S.A., Lin, H.Y., Bloch, K.D., and Peterson, R.T. (2008). Dorsomorphin inhibits BMP signals required for embryogenesis and iron metabolism. *Nat. Chem. Biol.* **4**, 33–41.

Zeisberg, E.M., Tarnavski, O., Zeisberg, M., Dorfman, A.L., McMullen, J.R., Gustafsson, E., Chandraker, A., Yuan, X., Pu, W.T., Roberts, A.B., et al. (2007). Endothelial-to-mesenchymal transition contributes to cardiac fibrosis. *Nat. Med.* **13**, 952–961.

Zhang, H., and Bradley, A. (1996). Mice deficient for BMP2 are nonviable and have defects in amnion/chorion and cardiac development. *Development* **122**, 2977–2986.

Zhang, J.-L., Qiu, L.-Y., Kotzsch, A., Weidauer, S., Patterson, L., Hammerschmidt, M., Sebald, W., and Mueller, T.D. (2008). Crystal structure analysis reveals how the Chordin family member crossveinless 2 blocks BMP-2 receptor binding. *Dev. Cell* **14**, 739–750.

Zhang, S., Dehn, S., DeBerge, M., Rhee, K.-J., Hudson, B., and Thorp, E.B. (2014). Phagocyte-myocyte interactions and consequences during hypoxic wound healing. *Cell. Immunol*. **291**, 65–73.

Zhao, N., Zhang, A.-S., and Enns, C.A. (2013). Iron regulation by hepcidin. *JCI* **123**, 2337–2343.

Zuniga, E., Rippen, M., Alexander, C., Schilling, T.F., and Crump, J.G. (2011). Gremlin 2 regulates distinct roles of BMP and Endothelin 1 signaling in dorsoventral patterning of the facial skeleton. *Development* **138**, 5147–5156.